TECHNISCHE UNIVERSITÄT WIEN
Vienna University of Technology

D I P L O M A R B E I T

Mathematical models for action potential propagation in unmyelinated nerve fibres of warm blooded animals

ausgeführt am Institut für

Analysis and Scientific Computing

der Technischen Universität Wien

unter Anleitung von Ao.Univ.Prof. Dipl.-Ing. DDDr. Frank Rattay

durch

Reimar Madzak

Hartlebengasse 1-17/5/3

1220 Wien

Acknowledgements

I want to thank Prof. Frank Rattay for his scientific support in numerous meetings and for the help during the working process of my diploma thesis. I also want to thank my fellow students and friends for their constructive comments and extensive discussions, especially DI Cornelia Wenger for her assistance and ideas, Evelyn Anninger, Julia Hofecker, and Andrea Hahn for their helpful discussions, and Dr. Julia Lajta-Novak for her English support.

A special thanks goes to my family, who supported and motivated me in various ways throughout my study.

Abstract

Many of the mathematical models for cell membranes that have been investigated so far deal with non-myelinated nerve fibres of cold blooded animals or myelinated nerve fibres; this diploma thesis examines a slightly adapted Hodgkin-Huxley (HH) model, which shall model a non-myelinated nerve fibre of warm blooded animals. This model is compared with other membrane models found in literature. The original HH model was developed in 1952 for the unmyelinated giant axon of the squid. By changing the maximal ionic conductances g_{ion}, the ion channels are adapted so that g_{Na} almost equals that of the model which was developed by Chiu, Ritchie, Rogart, Stagg, and Sweeney (CRRSS) for mammalian myelinated nerve fibres. Changing the ionic conductances is necessary to avoid the heat block, a phenomenon that prohibits spike propagation at high temperatures.

In this thesis, the local models, where current flow along the axon is prevented, as well as different propagation models are examined and compared with each other. Adapted HH models with different factors for the ionic conductances are analyzed, and models for myelinated nerve fibres with different insulating properties are investigated.

Comparison shows that the total number of ions that cross the cell membrane through the ionic channels in the HH model during an action potential is smaller than that in any other model. The total number of sodium ions that cross the membrane at some distance from the stimulated region in the CRRSS model is, for example, three times the number of sodium ions that pass the corresponding membrane area in the HH model. The injected stimulating threshold current in the HH model is also smaller than those in the other models. The conduction velocity of an action potential along the unmyelinated HH fibre is higher than that according to any other examined membrane model, and can be increased by modeling myelinated nerve fibres. In a $1\,\mu\mathrm{m}$ thick axon, the conduction speed can be heightened to $16\,\mathrm{m/s}$. As regards the shape of the action potentials, the spike in the adapted HH model is unusually short, which can be observed in the local model as well as in the propagation models. The spike is quite different to those in the CRRSS and the SRB model, which were created for modeling the membrane of a mammalian myelinated nerve fibre and a human myelinated nerve fibre, respectively. This indicates that the adapted HH model is not adequate for modeling the membrane of warm blooded animals.

One possible reason might be that the value of Q_{10} in the HH model is not constant but changes with temperature. Another reason might be that the HH model does not take account of different types of sodium channels.

Zusammenfassung

Viele bisher entwickelten mathematischen Modelle für Zellmembranen behandeln unmyelinisierte Nervenfasern von Kaltblütern oder myelinisierte Nervenfasern; diese Diplomarbeit beschäftigt sich insbesondere mit einem etwas veränderten Hodgkin-Huxley-Modell (HH-Modell), das unmyelinisierte Nervenfasern von Warmblütern modellieren soll. Dieses Modell wird mit anderen in der Literatur gefundenen Modellen verglichen. Das ursprüngliche HH-Modell wurde 1952 für die unmyelinisierten Riesenaxone der Tintenfische entwickelt. Durch eine Veränderung der maximalen Ionenleitfähigkeiten g_{ion} werden die Ionenkanäle denen des von Chiu, Ritchie, Rogart, Stagg und Sweeney (CRRSS) entwickelten Modells für myelinisierte Nervenfasern von Säugetieren angepasst. Eine Änderung der Ionenleitfähigkeiten ist nötig, um den Hitzeblock, ein Phänomen, das die Reizweiterleitung bei hohen Temperaturen verhindert, zu vermeiden.

In dieser Diplomarbeit werden lokale Modelle, bei denen der Stromfluss entlang des Axons verhindert wird, und verschiedene Modelle mit Ausbreitungseffekten untersucht und miteinander verglichen. Veränderte HH-Modelle mit unterschiedlichen Faktoren für die Ionenleitfähigkeiten werden analysiert, und Modelle für myelinisierte Nervenfasern mit verschiedenen Isolierungseigenschaften werden untersucht.

Ein Vergleich zeigt, dass die Ionenanzahl, die beim HH-Modell während eines Impulses durch die Ionenkanäle fließen, kleiner als bei den übrigen Modellen ist. Die Gesamtzahl der Natriumionen, die beispielsweise beim CRRSS-Modell die Zellmembran passieren, ist in einem vom Stimulationsbereich entfernten Abschnitt ungefähr drei mal so groß wie beim HH-Modell. Der Schwellwert für den Stimulusstrom ist beim HH-Modell ebenfalls kleiner als bei den anderen Modellen. Die Reizweiterleitungsgeschwindigkeit eines Aktionspotentials entlang einer HH-Zellmembran ist höher als bei den anderen untersuchten Modellen, und kann erhöht werden, indem man myelinisierte Nervenfasern modelliert. In einem 1 µm dicken Axon kann die Geschwindigkeit auf 16 $^{\mathrm{m}}/_{\mathrm{s}}$ erhöht werden. Die Form des Nervenimpulses beim HH-Modell ist ungewöhnlich kurz. Insbesondere hat das Aktionspotential eine andere Form als das des CRRSS- und des SRB-Modells, die die Zellmembran einer myelinisierten Nervenzelle eines Säugetiers bzw. eines Menschen modellieren. Dies zeigt, dass das adaptierte HH-Modell für die Modellierung einer Zellmembran von Warmblütern ungeeignet ist.

Ein möglicher Grund ist, dass das Q_{10} im HH-Modell nicht für alle Temperaturen gleich ist, sondern sich mit der Temperatur ändert. Ein anderer Grund könnte sein, dass das HH-Modell die verschiedenen Typen von Natriumionenkanälen nicht berücksichtigt.

Contents

Chapter 1

Introduction

The first quantitative description of axonal membrane currents was made by Alan Lloyd Hodgkin and Andrew Huxley[21] for the giant axon of the squid. Later, Bernhard Frankenhaeuser[12],[14] demonstrated that membrane currents measured in the frog node of Ranvier were similar to those of the squid axon and were composed of Na^+ and K^+ currents and a non-specific leakage current. Based on the quantitative analysis of these nodal currents, Frankenhaeuser and Huxley[15] were able to calculate action potentials which were similar to those measured.
Following a short description of action potentials and membrane currents in the rat[1], the first successful voltage-clamp experiments in mammalian nerve fibres were reported in the rabbit[5] and in the rat[4].
Because of the lack of human data, previous models of action potentials and slow excitability changes in human nerve fibres have been based on measurements from frog, rabbit, or rat nodes, although extracellular recordings from human nerve in vivo have also been taken into account[2],[2]. K^+ channel density differs substantially between frog and mammalian nodes[4],[5], and in rat fibres, K^+ channel distribution changes with age[3]. Therefore, it has been open to question whether data from laboratory animals can provide a satisfactory model of excitability in adult human axons. [42]

The aim of this thesis is the investigation of a nerve cell model for unmyelinated fibres of warm blooded animals at 37 ℃ body temperature on the basis of the model of Hodgkin and Huxley. The ion channel dynamic is adapted to avoid the heat block, a phenomenon that occurs at the original HH model at high temperatures, i.e. that blocks the propagation of

[1] Horáckova M., Nonner W. & Stämpfli R., 1968. Action potentials and voltage clamp currents of single rat Ranvier nodes. Proc. int. Union Physiol. Sci. 7, 198

[2] H. Bostock, D. Burke, and J.P. Hales, Differences in behaviour of sensory and motor axons following release of ischaemia. Brain, 117:225-234, 1994

a nerve impulse in the cell membrane. The idea is to multiply the maximum conductances of each ionic current by a constant factor in order to get almost the same maximum sodium conductance as in the CRRSS model. This adaption corresponds to an increase of ionic channels when considering the biological aspect of a nerve cell.

Chapter 2

Hodgkin and Huxley's space clamp experiment

In 1902, Julius Bernstein postulated that the cell membrane has pores which open during excitation, but it took fifty years until a quantitative description of the phenomena involved was found by the ingenious experiments of Alan Lloyd Hodgkin and Andrew Huxley on giant squid axons. They assumed that a gating mechanism is responsible for the ionic transport across the membrane and that sodium and potassium ions are responsible for exciting the axon. The ionic currents seemed to be independent of each other, but both could be described in a statistical manner. In order to quantify the voltage-dependent conductance of the membrane new electronic techniques were used. [34]

Within their experiments, Hodgkin, Huxley, and Katz inserted two electrodes consisting of fine silver wires down the axis of the fibre for a distance of about 30 mm. One of these electrodes recorded the membrane potential, the other was responsible for stimulation of the axon.

In the "space clamp" experiment there is no current flow along the axis, all parts of the membrane work under the same conditions because there are 'isopotentials' on the inside as well as on the outside of the membrane. This "local model", where current flow along the axis is prohibited, is often used to describe the reaction of the axon at a fixed point. The space clamp experiment can be used to produce a simultaneous action potential at all parts of the membrane by applying a current square pulse or any stimulus signal of arbitrary shape. As the whole injected current I_{inj} has to cross the membrane (and cannot leak away to the left or the right), it only splits into a capacitive and an ion current $I_{inj} = I_{cap} + I_{ion} = C_m \cdot \frac{\mathrm{d}V}{\mathrm{d}t} + I_{ion}$. More details on the model of the cell membrane can be found in the sections 6.3 and 6.4. [22],[34]

2.1 The voltage clamp

The space clamp experiment can be used for voltage clamp analysis where the voltage across the membrane is controlled and held at a constant level. A feedback amplifier, which is connected to the stimulating electrode regulates the current entering the electrode in such a way as to change the membrane potential suddenly and hold it at the new level. Under these conditions it was found that the membrane current consisted of a nearly instantaneous surge of capacity current, associated with the sudden change of potential, and an ionic current during the period of maintained potential. Note that at constant voltage the capacitive current is zero $\left(I_{cap} = C \cdot \frac{\mathrm{d}V}{\mathrm{d}t}\right)$!

In the voltage clamp experiment the time course of the voltage is given and the injected current is measured in order to find the nonlinear conductances for the ionic currents. For this purpose, the voltage is varied as a step or pulse function. In practise, this means that the voltage signal has a very large slope as the rise time is in the order of 1 µs. Within this short rise time interval a large current has to be injected and nearly all this current is needed to load the capacitor. After this short starting phase $\frac{\mathrm{d}V}{\mathrm{d}t}$ equals zero and all the injected current passes the membrane in form of ionic current until at the end of the pulse voltage a strong capacity current occurs again. In most experiments of Hodgkin and Huxley $\frac{\mathrm{d}V}{\mathrm{d}t}$ equals zero so that the ionic current can be obtained directly from the experimental record. This is the most obvious reason for using electronic feedback to keep the membrane potential constant. Within the pulse interval, I_{inj} equals I_{ion}.

By changing the bathing solution, the axon is laid, or by using blockers which stop the activity of special types of channels, the ionic currents can be determined individually. One way to separate sodium and potassium currents is to exchange the sodium component of the bath solution with larger cations which cannot pass the small sodium channels; thereby the potassium outward current is found. Because of $I_{inj} = I_{\mathrm{Na}} + I_{\mathrm{K}}$, the sodium current is also determined.

The main result of the voltage clamp experiment is the time course of g_{Na} and g_{K}, which is proportional to I_{Na} and I_{K}. It is important to note that the electrical membrane behaviour is not linear, which means that doubling the amplitude of the voltage pulse does not produce just the doubled time course of I_{Na} and I_{K}. Therefore Hodgkin and Huxley varied the amplitudes of the voltage pulses and, by fitting the transient behaviour of g_{Na} and g_{K}, they found a description for the squid membrane of the general current-voltage relation through four differential equations (see section 7.1). [22],[34]

2.2 The patch clamp

The patch clamp technique is a method to measure the electric current of single ion channels. It was developed in 1976 by Erwin Neher, Bert Sakmann, and their colleagues, and is a refinement of the voltage clamp which is used to measure the ion currents across a cell membrane while holding the membrane voltage at a set level.

Unlike in the case of the voltage clamp, where two electrodes are inserted into the cell, one micropipette with an inside diameter of 0.3 µm is pressed against the surface and onto some ion channels of a cell membrane in a patch clamp experiment. Suction produces low pressure on the inside of the pipette to get a seal between the membrane and the glass of the pipette. In this way, only those currents which pass through this very small patch of membrane are measured. This technique was used by Sigworth and Neher in 1980 for whole cell recordings. They filled the micropipette with a modified Ringer solution which was connected to an operational amplifier, which recorded the currents passing through $2-5$ Na^+ channels that were located within the opening of the pipette.

This technique can also be used to cut a small patch of membrane and put it in a bathing solution. Arbitrary solutions are put inside the pipette and in the bath before the current across the membrane is measured under voltage control. In this way, the patch clamp technique was used to find both the open times and the resulting current strengths of single channels under the control of different intra- and extracellular solutions and also under the influence of transmitters. [34]

Chapter 3

Gating of ion channels

A gating process is quantitatively represented by a single variable y being a function of time and voltage. y statistically describes the gating behaviour of a high number of channels of one special type, for example a potassium channel, lying in a small patch of membrane. $y = 1$ means that all gates are open, $y = 0$ means that all gates are closed.
The conductance of the membrane may be determined by the rate constants α and β. At a fixed voltage, β defines the change of the part of open gates which closes within a time unit Δt ($\beta \cdot y$ of open gates will close), whereas $\alpha \cdot (1 - y)$ of the closed gates—the probability of a gate to be closed is $(1 - y)$—open up at the same. Thus, one can calculate the probability that gates are open with the help of the following differential equation.

$$\frac{\mathrm{d}y}{\mathrm{d}t} = \big(\alpha(1 - y) - \beta y\big) \cdot k \tag{3.1}$$

k is the temperature coefficient which accelerates the gating process for temperatures higher than the original experimental temperature. [34],[37]

3.1 Time constant and steady state value

Equation (3.1) can also be written in the following form:

$$\frac{\mathrm{d}y}{\mathrm{d}t} = k \cdot \alpha - k \cdot (\alpha + \beta) \cdot y \tag{3.2}$$

Before a voltage step is applied, the probability of open gates may be $y(0) = y_0$ and according to equation (3.2) y increases exponentially to a steady state value y_∞:

$$y = y_\infty - (y_\infty - y_0) \cdot e^{-\frac{t}{\tau}} \tag{3.3}$$

where

$$y_\infty = \frac{\alpha}{\alpha + \beta}, \tag{3.4}$$

and

$$\tau = \frac{1}{k \cdot (\alpha + \beta)}. \tag{3.5}$$

As regards the function $y = e^{-t/\tau}$, after the time $t = \tau$ the value of y decays to $1/e$. As τ is the time scaling parameter for exponentially changing processes, τ is called the "exponential time constant" or just the "time constant" and determines the rate at which y approaches its steady state value y_∞. y_∞ and τ are the essential parameters of the gating process, they give information about the steady state and how quickly it will be reached. The voltage dependent parameters τ and y_∞ of different ion conductances in different membrane models are shown in figures 3.1 and 3.2. As a model for the cell membrane has more than one type of ion channel and the gating of the sodium channel is more complicated than of the potassium channel anyway (see section 3.2), several variables are used instead of y. One can see that at very negative potentials (e.g., $-75\,\mathrm{mV}$) n_∞ (n is the gating variable for the potassium channel) of the HH model is small, meaning that potassium channels would tend to close. At positive potentials (e.g., $50\,\mathrm{mV}$) n_∞ is nearly 1, meaning that channels tend to open. As regards the τ_n curve of the HH model, the parameter n relaxes slowly to new values at $-75\,\mathrm{mV}$ and much more rapidly at $50\,\mathrm{mV}$.

Unfortunately, the gating mechanism of living cells cannot be described by such a simple rule (equation (3.3)). Hodgkin and Huxley observed that during a depolarization step the increase of potassium conductance g_K follows an S-shaped time course, whereas on repolarization the decrease is exponential. This very flat response at the beginning of the voltage step does not confirm the time course of the gating variable in accord with the differential equation (3.1). By using the fourth power of n they gained better fitting and a good approximation to the experimental data. As they noted, such kinetics would be obtained if the opening of a potassium channel were controlled by four independent membrane-bound "particles". Supposing that each particle is in the correct position to set up an open channel with a probability n, the probability that all four particles are correctly placed is n^4. Hence, the potassium current of the HH model is represented by

$$I_\mathrm{K} = g_\mathrm{K} n^4 (V - V_\mathrm{K}). \tag{3.6}$$

V_K is the Nernst potential for the potassium ions. For more details on the Nernst potential, the reader is asked to have a look at section 6.5. The equations above except the last one for the potassium current hold for all gating variables. Nevertheless, the gating of the sodium channel is more complicated than that of the potassium channel.[17],[20],[21],[34]

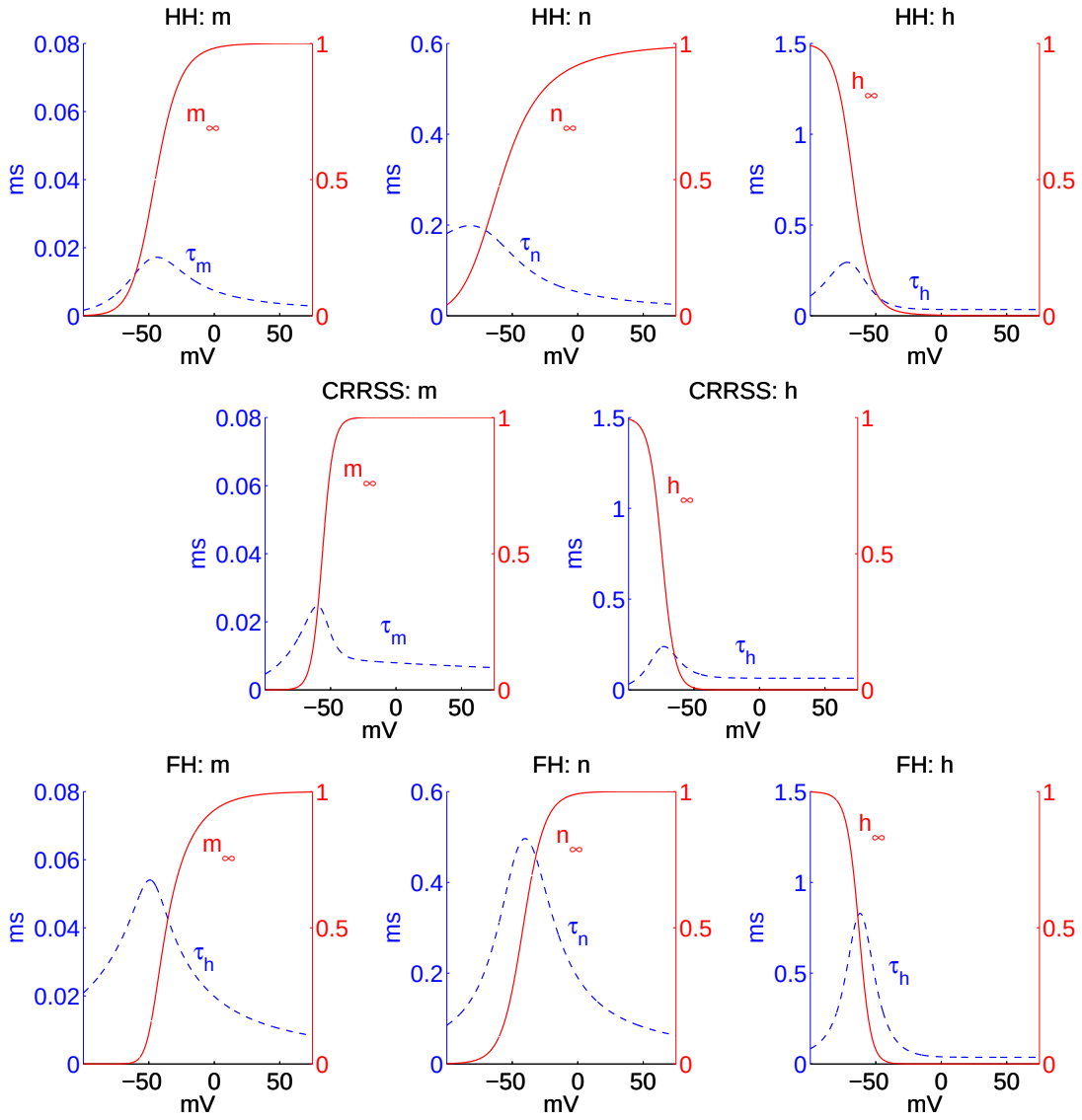

Figure 3.1: Steady state values y_∞ (red solid line) and time constants τ_y (blue dotted line) according to different gating variables y in the HH model, the CRRSS model, and the FH model as a function of the membrane voltage $V = V_i - V_e$ at 37 ℃.

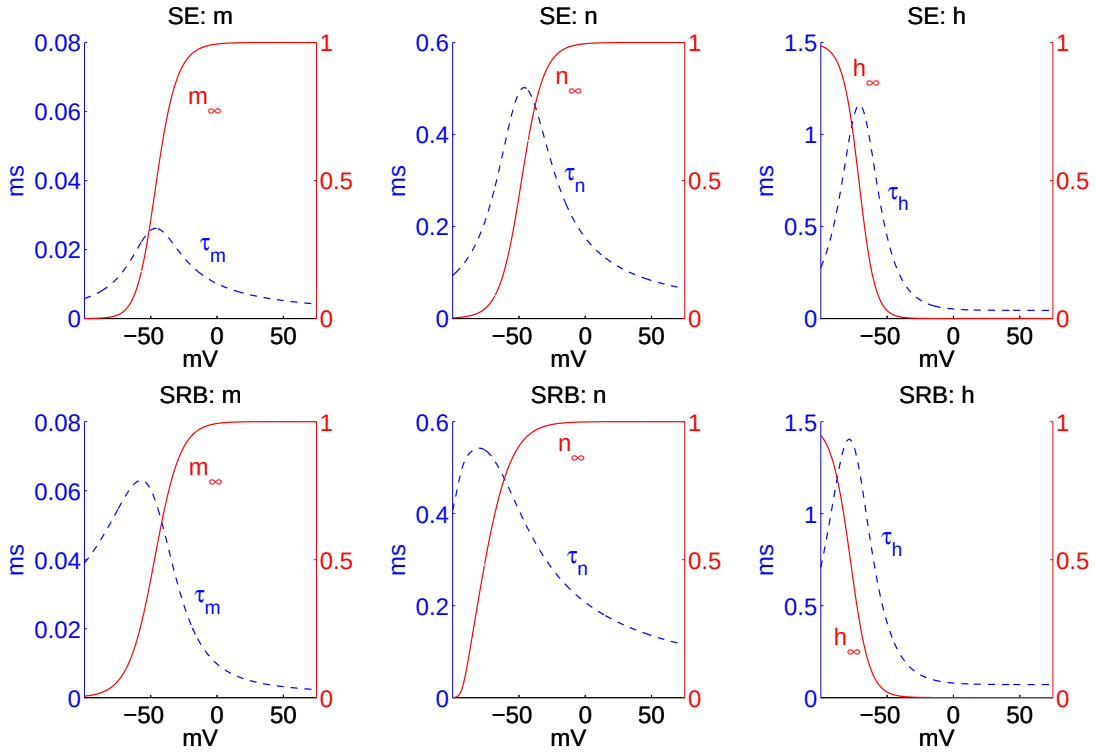

Figure 3.2: Steady state values y_∞ (red solid line) and time constants τ_y (blue dotted line) according to different gating variables y in the SE model, and the SRB model as a function of the membrane voltage $V = V_i - V_e$ at 37 ℃.

3.2 Activation and inactivation of sodium channels

Hodgkin and Huxley found out that during a depolarizing voltage step, which can be made possible by a voltage clamp experiment (see section 2.1), the sodium permeability of the membrane rises rapidly and then decays. This a remarkable difference to the potassium conductance, whose time course increases monotone to the steady state. Hodgkin and Huxley said that g_{Na} activates and then inactivates, nowadays one would say that Na^+ channels activate and then inactivate. In the Hodgkin-Huxley analysis, activation is the rapid process that opens Na^+ channels during a depolarization. A quick reversal of activation during a repolarization accounts for the rapid closing of channels after a brief depolarization pulse is terminated. According to the Hodgkin-Huxley view, if there were no inactivation process, g_{Na} would increase to a new steady state level in a fraction of a millisecond with any voltage step in the depolarizing direction, and would decrease to a new steady state level, again in a fraction of a millisecond, with any step in the hyperpolarizing direction. Without inactivation, such rapid opening and closing of channels could be repeated as often as desired. Sodium channels do behave exactly this way if they are modified by certain chemical treatments of natural toxins.

Inactivation is a slower process that closes Na channels during a depolarization. Once sodium channels have been inactivated, the membrane must be repolarized or hyperpolarized, often for many milliseconds, to remove the inactivation. Inactivated channels cannot be activated to the conducting state until their inactivation is removed. The inactivation process overrides the tendency of the activation process to open channels. Thus, inactivation is distinguished from activation in kinetics, which are slower, and in its effect, which is to close rather than to open during a depolarization. Inactivation of sodium channels accounts for the loss of excitability that occurs if the resting potential falls by as little as 10 or 15 mV—for example, when there is an elevated extracellular concentration of potassium ions, or after prolonged anoxia or metabolic block. Hodgkin and Huxley treated activation and inactivation as entirely independent of each other. Both depend on membrane potential; either can prevent a channel from being open; but one does not know what the other is doing.[17]

Due to the opposing gating processes activation and inactivation of sodium channels, there have to be two kinds of gating particles for the sodium current. Hodgkin and Huxley called them m and h. Three m particles control activation and one h particle, inactivation. Therefore, the probability that they are all in the permissive position is m^3h, and I_{Na} is represented by

$$I_{\mathrm{Na}} = g_{\mathrm{Na}} m^3 h (V - V_{\mathrm{Na}}). \tag{3.7}$$

In this way the sodium conductance g_{Na} will reach the maximum value only when $m = 1$

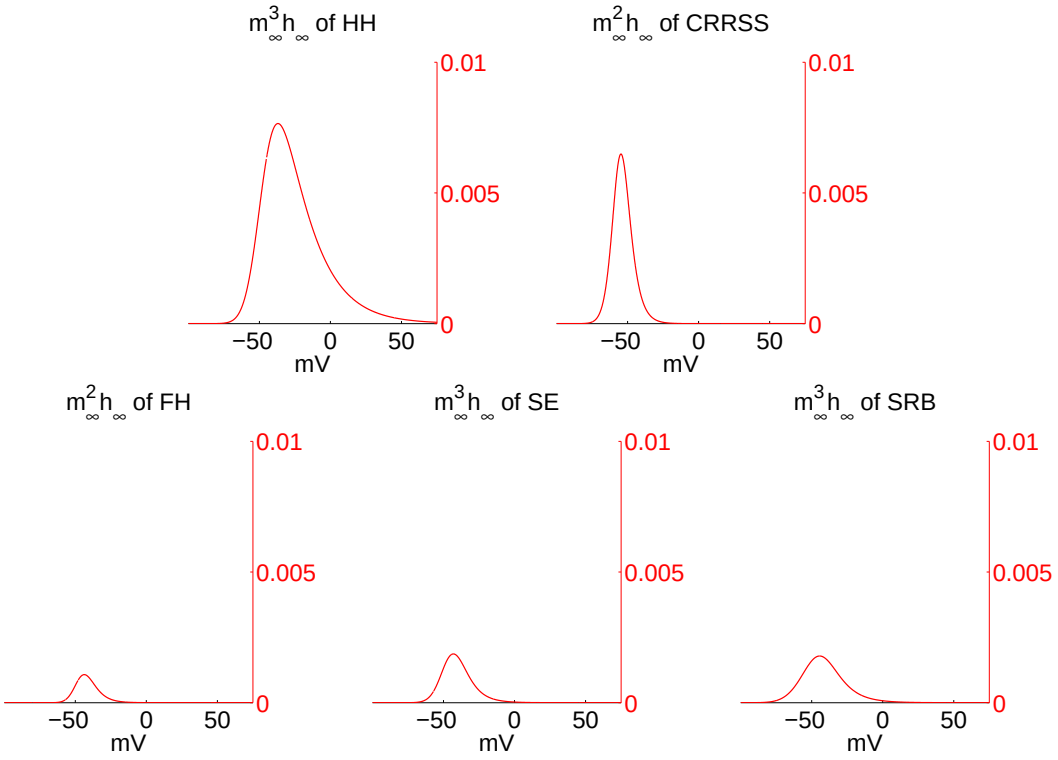

Figure 3.3: Steady state values of the gating variables for the sodium channel according different membrane models as a function of the membrane voltage $V = V_i - V_e$ at 37 °C.

and $h = 1$ at the same time, i.e. all the sodium gates of the membrane are open. Note that both, the variable for activation as well as for inactivation, stand for the probability that the Na^+ channel is open. The inactivation gate is assumed to be at one end of the channel and in the resting state it has a high probability h to be open. Nevertheless, there is no good conductance for the sodium ions, as long as, the three activation gates m in the same channel have a low probability to be open. Red solid lines in figures 3.1 and 3.2 indicate the probability m (activation of sodium channel), n (gating variable for potassium channel), and h (inactivation of sodium channel). [17],[34]

For the interpretation of the whole sodium channel, it is more significant to look at the steady state values of m^3h (HH model), m^2h (CRRSS model), m^2h (FH model), m^3h (SE model), and m^3h (SRB model) which are plotted in figure 3.3. One can see, that at very negative potentials the permeability of a sodium channel to open is very small meaning that sodium channels would tend to close. Due to inactivation this can also be observed at higher potentials.

Chapter 4

Conduction velocity and fibre diameter

Propagation velocity is proportional to fibre diameter, that is a common assumption among scientists, which is the consequence of many studies.

In 1937, Joseph Erlanger and Herbert Spencer Gasser found out that different peaks in the compound action potential[1]—the summed activity of hundreds of axons—of the frog peroneal nerve represent the activity of fibre groups of different conduction velocities. Measurements of the histological sections of nerves facilitate the creation of a histogram of the nerve fibres. As quoted in "Nerve and Muscle Excitation", in 1943, Gasser found out that such a histogram for a human sensory nerve shows two peaks, one at about 3 µm and the other at about 12 µm. The observed compound action potential, which was measured 4 cm distant from the stimulated region, had two well-defined elevations, one large at about 0.7 ms and another at 2.4 ms after the stimulus. In several studies, Erlanger and Gasser showed that the first or α peak was due to the large-diameter fibre group. Their first, and most necessary assumption was that the conduction velocity of each fibre was proportional to its outside diameter. By delaying the contribution of each size of the fibre by the appropriate conduction time and summing, they could obtain a fair representation of the compound action potential. Assuming that individual spike amplitudes were proportional to fibre diameters, they were able to obtain much better fits to the compound action potential. As quoted in "Nerve and Muscle Excitation", J.B. Hush in 1939 found out that their assumptions also held for cat neurons. [25]

Following Douglas Junge [25], the cable theory that was first worked out for transatlantic telegraph cables by Lord Kelvin in 1855, is the simplest theory that explains the behaviour

[1] Unlike the action potential of an individual axon which is all-or-none, the compound action potential is graded and varies in size with the stimulus amplitude. This is because increasing the stimulus brings more and more axons into play, each of which contributes to the total record.

of axons and muscle fibres. The axon is considered as a conductive cylinder surrounded by a dielectric layer which is all immersed in a highly conductive medium. The electric equivalent model is similar to the one at the top of figure 8.1, without the segmentation of the fibre into sections of the length Δx and with constant (inner-)axonal and membrane conductances. The axonal resistance R_a (which is the reciprocal of the axonal conductance G_a) varies inversely with the square of the fibre diameter. A three times thicker axon implicates a ninth of axonal resistance. The axonal resistance of 1 cm of the axon is given by

$$R_{a,1\,\mathrm{cm}} = \rho_a \cdot \frac{4}{d^2 \cdot \pi}, \tag{4.1}$$

where ρ_a is the resistivity (or specific resistance) of the axon, d the diameter of the axon. When R_a is lower, more current flows from the active to the inactive region, and the inactive region is excited more rapidly. This effect causes an increase in conduction velocity with increasing diameter (lower R_a). The membrane resistance R_m, which is the reciprocal of the membrane conductance G_m, varies inversely with the first power of the diameter. The membrane resistance of 1 cm of the axon is given by

$$R_{m,1\,\mathrm{cm}} = r_m \cdot \frac{1}{d \cdot \pi}. \tag{4.2}$$

r_m symbolizes the resistance of the membrane, the quantity is defined with respect to $1\,\mathrm{cm}^2$ of membrane and its unit is $\Omega\mathrm{cm}^2$, d is the diameter of the axon. However, R_m has an opposite effect from that of R_a. As more current flows across the membrane, a smaller membrane resistance produces a lesser depolarization of the inactive region and excites it less rapidly. Since the effect of diameter is stronger on R_a, the conduction velocity varies approximately with the first power of fibre diameter.

The influence of fibre diameter can be derived from equation (8.5) too. For this purpose, it is assumed that the solution of equation (8.5) is computed for an unmyelinated nerve fibre ($l = \Delta x$) of diameter d at the supporting points $x_n = n \cdot \Delta x$. Comparing a propagating action potential which is far away from the point of generation, and therefore which is not influenced by the stimulus signal with one of another nerve fibre with a diameter of $d_1 = k \cdot d$, one gets exactly the same coefficients in equation (8.5) if a new choice for $\Delta x_1 = \sqrt{k} \cdot \Delta x$ is made. Therefore, one gets the same results at the points of support at the same times as in the first case, but now at distances $\sqrt{k} \cdot \Delta x$. This means that velocity of propagation is proportional to the square root of diameter in unmyelinated nerve fibres, the rule of thumb is 'velocity in $^{\mathrm{m}}/_{\mathrm{s}}$ is 1.1 times $\sqrt{d}$ in µm'.

In the case of myelinated nerve fibres—when assuming that the nodal distance Δx is proportional to d and that the gap width l of the node of Ranvier is independent of d—a changed diameter $d_1 = k \cdot d$ would demand for $\Delta x_1 = k \cdot \Delta x$ to get the same values at the supporting

points. This is in agreement with the empirical rule 'velocity in ms is 4.5 times d in µm' for human applications. Another rule of thumb says that for fibres thicker than 11 µm, $v = 6 \cdot d$. Furthermore, it is seen with these assumptions that the duration and even the shape of the action potential is independent of the diameter for both the myelinated and the unmyelinated fibre.

Comparing the equations for the propagation velocities of the myelinated and the unmyelinated nerve fibre, one can see that in very small fibres ($d < 0.25\,\mu m$) action potentials propagate quicker within unmyelinated axons than within myelinated ones. With other assumptions the diameter at which unmyelinated axons are quicker is even larger. [34]

Chapter 5

Biological Background

5.1 Cells and Nervous System

A typical neuron has four morphologically defined regions: the cell body, dendrites, the axon, and presynaptic terminals (see figure 5.1).
The cell body (soma) is the metabolic center of the cell. It contains the nucleus, which stores the genes of the cell, as well as the endoplasmatic reticulum, an extension of the nucleus where the cell's proteins are synthesized. The cell body usually gives rise to two kinds of processes: several short dendrites and one, long, tubular axon. Dendrites branch out in tree-like fashion and are the main apparatus for receiving incoming signals from other nerve cells. In contrast, the axon extends away from the cell body and is the main conducting unit for carrying signals to other neurons. An axon can convey electrical signals along distances ranging from 0.1 mm to 3 m. These electrical signals, called "action potentials", are rapid, transient, all-or-none nerve impulses, with an amplitude of 100 mV and a duration of about 1 ms. Action potentials are initiated at a specialized trigger region at the origin of the axon called the "axon hillock" (or "initial segment" of the axon); from there they are conducted down the axon without failure or distortion at rates of 1-100 $^{m}/_{s}$. The amplitude of an action potential traveling down the axon remains constant because the action potential is an all-or-none impulse that is regenerated at regular (in terms of periodical) intervals along the axon. Action potentials constitute the signals by which the brain receives, analyzes, and conveys information. These signals are highly stereotyped throughout the nervous system, even though they are initiated by a great variety of events in the environment that impinge on our bodies—from light to mechanical contact, from odorants to pressure waves. Thus, the signals that convey information about vision are identical to those that carry information about odors. The information conveyed by an action potential is determined not by the form of the signal but by the pathway the signal travels in the brain. The brain analyzes

and interprets patterns of incoming electrical signals and in this way creates our everyday sensations of sight, touch, taste, smell, and sound.
To increase the speed by which action potentials are conducted, large axons are wrapped in a fatty, insulating sheath of myelin. The sheath is interrupted at regular intervals by the nodes of Ranvier. At these uninsulated spots on the axon the action potential becomes regenerated. Near its end, the tubular axon divides into fine branches that form communication sites with other neurons. The point at which two neurons communicate is known as a "synapse". The nerve cell transmitting a signal is called the presynaptic cell, the one receiving the signal the postsynaptic cell. The presynaptic cell transmits signals from the swollen ends of its axon's branches, called "presynaptic terminals". However, a presynaptic cell does not actually touch or communicate anatomically with the postsynaptic cell since the two cells are separated by a space, the synaptic cleft. Most presynaptic terminals end on the postsynaptic neuron's dendrites, but the terminals may also end on the cell body or, less often, at the beginning or end of the axon of the receiving cell.[26]

5.1.1 Ion channels

Physiologists have long known that ions play a central role in the excitability of nerve and muscle. In the late nineteenth century, Sidney Ringer showed that a solution containing a definite proportion of sodium, potassium and calcium ions lets a frog heart continue beating. In the early twentieth century, Julius Bernstein correctly proposed that excitable cells are surrounded by a membrane selectively permeable to potassium ions at rest and that during excitation the membrane permeability to other ions increases. Nowadays, one knows that neuronal signaling depends on rapid changes in the electrical potential across nerve cell membranes. Individual sensory cells can generate changes in membrane potential in response to very small stimuli: receptors in the eye respond to a single photon of light, olfactory neurons detect a single molecule of odorant, and hair cells in the inner ear respond to tiny movements of atomic dimensions. Signaling in the brain depends on the ability of nerve cells to respond to those small stimuli by producing rapid changes in the electrical potential across the nerve cell membranes.[17],[26]

5.1.2 Membrane potential and action potential

Bernstein's "membrane hypothesis" explained the resting membrane potential of nerve and muscle as a diffusion potential set up by the tendency of positively charged ions to diffuse from their high concentration in cytoplasm to their low concentration in the extracellular solution. During excitation the internal negativity would be lost transiently as other ions are

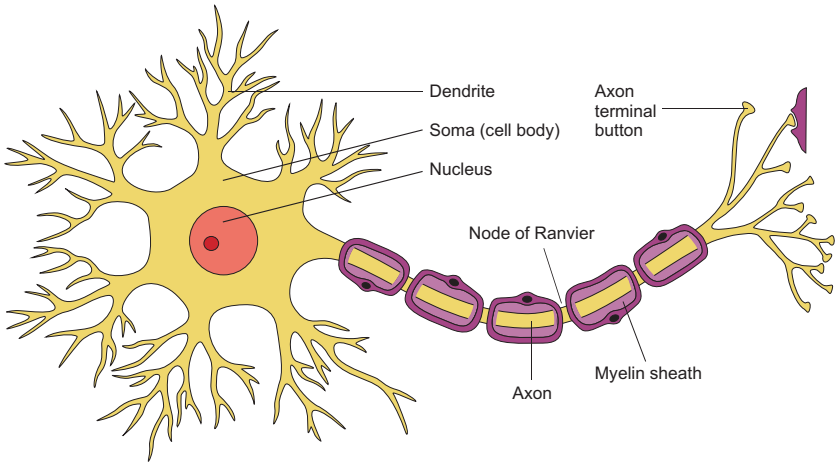

Figure 5.1: Structure of a neuron, adapted from [1]. Most neurons in the vertebrate nervous system have several main features in common. The cell body contains the nucleus, the storehouse of genetic information, and gives raise to two types of cell processes, axons and dendrites. Axons are the transmitting element of neurons, they can vary greatly in length; some can extend more than 3 m within the body. Most axons in the central nervous system are very thin (between 0.2 and 20 µm in diameter) compared with the diameter of the cell body (50 µm or more). Many axons are insulated by a fatty sheath of myelin that is interrupted at regular intervals by the nodes of Ranvier. The action potential, the cell's conducting signal, is initiated either at the axon hillock, the initial segment of the axon, or in some cases slightly farther down the axon at the first node of Ranvier. Branches of the axon of one neuron transmit signals to another neuron at a site called the synapse. The branches of a single axon may form synapses with as many as 1000 other neurons. Whereas the axon is the output element of the neuron, the dendrites are input elements of the neuron. Together with the cell body, they receive synaptic contacts from other neurons.[26]

allowed to diffuse across the membrane, effectively short circuiting the K^+ diffusion potential. [17]

During an action potential the membrane potential changes quickly, up to 500 volts per second. These rapid changes in membrane potential are mediated by ion channels, a class of integral membrane proteins found in all cells of the body. The ion channels of nerve cells are optimally tuned for rapid information processing. The channels of nerve cells are also heterogeneous, so that different types of channels in different parts of the nervous system can carry out specific signaling tasks.

Ion channels have three important properties: (1) They conduct ions, (2) they recognize and select specific ions, and (3) they open and close in response to specific electrical, mechanical, or chemical signals. The channels in nerve and muscle conduct ions across the cell membrane at extremely rapid rates, thereby providing a large flow of ionic current: up to 100 million ions may pass through a single channel per second. This current flow causes the rapid changes in membrane potential required for signaling.

Despite their ability to conduct ions at high rates, ion channels are surprisingly selective: Each type allows only one or a few types of ions to pass. For example, the membrane potential of nerve cells at rest is largely determined by channels that are selectively permeable to K^+. Typically, these channels are 100-fold more permeable to K^+ than to Na^+. During the action potential, however, ion channels 10- to 20-fold more permeable to Na^+ than to K^+ are activated. Thus, a key to the great versatility of neuronal signaling is the activation of different classes of ion channels, each of which is selective for specific ions.

Finally, many channels are regulated or gated; they open and close in response to various stimuli. Voltage-gated channels are regulated by changes in voltage, ligand-gated channels by chemical transmitters, and mechanically gated channels by pressure or stretch. An individual channel is usually most sensitive to one type of signal. In addition to the gated channels, there are nongated channels that are normally open in the cell at rest. These resting channels contribute significantly to the resting potential.[26]

Chapter 6

Electrical properties

6.1 Structure of the cell membrane

Cell membranes consist of bimolecular lipid layers with embedded proteins. Each of the phospholipid molecules has two about 2 nm long hydrocarbon chains which have a very symmetrical structure, which signifies that there is no polar behaviour. This results in the hydrophobic (lipophilic, fatty) property of the hydrocarbon chains. The small heads, on the other hand, are not symmetric. Consequently, they are account for the hydrophilicity of this part of the lipid. As a consequence of its complex structure, it is not a dipole like a water molecule but an even more complicated multipole.
There are several possibilities how emulsified lipids order in water, one is a spherical arrangement where the hydrophobic chains form the center and the hydrophilic heads face the water molecules around. The arrangement within the cell membrane is similar. Two lipids face one another with their hydrophobic chains, their hydrophilic heads face the liquid of the intracellular and the extracellular medium. As a consequence of the molecular structure, the lipid bilayer is mechanically stable, and even when a microelectrode is carefully introduced into the cell, the gap in the membrane is filled and ionic separation is not disturbed.
Because of its structure the cell membrane is fluid and stable, into which so-called domains are embedded. These have proteins embedded which are responsible for specific transport across the membrane, they have the function of "pores". The structure of two membrane pores can differ in a wide range and as a consequence of that, have specific functions. [31],[34]

6.2 Ohm's law is central

All matter is made up of charged particles. They are normally present in equal numbers, so most bodies are electrically neutral. Quantity of charge (symbolized Q) is measured in

coulombs (abbreviated C), where the charge of a proton is $e = 1.6 \cdot 10^{-19}$ C.
Electrical phenomena arise whenever charges of opposite signs are separated or can move independently. Any net flow of charges is called a current. Current is measured in amperes (abbreviated A), where one ampere corresponds to a steady flow of one coulomb per second. By the convention of Benjamin Franklin, positive current flows in the direction of movement of positive charges. Hence if positive and negative electrodes are placed in Ringer's solution, Na^+, K^+, and Ca^{2+} ions will start to move toward the negative pole, Cl^- ions will move toward the positive pole, and an electric current is said to flow through the solution from positive to negative pole.
The size of current will be determined by two factors: the potential difference between the electrodes and the electrical conductance of the solution between them. Potential difference is measured in volts (abbreviated V) and is defined as the work needed to move a unit test charge in a frictionless manner from one point to another. To move a coulomb of charge across a 1-V difference requires a joule of work. In common usage the words "potential", "voltage", and "voltage difference" are used interchangeably to mean potential difference, especially when referring to a membrane. Electrical conductance (symbolized g) is a measure of the ease of flow of current between two points, it is measured in siemens (abbreviated S and formerly called mho which was derived from spelling "ohm" backwards and which expresses the fact that it is the multiplicative inverse of ohm, unit of the electrical resistivity). [17]

To describe the behavior of biological membranes, it is often convenient to employ electrical models, or analogues. These are approximations to the real membrane, but they have well-defined properties. In the study of ionic channels, we see how much can be learned by applying simple laws of physics. Ohm's law ($V = R \cdot I$) plays a central role in membrane biophysics because each ionic channel is modeled as an elementary conductor spanning the insulating lipid membrane. It shows the relation between voltage (symbolized V), resistance (symbolized R) and current (symbolized I). As the reciprocal of resistance is called conductance, Ohm's law can also be written in terms of conductance: [17],[25]

$$I = g \cdot V \tag{6.1}$$

Excitation and electrical signaling in the nervous system involve the movement of ions through ionic channels. The Na^+, K^+, Ca^{2+}, and Cl^- ions seem to be responsible for almost all of the action. Each channel may be regarded as an excitable molecule, as it is specifically responsive to some stimulus: a membrane potential change, a neurotransmitter or other chemical stimulus, a mechanical deformation, and so on. The channel's response, called "gating", is apparently a simple opening or closing of the pore. The open pore has the important property of "selective permeability", allowing some restricted class of small ions to

flow passively down their electrochemical activity gradients at a rate that is very high ($> 10^6$ ions per second) when considered from a molecular point. We consider the high throughput rate as a diagnostic feature distinguishing ionic channel mechanisms from those of other ion transport devices such as the Na^+-K^+ pump (Na^+-K^+-ATPase). An additional major feature is a restriction to downhill fluxes not coupled stoichiometrically to the immediate injection of metabolic energy.
How do gated ionic fluxes through pores make a useful signal for the nervous system? For electrophysiologists the answer is clear. Ionic influxes are electric currents across the membrane and therefore they have an immediate effect on membrane potential. Other voltage-gated channels in the membrane detect the change in membrane potential, and they in turn become excited. In this way the electric response is made regenerative and self-propagating. [17]

6.3 The membrane as a capacitor

The lipid bilayer of biological membranes separates internal and external conducting solutions by an extremely thin insulating layer. One lipid has a length of about 3 nm, so the cell is surrounded by an about 6 nm thick membrane. Such a narrow gap between two conductors forms, of necessity, a significant electrical capacitor.
This separation of charge results in a potential difference between the inside and the outside of the membrane. Capacitance (symbolized C) is a measure of how much charge needs to be transferred from one conductor to another to set up a given potential and is defined by $C = \frac{Q}{V}$. The unit of capacitance is the farad (abbreviated F). A 1 F capacitor will be charged to 1 V when 1 C of charge is on one conductor and -1 C on the other. The rate of change of the potential under a current I_{cap} is obtained by differentiating the last equation with respect to t. With 1 to 2 $\mu F/cm^2$ the capacitance of the membranes is relatively large because of the very thin sheets of the lipid bilayers. [17],[31]

$$I_{cap} = \frac{\mathrm{d}Q}{\mathrm{d}t} = C \cdot \frac{\mathrm{d}V}{\mathrm{d}t} \tag{6.2}$$

6.4 Mathematical model for a patch of cell membrane

The lipid bilayer contains many conducting channels, through which ions can pass. The ionic current is caused by ions that diffuse down their concentration gradient either from the inside to the outside or the other way round. An ionic channel is modeled as an elementary conductor spanning the insulating lipid membrane, the current across the ion channel can be calculated by Ohm's law ($I_{ion} = \frac{V}{R}$) as long as the cell membrane is not excited, i.e. does

not produce an action potential. In contrast to its constant capacitance, the resistance of a cell membrane depends to very large extend on the voltage sensitive gating mechanism of the ionic channels. Only in cases close to the steady state one can approximate membrane resistances by constants.
The resulting model of the currents across the membrane is the sum of a capacitance current and an ionic current. A current I_M that crosses the membrane is therefore split into a capacitance current which involves a change in ion density at the outer and the inner surface of the membrane, and an ionic current which depends on the movement of charged particles through the membrane:

$$I_M = I_{cap} + I_{ion} = C \cdot \frac{\mathrm{d}V}{\mathrm{d}t} + I_{ion} \tag{6.3}$$

I_M is the total current through the membrane, I_{ion} is the ionic current, C is the membrane capacitance, and t is time. Equation (6.3) is the main equation for internal stimulation of the soma or any other compartment where current flow to other processes or neighbored compartments is prevented. In most experiments of Hodgkin, Huxley, and Katz, $\frac{\mathrm{d}V}{\mathrm{d}t}$ equals zero, so that the ionic current can be obtained directly from the experiment records. This is the most obvious reason for using electronic feed-back to keep the membrane potential constant. As an injected current is prevented to flow to other processes or neighbored compartments, it all has to pass the membrane and therefore, $I_{inj} = I_M = \ldots$ This situation can be caused by a space clamp experiment (see chapter 2). Thus, a solution of equation (6.3) when applying an injected current of arbitrary shape is more or less a good approximation of the expected response of the nerve cell under space clamp condition, depending on the model for the ionic currents. [17],[22],[34],[37]

The behavior of a piece of membrane (patch) can be simulated by an electric circuit consisting of a voltage source, capacitance and resistance (see figure 6.1). If we assume an inside potential V_i and an external potential V_e we obtain the voltage $V = V_i - V_e$ across the membrane. The ionic current can be approximated either by an electric circuit consisting of a constant resistivity (left circuit in figure 6.1) or of a nonlinear resistivity that depends on voltage and time (right circuit in figure 6.1). One proceeds on the first assumption if the axon is not excited but stimulated by a subthreshold current; in this case the ionic current I_{ion} equals—according to Ohm's law—$\frac{V}{R}$ or in terms of conductance: $I_{ion} = g \cdot V$. If the stimulating current is high enough to reach or exceed threshold, the resistance cannot be approximated to be constant. In this case, the ionic current has to be calculated by one of the mathematical models, which some of them are presented in chapter 7. [17],[34]

The solution of the differential equation (6.3) when considering constant resistance (i.e. when the system is only slightly disturbed by an injected current I_{inj}) is

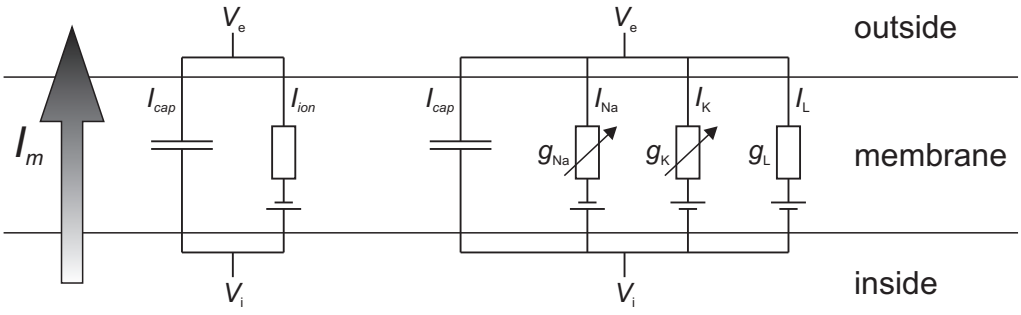

Figure 6.1: Electrical models for a patch of membrane. Left: The model with constant conductance (resistance) can be appropriate for subthreshold analysis. Voltage of resting state is represented as a voltage source. Right: The model includes active gating mechanism and has voltage depending conductances, which is indicated by the arrows across the conductances (resistances). The additional voltage, resulting from the differences in the ionic concentrations on both sides of the membrane, is simulated by batteries. Adapted from [34]

$$V(t) = RI_{inj} \cdot \left(1 - e^{-\frac{t}{RC}}\right) \tag{6.4}$$

The voltage exponentially follows the value which is defined by the pure ohmic resistance. The time constant of the membrane $\tau = R \cdot C$ defines how quickly the transient behavior returns to the steady state. After the pulse the voltage drops down to zero with the same exponential behavior. By splitting the total current across the membrane, one can calculate the ohmic part with $I_R = I_{inj} \cdot \left(1 - e^{-\frac{t}{RC}}\right)$ (within the pulse interval), and the capacitive part with $I_C = I_{inj} \cdot e^{-\frac{t}{RC}}$. [34]

6.5 Membrane resting potential and action potential

As regards the conveyance of information inside the body, the cell membrane is of special interest. If a cell is in resting state and not excited by any stimulus, one can measure a potential difference between the inside and the outside of each cell, whether it is a blood cell, a muscle cell or any other type of cell. The so-called resting potential is of the order of $-70\,\mathrm{mV}$ which means that the inside is negative to the outside, as every membrane potential (or voltage) is measured 'inside minus outside'.

There are two prerequisites to obtain a voltage difference V at the cell. First, there has to be a different ion concentration at the inside and the outside of a cell. Second, there has to be a different permeability for the ions to cross the membrane through appropriate ion channels. Table 6.1 displays ionic concentrations of different ions at the inside of the cell and the extracellular fluid.

All systems are moving towards an equilibrium, a state where the tendency for further change vanishes. A first approach in finding this state was made by Walther Nernst, who described the voltage across the membrane when only one type of ions is involved. His basic idea was that the electric work that is needed to bring n moles of ions ($1\,\text{mol} = 6.0225 \cdot 10^{23}$) from concentration c_1 to concentration c_2 is equal to the osmotic work that compresses these ions from volume V_1 to volume V_2. According to the laws of gasdynamics, the osmotic energy $\mathrm{d}W$ that is needed to compress the volume $\mathrm{d}V$ is given by the product of the pressure p and the volume $\mathrm{d}V$, i.e. $\mathrm{d}W = p \cdot \mathrm{d}V$. The total work therefore is

$$W_{osmotic} = -\int_{V_1}^{V_2} p\,\mathrm{d}V \tag{6.5}$$

By applying the ideal gas law $p \cdot V = n \cdot R \cdot T$ with the gas constant $R = 8.31441\,\text{J/mol·K}$, one gets

$$W_{osmotic} = -\int_{V_1}^{V_2} \frac{nRT}{V}\,\mathrm{d}V = -nRT \cdot \ln\frac{V_2}{V_1} \tag{6.6}$$

Introducing the concentrations $c_1 = \frac{n}{V_1}$ and $c_2 = \frac{n}{V_2}$, one finally gets

$$W_{osmotic} = nRT \cdot \ln\frac{c_2}{c_1} \tag{6.7}$$

The electric work on the other hand that moves a charge Q against the voltage V is given by

$$W_{eletric} = Q \cdot V \tag{6.8}$$

With $Q = n \cdot z \cdot F$, where z is the valence (e.g. for K^+ ions $z = 1$) and F is the Faraday constant $F = 9.64845 \cdot 10^4\,\text{C/mol}$, equation (6.8) reads as

$$W_{eletric} = n \cdot z \cdot F \cdot V. \tag{6.9}$$

Setting $W_{electric} = W_{osmotic}$ results in the "Nernst equation" for the voltage across the membrane V_m:

$$V_m = \frac{R \cdot T}{z \cdot F} \ln\frac{c_2}{c_1} \tag{6.10}$$

Table 6.1: Different ionic concentrations at the inside and the outside of a squid axon [31], a mammalian muscle [31], a frog muscle [27], and a motoneuron [31] in mMol/l

	Squid axon		Mammalian muscle		Frog muscle		Motoneuron	
Ion	outside	inside	outside	inside	outside	inside	outside	inside
Na^+	460	50	120	9	120	9.2	150	15
K^+	10	400	2.5	140	2.5	140	5.5	150
Cl^-	540	50	120	4	120	3-4	125	9
Ca^{2+}			1	10^{-3}				

The Nernst potential is determined using the concentration of the ion inside and outside the cell. Suggesting that only K^+ ions are involved, the membrane potential can be calculated:

$$V_m = \frac{R \cdot T}{F} \ln \frac{[K^+]_e}{[K^+]_i} \tag{6.11}$$

The Nernst potential for the potassium ions is often called 'potassium potential' V_K, just as the sodium potential V_{Na} and the leakage potential V_L. [17],[34]

The Nernst potential is an essential part in most mathematical descriptions of ionic currents, as can be seen in the formulas of chapter 7, and also appears in the equivalent circuits (e.g. see figure 6.1). If the membrane were only modeled as a capacitor and a conductor in parallel, one immediately would recognize a deviation: Ionic current in the pores would go to zero at 0 mV and not at their equilibrium potentials. As a consequence, one would suggest that a concentration gradient which is the reason for the equilibrium potential is like a battery with an electromotive force in series with the resistor. The modified current-voltage law of Ohm becomes, e.g. for the potassium current, $I_K = g_K(V - V_K)$. The electromotive force is V_K and the net driving force on K^+ ions is now $V - V_K$ and not V. In the equivalent currents, the resting potential according to the ionic current one is dealing with is represented as a battery. [17]

However, the Nernst equation gives only an incomplete description of the voltage difference across the cell membrane. The consideration that the membrane were only permeable to potassium ions would result in a static equilibrium, which means that after achieving this state, there would not be any ion transfer. Actually, there is a so-called steady state where different ions cross the membrane without having any effect on the membrane potential.
To get a better, completer, description of the resting potential, one has to take into account that the cell membrane is slightly permeable for other ions too. Regarding that the membrane is permeable to sodium ions as well, they diffuse because of their concentration gradient from the extracellular medium into the cell, potassium ions from the inside out of the cell. The resulting little bit smaller absolute value of the membrane potential can better be described by the Goldman equation, which regards the sodium and the chloride ions as well. Within his 'constant field theory', Goldman assumed that ions that cross the membrane move under the influence of electric fields and concentration gradients, just as they would do in free solutions. Another assumption was that ionic concentration at the edges of the membrane are proportional to those in the aqueous solutions in contact there. A third was that the electrical potential gradient is constant within the membrane. The Goldman equation is written in equation (6.12). [31],[34]

$$V_m = \frac{R \cdot T}{F} \cdot \frac{P_K \cdot [K^+]_e + P_{Na} \cdot [Na^+]_e + P_{Cl} \cdot [Cl^-]_i}{P_K \cdot [K^+]_i + P_{Na} \cdot [Na^+]_i + P_{Cl} \cdot [Cl^-]_e} \tag{6.12}$$

$[K^+]$ is the potassium concentration, the suffixes e and i stand for external and internal, respectively. P_K, is the permeability of the potassium channel, measured in $^{cm}/_{s}$. It is defined as $\frac{u\beta RT}{\alpha F}$ where u is the mobility of the ion in the membrane, β is the partition coefficient between the membrane and the aqueous solution, and α is the thickness of the membrane. Note that sodium and potassium ions are cations, but chloride ions are anions, therefore $[Cl^-]_i$ appears in the numerator of the Goldman equation. [34]

Within the assumption that the membrane at rest is not only permeable to potassium ions, one gets a completer description as it takes the steady state into account. A simultaneous change of K^+ and Na^+ implies a steady voltage but no static state according to the ionic system. The ionic currents at rest are very small, but without the Na^+-K^+-ATPase the concentration gradient would decrease and so would the membrane voltage. The Na-K-ATPase guarantees the maintenance of the concentration gradient as it replaces a K^+ ion of the extracellular medium with a Na^+ ion of the inside of the cell. This process requires energy in form of ATP.

The Goldman equation allows a good quantitative description of the membrane potential; for qualitative analysis it is more suitable to work on equivalent circuits. [31]

The considerations for the resting potential made above are valid for each type of cell. However, neurons (nerve cells) and muscle cells have electrically excitable membranes, which is noticeable by the occurrence of action potentials.

Investigations show that whenever a nerve (or muscle) cell is stimulated by a negative current pulse, the membrane reacts with an exponential hyperpolarization which decreases with increasing distance from the stimulating electrode. An analogue effect can be observed when the cell is stimulated by a small positive current pulse, which implicates an exponential depolarization.

A phenomenon arises when the depolarizing pulse increases the membrane voltage up to a certain point—the so-called threshold—which differs from cell to cell. Once the threshold is reached or exceeded, the nerve cell reacts with an action potential which does not decrease with increasing distance from the stimulating electrode. When an axon of a neuron is sufficiently disturbed, there first is a steep depolarization phase which is followed by an overshoot. The membrane potential climbs from about -50 to $-70\,\mathrm{mV}$ up to about $+40\,\mathrm{mV}$ where it has its maximum value. The following steep decrease of the membrane potential is called the repolarization phase which is followed by the hyperpolarization phase where the membrane potential is lower than the resting potential. [31]

When the membrane potential is suddenly depolarized, the initial pulse of current through the capacitance of the membrane is followed by large currents carried by ions. According to the results of Hodgkin and Huxley, depolarization leads to a rapid increase in permeability of

sodium ions. The influx of sodium ions, which move under the influence of concentration and potential difference, cause the rising phase of the action potential. Throughout the change in voltage, the potassium channels open and allow the highly concentrated inside potassium ions to flow outside.

The current carried by sodium ions rises rapidly to a peak and then decays to a low value; that carried by potassium ions rises much more slowly along an S-shaped curve, reaching a plateau which is maintained with little change until the membrane potential is restored to its resting value. For more details on the sodium and potassium currents, have a look at chapter 3. [19],[34]

Chapter 7

Models for the ionic channels

7.1 Model of Hodgkin and Huxley (HH)

The general aim of the series of papers of Hodgkin, Huxley and Katz ([18],[19],[20],[21],[22]) was to determine the laws which govern movements of ions during electrical activity at the giant axon from the squid. Within their voltage clamp experiments with the giant axon (see section 2.1) the authors found out that the membrane current consisted of a capacitance current and an ionic current (see e.g. equation (6.3)). The ionic current could be resolved into a transient component associated with movement of sodium ions, and a prolonged phase of potassium current. Both currents varied with the permeability of the membrane to sodium or potassium and with the electrical and osmotic driving force. They could be distinguished by studying the effect of changing the concentration of sodium in the external medium. [22]

Unlike today's convention that the voltage difference across the membrane is measured $V = V_i - V_e$, Hodgkin and Huxley measured $V^* = V_e - V_i$. They regarded the resting potential as a positive quantity and the action potential as a negative variation. Neurophysiologists call an outward membrane current (positive charges that flow out of the cell) positive and an inward current negative. This "inward negative" convention is also not in accordance with the one of Hodgkin and Huxley, who named inward current positive (inward positive). For this thesis, the equations of the original HH papers were adapted to fit to modern convention. [22],[29]

The HH equations are a very powerful tool for analyzing the membrane properties because they predict the membrane behaviour for arbitrary shapes of stimulating signals. Although many other equations are in use, even today no other membrane model finds as many applications as the HH model. [34]

The quantities of equation (6.3) depend on the diameter and the length of the fibre. In order to be independent of geometrical parameters, equation (6.3) can be formulated for

$1\,\mathrm{cm}^2$ of the membrane by dividing the current and capacitance through the membrane area involved. All currents become current densities and c the capacitance per cm^2.

$$\frac{\mathrm{d}V}{\mathrm{d}t} = \big(-(i_{\mathrm{Na}} + i_{\mathrm{K}} + i_{\mathrm{L}}) + i_{stim}\big)\frac{1}{c} \tag{7.1}$$

V is the 'reduced membrane voltage' $V = V_i - V_e - V_{rest}$ which implies that $V = 0$ in the resting state. c is the membrane capacitance per unit area, i_{ion} the current density according to a specific ion, i_{stim} the density of the injected current I_{inj}. [22],[34]

In their paper "The components of membrane conductance in the giant axon of Loligo" the authors showed that the ionic permeability of the membrane can be satisfactorily expressed in terms of ionic conductances. The individual ionic currents are obtained from these by the relations

$$i_{\mathrm{Na}} = g_{\mathrm{Na}} m^3 h (V - V_{\mathrm{Na}}) \qquad i_{\mathrm{K}} = g_{\mathrm{K}} n^4 (V - V_{\mathrm{K}}) \qquad i_{\mathrm{L}} = g_{\mathrm{L}} (V - V_{\mathrm{L}}) \tag{7.2}$$

g_{Na}, g_{K} and g_{L} are the maximum sodium, potassium and leakage conductances, m, n and h are dimensionless variables, called gating variables, that vary from 0 to 1 as a function of voltage and time, V_{Na} and V_{K} are the equilibrium potentials (Nernst potentials) for the sodium and potassium ions, and V_{L} is the potential at which the 'leakage current' due to chloride and other ions is zero.

$$\frac{\mathrm{d}m}{\mathrm{d}t} = \big(-(\alpha_m + \beta_m)m + \alpha_m\big)k \tag{7.3}$$

$$\frac{\mathrm{d}h}{\mathrm{d}t} = \big(-(\alpha_h + \beta_h)h + \alpha_h\big)k \tag{7.4}$$

$$\frac{\mathrm{d}n}{\mathrm{d}t} = \big(-(\alpha_n + \beta_n)n + \alpha_n\big)k \tag{7.5}$$

k is the temperature coefficient that accelerates the dynamic of the gating variables at temperatures higher than 6.3℃. α's and β's are rate constants that vary with voltage but not with time and have dimensions of $1/\mathrm{ms}$. They are given by the following equations. [21]

$$\alpha_m = \frac{2.5 - 0.1V}{e^{2.5-0.1V} - 1} \qquad \beta_m = 4 \cdot e^{-\frac{V}{18}} \tag{7.6}$$

$$\alpha_n = \frac{0.1 - 0.01V}{e^{1-0.1V} - 1} \qquad \beta_n = 0.125 \cdot e^{-\frac{V}{80}} \tag{7.7}$$

$$\alpha_h = 0.07 \cdot e^{-\frac{V}{20}} \qquad \beta_h = \frac{1}{e^{3-0.1V} + 1} \tag{7.8}$$

Hodgkin, Huxley and Katz found out that the rate at which the ionic current changed with time was increased about threefold for a rise of 10℃. Thus, the temperature coefficient is determined by equation (7.9). [22]

$$k = 3^{0.1T - 0.63} \tag{7.9}$$

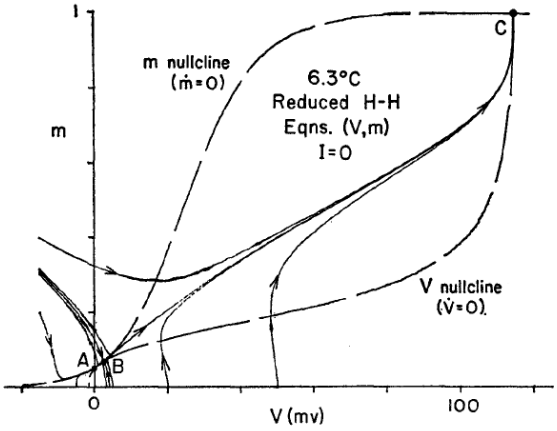

Figure 7.1: Phase plane of V, m reduced HH system, with h and n fixed at their resting values and without any stimulating current. Solutions of equations follow paths marked with arrow-heads. Three singular points occur at intersections of nullclines (curves on which $\dot{V} = 0$ and $\dot{m} = 0$ respectively.) Threshold phenomenon appears at saddle point B. Stimulus displaces phase point from resting singular point A, and is followed by either return to A or passage to singular point C (excitation), depending on the shock strength. Adapted from [8]

$$V_{\mathrm{Na}} = 115 \qquad g_{\mathrm{Na}} = 120 \qquad c = 1 \qquad m(0) = 0.05 \tag{7.10}$$

$$V_{\mathrm{K}} = -12 \qquad g_{\mathrm{K}} = 36 \qquad V_{rest} = -70 \qquad n(0) = 0.32 \tag{7.11}$$

$$V_{\mathrm{L}} = 10.6 \qquad g_{\mathrm{L}} = 0.3 \qquad V(0) = 0 \qquad h(0) = 0.6 \tag{7.12}$$

In contrast to all the other models the HH model has a curiosity: it also allows the generation of an action potential by stimulation with inverse signals, that is with negative currents from the inside. [34]

An approach in analyzing the behavior of the HH model was taken by Richard FitzHugh in 1960. He first approximated the four equations by a reduced system of two equations by arbitrarily setting h and n constant and equal to their resting values. After investigation of the effect on the behavior of this reduced system produced by changing h and n to other constant values, he reintroduced h and n (separately or together) as variables to give the V, m, h and V, m, n reduced systems and finally the complete V, m, h, n system. This synthetic process leads to a better understanding of the complete system than can be obtained by considering all the variables at once, and suggests how modifications in the separate equations will affect the behavior of the complete system.

The reduced system with two differential equations has three singular points (labeled A, B, and C in figure 7.1) which are the intersections of the two nullclines $\dot{V} = 0$ and $\dot{m} = 0$. The two stable points correspond to the resting state (A) and the excited state (C), the third is a

saddle point (B). There are two paths, called the 'stable separatrices' along which solutions approach this saddle point as $t \to \infty$, which can be called 'threshold separatrices'. Together they form a boundary in the phase plane in which a threshold phenomenon occurs. This had already been investigated by FitzHugh in 1955 [7]. An instantaneous positive (anodic) current pulse (brief enough to be considered as instantaneous or proportional to a delta function) at $t = 0$ will displace the phase point of the resting system from A to some point horizontally and to the right from A. This displacement in V will be denoted ΔV. The threshold value ΔV_θ of ΔV is that which brings the state point to rest on the threshold separatrix. If a current pulse displaces the phase point of the resting system from the resting point by $\Delta V \neq \Delta V_\theta$, it will eventually approach either C or A, resulting in an "all" or a "none" response.

Because of the small angles between the nullclines at their two lower intersections (labeled A and B in figure 7.1), the locations of these intersections are very sensitive to slight movements of the V nullcline. If the V nullcline is lowered, A moves to the right and B to the left, so that A and B approach each other. This changes the resting potential (the value of V at A) positively, and, in decreasing the separation of A and B, decreases the magnitude of ΔV_θ. As a critical value of i_{stim} (or h or n) is passed, A and B coalesce and then vanish. C, which is the only remaining singular point, is approached by all solutions, including those starting at the original resting point. One result of this is that a step change i_0 of i_{stim} at $t = 0$ will have a positive threshold value for excitation, or rheobase[1], at which the nullclines are just tangent. Similar results are found when h or n are changed instead of i_{stim}. Changing any one of the parameters i_{stim}, h, or n can modify the effect of another so that, for instance, a decrease of h or an increase of n will increase the magnitude of the rheobase. These changes in excitability in the V, m reduced system are also what one would expect qualitatively from the physical significance of the variables i_{stim}, h, and n in the HH model.

Conversely, when the V nullcline is raised, by changing i_{stim}, h, or n in opposite directions from those considered above, A and B move apart, changing the resting potential negatively and increasing the magnitude of the shock threshold ΔV_θ. Eventually, points B and C approach, coalesce, and vanish, leaving A as the only singular point. The system is now inexcitable, and each parameter (i_{stim}, h, n) has a critical value at which this happens.

This system shows no recovery to the resting state, for which changes in h and n are required. Thus, the action potential (V plotted against t) with h and n at their resting values, shows a rising phase similar to that of a real nerve, followed by a permanent plateau with V about equal to V_{Na}. The time course of the V, m reduced HH system can be seen in the left of

[1]The rheobase is the supremum of the subthreshold current strengths or the minimum of the threshold current strengths. One theoretically needs an infinitely long impulse for $i_{stim} = i_{rheobase}$ to obtain an action potential.[34]

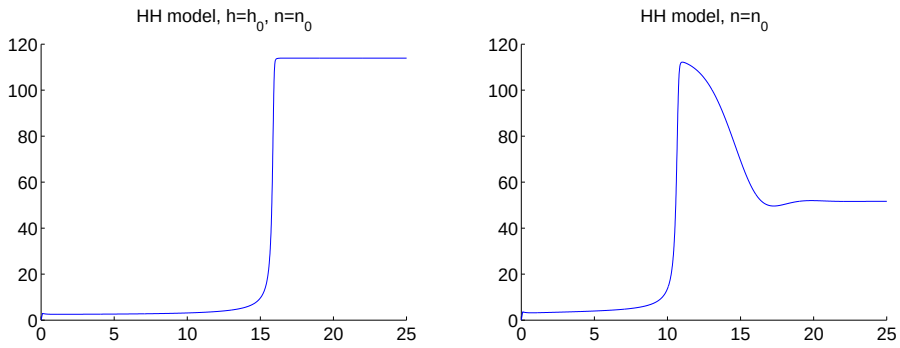

Figure 7.2: Time course of V according to the V, m reduced HH system (left) and of the V, m, h reduced HH system (right) at the original temperature of 6.3 ℃. In the first case, the gating variables h and n are set constant and equal to their resting values, in the second case, n is set constant and equal to its resting value. Minimal stimulus i_{stim} for a pulse width of 0.1 ms is 30 $\mu A/cm^2$ for the V, m reduced HH system and 37 $\mu A/cm^2$ for the V, m, h reduced HH system.

figure 7.2.

Within the V, m, h reduced system where only n is held constant, V, m, and h are coordinates of a three-dimensional phase space in which the solutions of the reduced HH equations appear as paths. The function $h_\infty(V)$ is a monotonically decreasing S-shaped curve (see, e.g. figure 3.1). Therefore, when V goes positive, as during the rising phase on the action potential, h_∞ decreases, and h pursues it. Consider first the case of stimulation by an instantaneous shock producing an initial displacement ΔV. If ΔV is just threshold for the V, m reduced system the phase point lies initially on the threshold separatrix. Initially, $h = h_\infty(0)$ and the (V, m) phase plane is as shown in figure 7.1. As t increases, since $V > 0$, h decreases, the V nullcline in the (V, m) plane moves upward, and saddle point B moves to the right, carrying the threshold separatrix with it away from the moving phase point. At any instant $t > 0$, therefore, the phase point finds itself no longer on the threshold separatrix, but on a subthreshold path, so that it returns toward A. If ΔV is made more positive by increasing the shock strength, the phase point will initially lie beyond the threshold separatrix and may get so far as to cross the V nullcline and start moving to the right and upward toward the excited point C. But the threshold separatrix is also moving to the right, and whether excitation actually takes place will depend on whether the phase point is overtaken by the separatrix and forced to turn back toward A.

In the case of stimulation by a positive step current, the rheobase also is increased when changes in h are allowed. i_{stim} must be greater than for the V, m system in order to allow the phase point to pass between the two nearly tangent nullclines before these have had a

chance to collide and produce a saddle point B with a threshold separatrix, which can then pursue the phase point, head it off, and turn it back toward A. Thus the effect of allowing h to vary is to produce accommodation; i.e., an increase of rheobase or shock threshold. The time course of V of the reduced V, m, h system can be seen in the right of figure 7.2. The minimal stimulating current strength to produce an action potential has raised from $30\,\mu A/cm^2$ at the V, m reduced HH system to $37\,\mu A/cm^2$ at the V, m, h reduced HH system when stimulated for 0.1 ms.

The introduction of h as a variable produces an action potential having a distinct peak, followed by a lower plateau which may be looked on as the result of partial recovery. The rather complex process of interaction between the variables can be described as follows. By the time the phase point has nearly reached C, C has started to move to the left, as a result of the decrease in h. As C continues to move to the left, the phase point follows it closely. As V simultaneously turns and starts to become more negative again, $h_\infty(V)$ reverses its decreasing trend and begins to increase again toward h. The latter therefore begins to decrease even more slowly than before. This slows down the motion of C to the left, and the behaviour of the system from now on will depend very much on whether C finally stops moving before it can meet B, which is approaching it along the m nullcline. If B and C do meet and vanish, the phase point must return to A. It happens that the addition of the third variable h to the V, m system does not change the number of the singular points, but as FitzHugh has shown, the addition of the fourth variable n does so. [8]

In one of his papers, FitzHugh classified mathematical models according to their threshold phenomena. He introduced the discontinuous threshold phenomenon (DTP), the singular-point threshold phenomenon (STP), and the quasi threshold phenomenon (QTP). According to this classification, the V, m, the V, m, h as well as the V, m, n reduced system each have a STP, whereas the complete V, m, n, h system has a QTP. In a QTP, there is no saddle point in the complete system, and any intermediate response between "all" and "none" is obtainable by an accurate enough adjustment of the stimulus intensity. FitzHugh's synthetic process to first investigate the reduced systems and then dealing with the full system is an example of how a QTP in a four-dimensional phase space can be represented by a STP in a moving two-dimensional subspace. As quoted in [8], this is related to Lotka's [2] interpretation of a quasi-equilibrium state which has a slowly changing non-equilibrium variable as a "moving (stable) equilibrium". A QTP could be described from this point of view as one type of "moving unstable equilibrium". [7],[8]

Like all theories, the HH model of the squid giant axon membrane requires testing. Predictions of the results of a variety of experiments have been made, starting from their equations,

[2] A.J. Lotka. Elements of Physical Biology, Baltimore, The Willians & Wilkins Co., 1925

of which some do and some do not agree with experimental results. The HH model is not universally accepted; there are some prediction from the model which are definitely false, and these indicate that even if the model is basically valid, it needs to be modified.
Solving the HH equations by a numerical method with a desk calculator found good agreement with experiment for, e.g., the membrane (space clamped) action potential at two temperatures, the propagated action potential and conduction velocity, net fluxes of sodium and potassium ions per impulse, the absolute refractory period, the value of threshold to short current pulses, as well as for other phenomena.
On the other hand, membrane action potentials computed with a digital computer—solving the equations with a desk calculator was so time-consuming that a digital computer was programmed to do this—at very near threshold show not only the variation of spike height to be expected from experiment, but also an apparently continuous gradation of responses of all intermediate heights between subthreshold active response and a full-sized action potential. This is an apparent violation of the all-or-none law which forbids such intermediate sized responses and which is obeyed by the squid axon experimentally. The discrepancy is, however, only apparent, the result of the greater accuracy of the digital computer than that of a real axon. The latter is affected by spontaneous fluctuations that practically eliminate the possibility of intermediate responses in a normal axon. This is shown by the fact that when the stimulus is set just as threshold, a real axon gives action potentials for only a certain proportion of stimuli, whereas the equations, not containing any statistical variation, always give the same result. The analog computer, with its electrical noise, also shows randomness near threshold, and is thus more lifelike than the digital computer. There has no attempt been made to include statistical variation in the equations in order to represent this phenomenon. This apparent disagreement between the model and the experiment is therefore not serious.[11]

7.1.1 Modifications

This section provides some ideas in which the HH model can be modified or improved, as it has been done several times in history. The following adaptions of the HH model are quoted in the book "Biological engineering" [11], which was written by Richard FitzHugh and Herman P. Schwan in 1969. The first modification concerns the situation when tetraethylammonium chloride (TEA) is injected into the axon. The obtained plateau action potential with bistable behavior can be closely imitated if the equations are modified by increasing the relaxation time of variable n by a factor of 100 or so.[3]

Computations by Huxley on the effect of changes of calcium concentration on the squid

[3]Richard FitzHugh, J. Gen. Physio., 43:867, 1960; E.P. George, Nature, 186:889, 1960; E.P. George and E.A. Johnson, Australian J. Exptl. Biol. Med. Sci., 39:275, 1961

axon were made by changing $m_\infty(V)$ to $m_\infty(V + \Delta V)$, $\tau_m(V)$ to $\tau_m(V + \Delta V)$, and $h_\infty(V)$, $\tau_h(V)$, $n_\infty(V)$ and $\tau_n(V)$ similarly. Here $\Delta V = K \cdot \ln \frac{[\mathrm{Ca}]}{[\mathrm{Ca}]_n}$, [Ca] is the calcium concentration used, $[\mathrm{Ca}]_n$ is the normal concentration, and $K = -9.32\,\mathrm{mV}$. These changes were based on experimental findings. The effect of these changes is to shift all the steady state and relaxation time functions along the V axis to the right for an increase of [Ca]. [4]

Not each modification was an improvement, as the example of E.B. Wright and T. Tomita shows. They used the HH equations to predict the effect of changing external sodium and potassium concentrations by changing the values of V_{Na} and V_{K}. Instead of recalculating the (new) resting values of V, m, n, and h, the authors used $V = 0$ and reset m, n, and h to arbitrary values for their initial conditions which produced an error in their solutions. [5]

As quoted in [8], Goodall and Martin[6] solved a set of differential equations which, for greater convenience in adjusting parameters, were slightly different from the HH equations. They used an additional chloride current and a sixth instead of a fourth power in their potassium conductance to obtain action potentials like those of muscle, and by altering the potassium time constant, an oscillating plateau.

In this thesis, the maximum sodium, potassium and leakage conductances g_{Na}, g_{K} and g_{L} are heightened by a factor of 12. The reason is that the HH model does not work at temperatures higher than 33 ℃ (see e.g. section 9.1), but which is necessary when applying the HH model to a human being with a temperature of 37 ℃. The CRRSS model was developed for a mammalian myelinated nerve cell, so the sodium conductance of the CRRSS model of $1445\,\mathrm{mS/cm^2}$ was approximated by multiplying the conductance of the HH model by a factor of 12. The new conductances—in order not to change the ratio as well as the initial conditions, the other conductances are multiplied by the same factor too—are: $g_{\mathrm{Na}} = 1440$, $g_{\mathrm{K}} = 432$, and $g_{\mathrm{L}} = 3.6\mathrm{mS/cm^2}$.

Since for other excitable membranes the voltage-clamp techniques are more difficult than for the squid axon, it is natural to take the HH model as a starting point and modify it to describe new membranes, instead of starting all over again from the beginning to develop a new model. It is a useful procedure as long as its dangers are recognized; it might turn out that a different cell operated on different principles than the squid axon does. [11]

As quoted in [11], the voltage-clamp technique has been applied to the single node of Ranvier of the myelinated nerve fibres of the frog and the toad, and modifications of the HH model have been found which duplicates these results. They differ from the HH equations in the functions used for the steady state values and relaxation times, in some of the constants,

[4] A.F. Huxley, Ann. N.Y. Acad. Sci, 81:221, 1959

[5] J. Cellular Comp. Physiol., 65:211, 1965

[6] Goodall, M.C. and Martin, T.E, Analogue computer solutions of Hodgkin-Huxley, Program and Abstracts of the Biophysical Society, Cambridge, Massachusetts, 1958

and in the fact the sodium and potassium currents are nonlinear in V.

7.2 Model of Chiu, Ritchie, Rogart, Stagg, and Sweeney (CRRSS)

In 1979, Chiu, Ritchie, Rogart, and Stagg made some voltage-clamp studies in order to model single rabbit myelinated nerve fibres. These studies were carried out at a temperature of 14 ℃ with the method of Dodge & Frankenhaeuser[7]. Mammalian membrane fibres had already been investigated by Horáckova et al.[8] and by Nonner & Stämpfli[9] earlier. Although no detailed analysis had been made, they had found out that the potassium currents seem to be entirely lacking. The analysis of Chiu et al. shows that except the absence of the potassium currents the currents in the rabbit node are well described by the Hodgkin-Huxley formulation. Unfortunately, the authors did not publish all the data which are necessary for simulation although the complete model was used in the paper to demonstrate good agreement with the experiment. The missing values can be found by fitting data of the measurements presented in their figures. By recalculation, one can find similar values to those obtained by Sweeney and his colleagues[43], who transformed the original data to find a model for warm-blooded axons. The CRRSS model, named after Chiu, Ritchie, Rogert, Stagg and Sweeney describes the sodium and leakage currents in mammalian myelinated fibres at 37 ℃. [5],[36]

As a consequence of the absence of the potassium currents, the ionic currents are split into two components, a sodium and a leakage current. The main equation (7.13) as well as the equations for the gating variables (7.14) and (7.15) are similar to the HH equations.

$$\frac{\mathrm{d}V}{\mathrm{d}t} = \big(-(i_{\mathrm{Na}} + i_{\mathrm{L}}) + i_{stim} \big) \frac{1}{c} \tag{7.13}$$

$$\frac{\mathrm{d}m}{\mathrm{d}t} = \big(-(\alpha_m + \beta_m)m + \alpha_m \big) k \tag{7.14}$$

$$\frac{\mathrm{d}h}{\mathrm{d}t} = \big(-(\alpha_h + \beta_h)h + \alpha_h \big) k \tag{7.15}$$

[7]Dodge F.A & Frankenhaeuser B., 1958. Membrane currents in isolated frog nerve fibre under voltage clamp conditions. Journal of Physiology 143, 76-90.

[8]Horáckova M., Nonner W. & Stämpfli R., 1968. Action potentials and voltage clamp currents of single rat Ranvier nodes. Proc. int. Union Physiol. Sci. 7, 198

[9]Nonner W. & Stämpfli R., 1969. A new coltage clamp mathod. In "Laboratory Techniques in Membrane Biophysics", ed. Passow H. & Stämpfli R., Berlin: Springer-Verlag

The sodium currents in rabbit nodes were fitted by the HH model using m^2h kinetics.

$$i_{\mathrm{Na}} = g_{\mathrm{Na}} m^2 h (V - V_{\mathrm{Na}}) \qquad i_{\mathrm{L}} = g_{\mathrm{L}} (V - V_{\mathrm{L}}) \tag{7.16}$$

$$\alpha_m = \frac{97 + 0.363V}{1 + e^{\left(\frac{31-V}{5.3}\right)}} \qquad \beta_m = \frac{\alpha_m}{e^{\left(\frac{V-23.8}{4.17}\right)}} \tag{7.17}$$

$$\alpha_h = \frac{\beta_h}{e^{\left(\frac{V-5.5}{5}\right)}} \qquad \beta_h = \frac{15.6}{1 + e^{\left(\frac{24-V}{10}\right)}} \tag{7.18}$$

The transient inward sodium current is responsible for the fast initial depolarization phase of the action potential, while the repolarizing phase is accounted for by leak alone. The computed shape of the action potential was in good agreement with the experimentally obtained action potential. [5]

The Q_{10} is equal to the one of the HH model; as the standard temperature of the CRRSS model is 37 ℃, the temperature coefficient k can be calculated by

$$k = 3^{0.1T - 3.7} \tag{7.19}$$

T is the temperature in ℃. The constants and the initial values or rather the resting values are [43]

$$V_{\mathrm{Na}} = 115 \qquad g_{\mathrm{Na}} = 1445 \qquad m(0) = 0.003 \tag{7.20}$$

$$V_{\mathrm{L}} = -0.01 \qquad g_{\mathrm{L}} = 128 \qquad h(0) = 0.75 \tag{7.21}$$

$$V_{rest} = -80 \qquad c = 2.5 \qquad V(0) = 0 \tag{7.22}$$

Even though the CRRSS model neglects the potassium currents, voltage sensitive potassium channels do exist in such fibres. The experiments of Röper and Schwarz showed that in rat myelinated nerve at least two potassium conductance can be distinguished, suggesting the existence of two different types of K^+ channels: those with fast and those with slow gating kinetics, in the ratio 4:1. Although they have no significant influence in the intact membrane, it is notable that these fast and slow voltage-sensitive potassium channels exist in the nodal, the paranodal (the area between node and internode), and in the internodal regions. The density of the slow potassium channels is maximal in the nodal membrane and decreases to $\frac{1}{31}$ in the internode. By contrast, the distribution of the fast potassium channels differs, their density being maximal in the paranode and descreasing to one sixth in the node and paranode. However, no sodium channels seem to be present in the myelinated parts of the membrane. See also Sherratt et al.[10], Kokis & Waxman[11]. [34],[40]

[10] Sherratt R.M., Bostock H. and Sears T.A., 1980. Effects of 4-aminopyridine on normal and demyelinated nerve fibres. Nature 283, 570-572

[11] Kokis J.D and Waxman S.G., 1987. Ionic channel organization of normal and regenerating mammalian axons. In "Progress in Brain Research" Ed. Seil F.J., Herbert E. and Carlson. Amsterdam Elsevier 71, 89-101

7.3 Model of Frankenhaeuser and Huxley (FH)

In 1964, Frankenhaeuser and Huxley published their investigation on the action potential in the myelinated nerve fibre of the toad. Analogue to the voltage clamp experiments of Hodgkin and Huxley, they analyzed the recorded current after changing the membrane potential step by step.

The membrane current densities are treated as the sum of a capacitive current density and an ionic current density which is split into a leak current density i_{L}, an initial current density and a complex delayed current density. Earlier, it was shown by Dodge and Frankenhaeuser[6] that the initial current is mainly carried by sodium ions, and by Frankenhaeuser[12] that the delayed current in the myelinated nerve fibre is carried essentially by potassium ions. Some of the complex delayed current was separated as a 'non-specific current' i_{P} which is to large extent carried by sodium but possibly also by other ions such as calcium[13]. [6],[15]

$$\frac{\mathrm{d}V}{\mathrm{d}t} = \big(- (i_{\mathrm{Na}} + i_{\mathrm{K}} + i_{\mathrm{P}} + i_{\mathrm{L}}) + i_{stim}\big)\frac{1}{c} \tag{7.23}$$

$$\frac{\mathrm{d}m}{\mathrm{d}t} = \big(- (\alpha_m + \beta_m)m + \alpha_m\big)k \tag{7.24}$$

$$\frac{\mathrm{d}n}{\mathrm{d}t} = \big(- (\alpha_n + \beta_n)n + \alpha_n\big)k \tag{7.25}$$

$$\frac{\mathrm{d}h}{\mathrm{d}t} = \big(- (\alpha_h + \beta_h)h + \alpha_h\big)k \tag{7.26}$$

$$\frac{\mathrm{d}p}{\mathrm{d}t} = \big(- (\alpha_p + \beta_p)p + \alpha_p\big)k \tag{7.27}$$

Notation is identical to the models mentioned above. There is another differential equation for the gating variable p which appears in the equation for the non-specific current density i_{P}. Voltage clamp experiments indicate that the sodium and potassium transport system can be described in terms of potassium permeability when permeability is defined by the 'constant

[12] Frankenhaeuser B. 1962. Delayed currents in myelinated bnerve fibres of Xenopus laevis investigated with voltage clamp technique. Journal of Physiology 160, 40-45. (Wuerd ich weglassen: Frankenhaeuser B. 1962. Instantaneous potassium currents in myelinated nerve fibres of Xenopus leavis. Journal of Physiology 160, 46-53.) Frankenhaeuser B. 1962. Potassium permeability in myelinated nerve fibres of Xenopus laevis. Journal of Physiology 160, 54-61

[13] Frankenhaeuser B. 1963. A quantitative description of potassium currents in myelinated nerve fibres of Xenopus laevis. Journal of Physiology 169, 424-430

field equation'. The specific permeabilities P_{Na}, etc. are measured in $^{\mathrm{cm}}/_{\mathrm{s}}$. [6],[13]

$$i_{\mathrm{Na}} = P_{\mathrm{Na}} m^2 h \frac{EF^2}{RT} \frac{[\mathrm{Na}]_o - [\mathrm{Na}]_i \cdot e^{\frac{EF}{RT}}}{1 - e^{\frac{EF}{RT}}} \qquad \alpha_m = \frac{0.36(V-22)}{1 - e^{\left(\frac{22-V}{3}\right)}} \qquad \beta_m = \frac{0.4(13-V)}{1 - e^{\left(\frac{V-13}{20}\right)}}$$

$$i_{\mathrm{K}} = P_{\mathrm{K}} n^2 \frac{EF^2}{RT} \frac{[\mathrm{K}]_o - [\mathrm{K}]_i \cdot e^{\frac{EF}{RT}}}{1 - e^{\frac{EF}{RT}}} \qquad \alpha_n = \frac{0.02(V-35)}{1 - e^{\left(\frac{35-V}{10}\right)}} \qquad \beta_n = \frac{0.05(10-V)}{1 - e^{\left(\frac{V-10}{10}\right)}}$$

$$i_{\mathrm{P}} = P_{\mathrm{P}} p^2 \frac{EF^2}{RT} \frac{[\mathrm{Na}]_o - [\mathrm{Na}]_i \cdot e^{\frac{EF}{RT}}}{1 - e^{\frac{EF}{RT}}} \qquad \alpha_h = -\frac{0.1(V+10)}{1 - e^{\left(\frac{V+10}{6}\right)}} \qquad \beta_h = \frac{4.5}{1 + e^{\left(\frac{45-V}{10}\right)}}$$

$$i_{\mathrm{L}} = g_{\mathrm{L}}(V - V_{\mathrm{L}}) \qquad \alpha_p = \frac{0.006(V-40)}{1 - e^{\left(\frac{40-V}{10}\right)}} \qquad \beta_p = -\frac{0.09(V+25)}{1 - e^{\left(\frac{V+25}{20}\right)}}$$

P_{Na} is the sodium permeability constant, m, n, h, and p are gating variables, E is the absolute value of the membrane voltage (unlike the reduced membrane voltage V which is zero at rest, E is $-70\,\mathrm{mV}$ at rest), F is the Faraday constant $F = 9.64845 \cdot 10^4\,^{\mathrm{C}}/_{\mathrm{mol}}$, R the gas constant $R = 8.31441\,^{\mathrm{J}}/_{\mathrm{mol \cdot K}}$, T the temperature in ℃, $[\mathrm{Na}]_o$ and $[\mathrm{Na}]_i$ are the ion concentration in $^{\mathrm{mMol}}/_{\mathrm{l}}$ of Na^+ ions outside and inside the membrane, α's and β's are rate constants.

It should be pointed out that the value of β_n depend to some extent on the previous history of the fibre. The equation for β_n used for this thesis was fitted to experimental data which were obtained from measurements after short current steps (about 1 ms). A different equation for β_n is appropriate for longer (5-15 ms) current steps. [14]

Frankenhaeuser and Moore determined temperature coefficients for simulations at temperatures other than 20 ℃. Their Q_{10} agrees rather well with the Q_{10} of 3 which was used by Hodgkin and Huxley for the squid fibre data. The only exception are the coefficients for α_m and β_m. In their investigation, Q_{10} values for P_{Na} and P_{Na} were also determined. [15],[16]

$$Q_{10}(\alpha_m) = 1.8 \qquad Q_{10}(\beta_m) = 1.7 \qquad m(0) = 0.0005 \tag{7.28}$$

$$Q_{10}(\alpha_n) = 3.2 \qquad Q_{10}(\beta_n) = 2.8 \qquad n(0) = 0.0268 \tag{7.29}$$

$$Q_{10}(\alpha_h) = 2.8 \qquad Q_{10}(\beta_h) = 2.9 \qquad h(0) = 0.8249 \tag{7.30}$$

$$Q_{10}(P_{\mathrm{Na}}) = 1.3 \qquad Q_{10}(P_{\mathrm{K}}) = 1.2 \qquad p(0) = 0.0049 \tag{7.31}$$

$$P_{\mathrm{Na}} = 0.008 \qquad E = V + V_{rest} \tag{7.32}$$

$$P_{\mathrm{K}} = 0.0012 \qquad V_{rest} = -70 \tag{7.33}$$

$$P_{\mathrm{P}} = 0.00054 \qquad V(0) = 0 \tag{7.34}$$

$$[\mathrm{Na}]_o = 114.5 \qquad [\mathrm{K}]_o = 2.5 \qquad V_{\mathrm{L}} = 0.026 \qquad c = 2 \tag{7.35}$$

$$[\mathrm{Na}]_i = 13.7 \qquad [\mathrm{K}]_i = 120 \qquad g_{\mathrm{L}} = 30.3 \qquad k = Q_{10}^{0.1T-2.0} \tag{7.36}$$

The leak conductance g_{L} in the FH equations is independent of potential and time. This is in contrast to the fact that g_{L} increases when NaCl or KCl is added to the ordinary Ringer's solution, the nerve cell is embedded in, which indicates that the leak current is carried by both Na^+ and K^+. Further, g_{L} increases somewhat after cathodal steps of long duration, which is an indication that g_{L} is, to some extent, potential and time dependent. This is neglected in the FH analysis. [15]

7.4 Model of Schwarz and Eikhof (SE)

In 1987, Schwarz and Eikhof developed their model which is of the FH type from voltage clamp experiments on rat nodes. Additionally, they showed that the results of their experiments performed in the cat nerve were essentially the same as those in the rat nerve fibres. The original SE model describes nodal currents, not densities. By assuming a nodal area of 50 μm^2, one obtains a model with current densities which is comparable to the other membrane models. This model is of special interest for medical application because most data were measured at 20 ℃ and 37 ℃. [36],[41]

An aim of Schwarz and Eikhof was to record membrane currents and action potentials at 37 ℃ as until then, only a few scattered notes about voltage and current clamp measurements in mammalian nerve fibres at body temperature were performed. [41]

$$\frac{\mathrm{d}V}{\mathrm{d}t} = \big(-(i_{\mathrm{Na}} + i_{\mathrm{K}} + i_{\mathrm{L}}) + i_{stim}\big)\frac{1}{c} \tag{7.37}$$

$$\frac{\mathrm{d}m}{\mathrm{d}t} = -(\alpha_m + \beta_m)m + \alpha_m \tag{7.38}$$

$$\frac{\mathrm{d}n}{\mathrm{d}t} = -(\alpha_n + \beta_n)n + \alpha_n \tag{7.39}$$

$$\frac{\mathrm{d}h}{\mathrm{d}t} = -(\alpha_h + \beta_h)h + \alpha_h \tag{7.40}$$

$$i_{\mathrm{Na}} = P_{\mathrm{Na}} m^3 h \frac{EF^2}{RT} \frac{[\mathrm{Na}]_o - [\mathrm{Na}]_i \cdot e^{\frac{EF}{RT}}}{1 - e^{\frac{EF}{RT}}} \qquad \alpha_m = \frac{1.87(V - 25.41)}{1 - e^{\left(\frac{25.41 - V}{6.06}\right)}} \qquad \beta_m = \frac{3.97(21 - V)}{1 - e^{\left(\frac{V - 21}{9.41}\right)}}$$

$$i_{\mathrm{K}} = P_{\mathrm{K}} n^2 \frac{EF^2}{RT} \frac{[\mathrm{K}]_o - [\mathrm{K}]_i \cdot e^{\frac{EF}{RT}}}{1 - e^{\frac{EF}{RT}}} \qquad \alpha_n = \frac{0.13(V - 35)}{1 - e^{\left(\frac{35 - V}{10}\right)}} \qquad \beta_n = \frac{0.32(10 - V)}{1 - e^{\left(\frac{V - 10}{10}\right)}}$$

$$i_{\mathrm{L}} = g_{\mathrm{L}}(V - V_{\mathrm{L}}) \qquad \alpha_h = -\frac{0.55(V + 27.74)}{1 - e^{\left(\frac{V + 27.74}{9.06}\right)}} \qquad \beta_h = \frac{22.6}{1 + e^{\left(\frac{56 - V}{12.5}\right)}}$$

$$E = V + V_{rest} \tag{7.41}$$

$$g_{\mathrm{L}} = 86 \qquad k = Q_{10}^{0.1T-3.7} \qquad c = 2.8 \tag{7.42}$$

$$V_{rest} = -78 \qquad V_{\mathrm{L}} = 0 \qquad V(0) = 0 \tag{7.43}$$

$$m(0) = 0.0077 \qquad Q_{10}(\alpha_m) = 2.2 \qquad Q_{10}(\beta_m) = 2.2 \tag{7.44}$$

$$n(0) = 0.0267 \qquad Q_{10}(\alpha_n) = 3 \qquad Q_{10}(\beta_n) = 3 \tag{7.45}$$

$$h(0) = 0.76 \qquad Q_{10}(\alpha_h) = 2.9 \qquad Q_{10}(\beta_h) = 2.9 \tag{7.46}$$

$$P_{\mathrm{Na}} = 0.00328 \qquad [\mathrm{Na}]_o = 154 \qquad [\mathrm{K}]_o = 5.9 \tag{7.47}$$

$$P_{\mathrm{K}} = 0.000134 \qquad [\mathrm{Na}]_i = 8.71 \qquad [\mathrm{K}]_i = 155 \tag{7.48}$$

7.5 Model of Schwarz, Reid, and Bostock (SRB)

Schwarz, Reid, and Bostock derived a mathematical model for action potentials of human myelinated nerve fibres. Their nerve material was obtained from patients that were undergoing nerve graft operations. The model is based on the FH equations and closely matches the recorded action potentials. Their study was undertaken to investigate the possible differences between action potentials and ionic currents in human and rat nodes of Ranvier. [42]

$$\frac{\mathrm{d}V}{\mathrm{d}t} = \big(-(i_{\mathrm{Na}} + i_{\mathrm{K},fast} + i_{\mathrm{K},slow} + i_{\mathrm{L}}) + i_{stim} \big) \frac{1}{c} \tag{7.49}$$

$$\frac{\mathrm{d}m}{\mathrm{d}t} = \big(-(\alpha_m + \beta_m)m + \alpha_m \big) k \tag{7.50}$$

$$\frac{\mathrm{d}n}{\mathrm{d}t} = \big(-(\alpha_n + \beta_n)n + \alpha_n \big) k \tag{7.51}$$

$$\frac{\mathrm{d}h}{\mathrm{d}t} = \big(-(\alpha_h + \beta_h)h + \alpha_h \big) k \tag{7.52}$$

$$\frac{\mathrm{d}p}{\mathrm{d}t} = -(\alpha_p + \beta_p)p + \alpha_p \tag{7.53}$$

$$i_{\mathrm{Na}} = P_{\mathrm{Na}} m^3 h \frac{EF^2}{RT} \frac{[\mathrm{Na}]_o - [\mathrm{Na}]_i \cdot e^{\frac{EF}{RT}}}{1 - e^{\frac{EF}{RT}}}$$

$$i_{\mathrm{K},fast} = g_{\mathrm{K},fast} n^4 (V - V_{\mathrm{K}})$$

$$i_{\mathrm{K},slow} = g_{\mathrm{K},slow} p (V - V_{\mathrm{K}})$$

$$i_{\mathrm{L}} = g_{\mathrm{L}} (V - V_{\mathrm{L}})$$

$$\alpha_m = \frac{4.6(V - 65.6)}{1 - e^{\left(\frac{-V+65.6}{10.3}\right)}} \qquad \beta_m = \frac{0.33(61.3 - V)}{1 - e^{\left(\frac{V-61.3}{9.16}\right)}}$$

$$\alpha_n = \frac{0.0517(V + 9.2)}{1 - e^{\left(\frac{-V-9.2}{1.1}\right)}} \qquad \beta_n = \frac{0.092(8 - V)}{1 - e^{\left(\frac{V-8}{10.5}\right)}}$$

$$\alpha_h = -\frac{0.21(V + 27)}{1 - e^{\left(\frac{V+27}{11}\right)}} \qquad \beta_h = \frac{14.1}{1 + e^{\left(\frac{55.2-V}{13.4}\right)}}$$

$$\alpha_p = \frac{0.0079(V - 71.5)}{1 - e^{\left(\frac{71.5-V}{23.6}\right)}} \qquad \beta_p = -\frac{0.00478(V - 3.9)}{1 - e^{\left(\frac{V-3.9}{21.8}\right)}}$$

$$E = V + V_{rest} \qquad V_{\mathrm{K}} = 0 \qquad V_{\mathrm{L}} = 0 \qquad V_{rest} = -84 \tag{7.54}$$

$$P_{\mathrm{Na}} = 0.00704 \qquad g_{\mathrm{K},fast} = 30 \qquad g_{\mathrm{K},slow} = 60 \qquad g_{\mathrm{L}} = 60 \tag{7.55}$$

$$c = 2.8 \qquad V(0) = 0 \qquad [\mathrm{Na}]_o = 154 \qquad [\mathrm{Na}]_i = 30 \tag{7.56}$$

$$m(0) = 0.0382 \qquad n(0) = 0.2563 \qquad h(0) = 0.6986 \qquad p(0) = 0.0049 \tag{7.57}$$

$$Q_{10}(\alpha_m) = 2.2 \qquad Q_{10}(\beta_m) = 2.2 \tag{7.58}$$

$$Q_{10}(\alpha_n) = 3 \qquad Q_{10}(\beta_n) = 3 \tag{7.59}$$

$$Q_{10}(\alpha_h) = 2.9 \qquad Q_{10}(\beta_h) = 2.9 \tag{7.60}$$

$$k = Q_{10}^{0.1T-3.7} \tag{7.61}$$

7.6 Model of FitzHugh

All models mentioned above have a similar behavior in regards to the electrostimulation process, thus, all these models belong to the same class of differential equations: They have a stable steady state; small disturbances produce small excursions of the states, but higher influences bring them against a pseudo limit circle from where the trajectories come back to the resting level. One can easily analyze the characteristics by reducing to two-dimensional models, such as the model of FitzHugh. [34]

In 1961, the 'Biophysical Journal' published a paper of Richard FitzHugh in which he made some phase plane analysis with a model he called "BVP model" after Bonhoeffer and Van der Pol. In literature, it is also often found as the Bohhoeffer Van der Pol FitzHugh (BVF) model. It has only two variables of state, which represent excitability and refractoriness, and its properties can therefore be visualized on a phase plane. FitzHugh's aims were to describe a large class of non-linear systems which show excitable and oscillatory behavior and the analysis of the stability of the singular points which represent the resting state. The model is not intended to be an accurate quantitative model of the axon, in the sense of reproducing the shape of experimental curves (see, e.g. figure 7.3). It rather tries to figure out the basic interaction between excitability and refractoriness. The algebraic form of the FitzHugh equations is not important and can be changed without altering the general properties of interest here. [9],[34]

The FitzHugh model is simple to analyze and needs less computation time than experimentally fitted equations. Time transformation and scaling allows the physiological interpretation

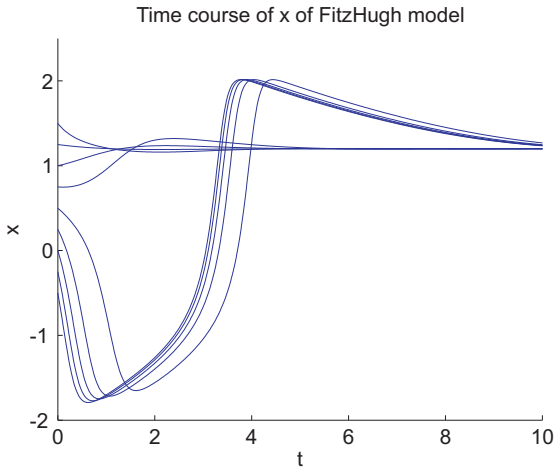

Figure 7.3: Time course of the main variable x of the FitzHugh model according to different starting values $x(0) = -0.5, -0.25, 0, \ldots, 1.5$; $y(0) = -0.625$ without any stimulus signal, with standard parameters and $\beta = 1$. From [34]

of the results. The modified equations give the nerve response to a stimulus signal $s(t)$. [34]

$$\frac{\mathrm{d}x}{\mathrm{d}t} = c \cdot \left(y + x - \frac{x^3}{3} - s \right) \cdot \beta \tag{7.62}$$

$$\frac{\mathrm{d}y}{\mathrm{d}t} = -\frac{(x - a + by)}{c} \cdot \beta \tag{7.63}$$

x may be interpreted as scaled voltage, s as the stimulus current density, and y as the recovery variable. The membrane voltage can be approximated by the following equation.

$$V = 25 \cdot (-x + 1.2) \tag{7.64}$$

For the standard parameters

$$a = 0.7, \qquad b = 0.8, \qquad c = 3 \tag{7.65}$$

the stable solution $\left(\frac{\mathrm{d}x}{\mathrm{d}t} = \frac{\mathrm{d}y}{\mathrm{d}t} = 0 \right)$ is $x_{rest} = 1.2$ and $y_{rest} = -0.625$. β is the time transformation factor that changes the time scaling, but does not influence the form of the solution. Warm blooded axon excitation behavior can be modeled with $\beta = 4$ to $\beta = 4$ when time is measured in ms, i.e. the solution is four times quicker than for the original problem with $\beta = 1$. For this thesis, $\beta = 7$ was chosen.[34]

The behavior of this model in the phase plane can be seen in figure 7.4. The state point or phase point representing the state of the system moves spontaneously in this plane along the paths (also called trajectories) which are represented by the blue lines in figure 7.4. Only a few representative paths have been drawn, but they should be thought of as completely

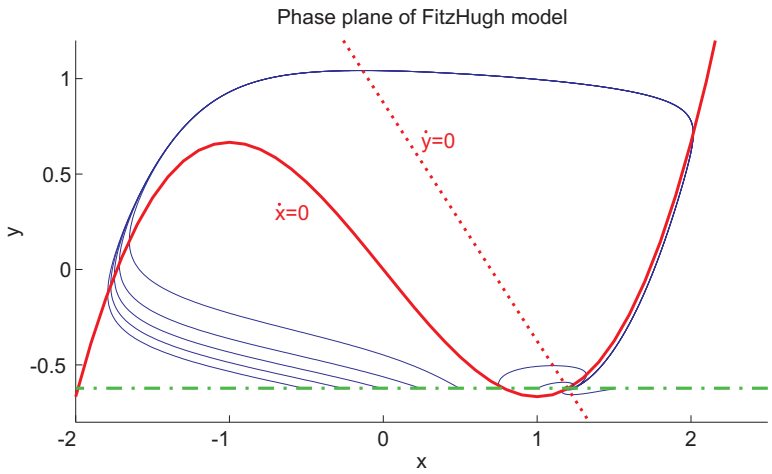

Figure 7.4: Phase plane of the FitzHugh model without any stimulus with standard parameters. Trajectories (blue lines) are responses to different starting values $x(0) = -0.5, -0.25, 0, \ldots, 1.5$; $y(0) = -0.625$. All solutions of the FitzHugh equations finally end in the resting point. This is the intersection of the curves $\dot{x} = 0$ and $\dot{y} = 0$. Green dotdashed line indicates the '(x) phase line' through the resting point. More details in the text. After [9]

filling the plane, like the stream lines of a fluid flow. Without a stimulus s the courses of the trajectories only depend on the starting point. At the highest and the lowest point of the trajectories there is $\dot{y} = 0$ and all the extremity points are situated on the y nullcline which is defined by $y = -\frac{x-a}{b}$ which is obtained by setting $\dot{y}$ equal zero in equation (7.63). The leftmost and the rightmost points of the curves are at the x nullcline which is defined by the 'N-shaped' curve $y = \frac{x^3}{3} - x$ which is obtained by setting $\dot{x}$ equal zero in equation (7.62). x and y nullclines are represented by the solid and dotted red lines in figure 7.4, respectively. This 'N-shaped' curve, which is typical for equations of nerve model, allows the existence of a 'separatrix' which separates the small excursions from the long ways of the spikes. A solution, which starts at a point above the separatrix, simulates a subthreshold response. Most of the curves starting above the separatrix follow in short pathways to the resting state and it is difficult to find starting values for solutions which pass through a large area called 'no man's land'. In practice, this means that one normally will not find a stimulus which can produce a subthreshold response that reaches, e.g., 90% of the amplitude of an action potential.
The trajectories of the phase plane of figure 7.4 are solutions of the FitzHugh model without a stimulus signal. Starting from the resting point, a stimulating signal has to drive the trajectory below or—which is the same— to the left of the separatrix in order to produce an action potential. [9],[34]

One has to be cautious when changing the standard parameters (7.65), the following limitations have to be taken into account:

$$1 - \frac{2b}{3} < a < 1, \qquad 0 < b < 1, \qquad b < c^2 \tag{7.66}$$

These conditions on a and b guarantee that without a stimulus signal the nullclines will intersect at only one singular point, which is a stable node or focus. This singular point represents the resting state. [9]

The FitzHugh equations can be more easily understood by considering separately the behavior of two subsystems. Except near the y nullcline, y is a more slowly changing variable than x. If y is kept constant at any value, the corresponding horizontal line in the (x, y) plane may be thought of as a phase line of a reduced system with a single variable of state x. The (x) phase line through the resting point (dotdashed green line in figure 7.4) has three singular points where it intersects the three branches of the x nullcline. The middle one is unstable and represents a threshold phenomenon. The other two are a stable excited point at the left and a stable quiescent point at the right. Displacement of the phase point from the resting point to some point to the left of the unstable threshold singular point produces excitation in the reduced system, and the phase point approaches the excited singular point. Considering the complete (x, y) system again, as a result of this negative change in x, y increases slowly, causing the phase line to move upward until the excited and threshold singular points meet and vanish. Then, in the (x) reduced system, the phase point rapidly approaches the only remaining singular point, the quiescent one on the right branch. Finally, y slowly decreases, and the phase point in the plane approaches the resting point. This description is similar to that given in [8] for the course of an impulse in the HH equations except that in the latter case the two subsystems were each of two dimensions instead of one (Hodgkin and Huxley's V and m together behave like x, h and n like y). [9]

Chapter 8

Propagation of the spike

Previous methods like the space clamped experiments can be used to simulate the reaction of fibres with long inserted electrodes. The injected stimulating current cannot leak away along the fibre and has to cross the membrane as capacitive or ionic current (see, e.g. section 6.4). It gives a good approximation of the behaviour of cell bodies because these are practically isopotential inside the membrane.
However, this model cannot describe the behaviour of an axon or muscle fibre, where the transmembrane potential may vary from point to point. Since the injected current leaks away to both sides along the axon, the membrane voltage becomes a function of distance. Therefore, the nerve fibre is segmented into several cylinders of length Δx, where each segment, or compartment, is represented as an electric circuit (see figure 6.1) so that the whole neuron is represented as an electric network (see figures 8.1 and 8.2). [25],[34]

The physiological reason for the propagation effect of an action potential along the fibre is the electrotonic coupling of nearby regions. Transmembrane current in the active region is inward, as Na^+ ions flow from outside to inside (which causes the internal potential to reverse and become positive in the active region). But since charge is neither added to nor subtracted from the whole system, the inward current in the active zone must be balanced by an equal outward current in the neighboring inactive regions. We know from artificial injection of current with microelectrodes that outward current in an inactive region of membrane is depolarizing. Thus, the outward current in an inactive region that is produced by inward current in an active region depolarizes the inactive membrane to threshold and excites it. As quoted in the book 'Nerve and muscle excitation', the sufficiency of this method of propagating the action potential was shown by Hodgkin in 1937[1]; he demonstrated that action potentials that arrived at a crushed portion of nerve could depolarize the inactive nerve beyond the

[1] A.L. Hodgkin, Evidence for electrical transmission in nerve, Part I. The Journal of Physiology. 90:183-210; Part II. The Journal of Physiology. 90:211-232

blocked area and could excite the inactive region if the block were small enough. [25]

Kirchhoff's current law says that at any node in an electrical circuit the sum of all inflowing currents is equal to the sum of all outflowing currents or, in other words, the sum of all currents at any node is zero. Considering that one compartment has only two neighbor segments, Kirchhoff's law for the n^{th} compartment according to the network model in figure 8.1 reads as:

$$I_{stim,n} = C_m \frac{\mathrm{d}(V_{i,n} - V_{e,n})}{\mathrm{d}t} + I_{ion,n} + G_a(V_{i,n} - V_{i,n-1}) + G_a(V_{i,n} - V_{i,n+1}) \tag{8.1}$$

or expressed in terms of resistance

$$I_{stim,n} = C_m \frac{\mathrm{d}(V_{i,n} - V_{e,n})}{\mathrm{d}t} + I_{ion,n} + \frac{V_{i,n} - V_{i,n-1}}{R} + \frac{V_{i,n} - V_{i,n+1}}{R} \tag{8.2}$$

C_m is the membrane capacitance, G_a the inneraxonal conductance, R the inneraxonal resistance, and $V_{i,n}(V_{e,n})$ the intracellular (extracellular) potential of the the n^{th} compartment. In contrast to the local model where any injected current has to pass the membrane either as capacitive or ionic current, the injected current in this network model is split into a capacitive current, an ionic current, an axonal current to the left, and an axonal current to the right of the considered segment.

Because the equations for the ionic currents are formulated with current densities, it is convenient to transform equation (8.2) by setting

$$R = \frac{4\rho_i \Delta x}{\pi d^2} \qquad \text{and} \qquad C_m = c_m \pi d \cdot l \tag{8.3}$$

where ρ_i is the resistivity (the specific resistance) of the axoplasm which is about $0.1\,\mathrm{k\Omega \cdot cm}$, d is the diameter of the axon, c_m is the capacitance per cm^2 of membrane, and l is the nodal gap width. One can treat the case of myelinated and of unmyelinated fibre in parallel if one sets $l = \Delta x$ for unmyelinated fibres. Equation (8.2) becomes [34]

$$\frac{\mathrm{d}(V_{i,n} - V_{e,n})}{\mathrm{d}t} = \frac{1}{c_m} \cdot \left(\frac{I_{stim,n}}{\pi d \cdot l} - i_{ion,n} + \frac{d}{4\rho_i \Delta x \cdot l} \cdot \Big(V_{i,n-1} - 2V_{i,n} + V_{i,n+1} \Big) \right) \tag{8.4}$$

By introducing the reduced membrane voltage $V_n = V_{i,n} - V_{e,n} - V_{rest}$ and by setting the extracellular potential equal to zero, equation (8.4) without any stimulus current can be written in the following form:

$$\frac{\mathrm{d}V_n}{\mathrm{d}t} = \frac{1}{c_m} \cdot \left(-i_{ion,n} + \frac{d}{4\rho_i \Delta x \cdot l} \cdot \Big(V_{n-1} - 2V_n + V_{n+1} \Big) \right) \tag{8.5}$$

Neglecting the extracellular potential is a simplification which was used by the pioneers when they examined the propagating action potential. As quoted in the book 'Electrical Nerve

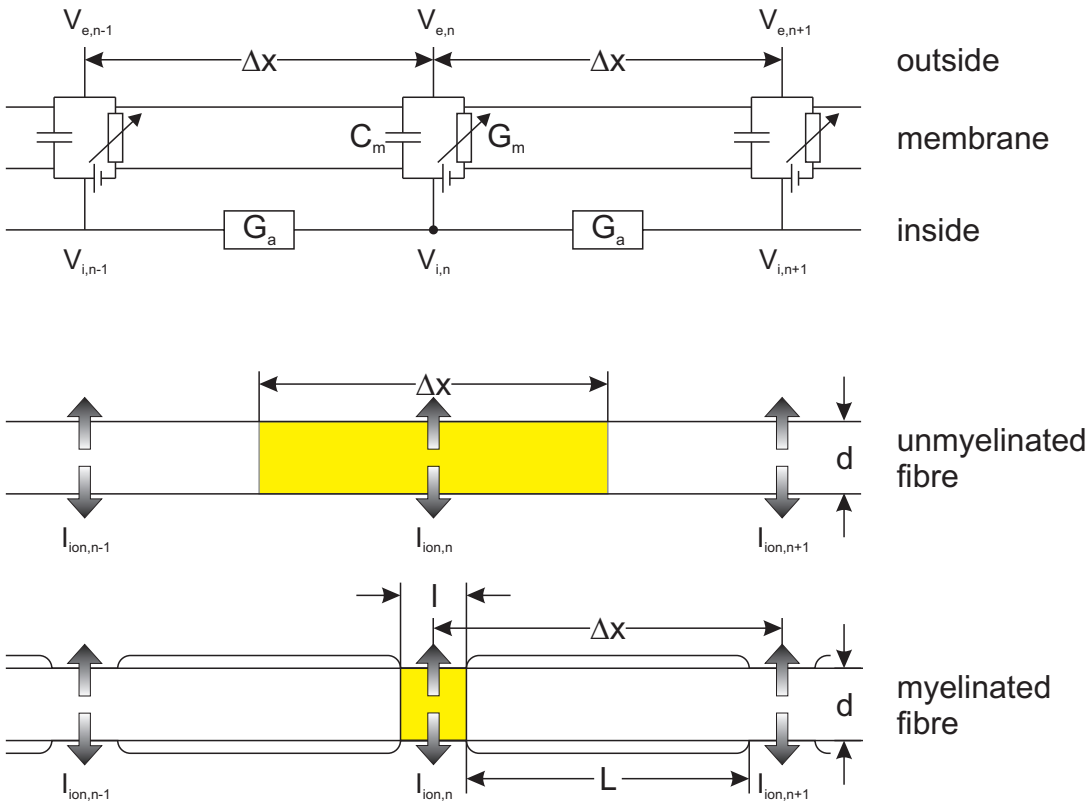

Figure 8.1: Electrical network to simulate the currents in an axon. Unmyelinated, as well as, myelinated fibres of diameter d are segmented into cylinders of length Δx. Myelinated fibres have active membrane parts only in the yellow area at the nodes of Ranvier. Here, ionic currents will only enter at a length l. The length of an internode is denoted as L. The membrane of every cylinder is simulated by an electric circuit (top diagram) consisting of membrane capacitance C_m, voltage source, and nonlinear membrane conductance. $V_{e,n}$ and $V_{i,n}$ are the external and the internal potential of the n^{th} segment. G_m symbolizes the nonlinear membrane conductance and G_a the conductance of axoplasm between two segments. $I_{ion,n}$ is the ionic current passing the membrane in the n^{th} segment. Adapted from [32]

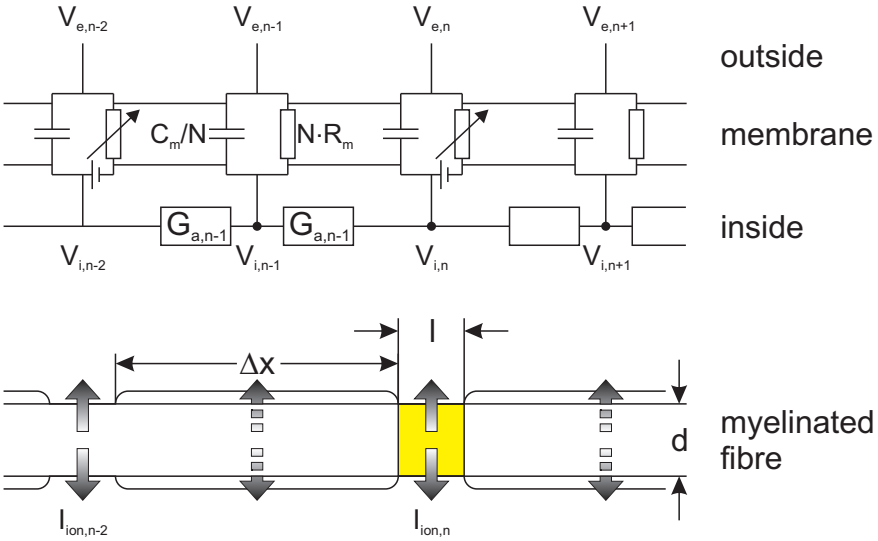

Figure 8.2: Electrical network for nerve fibres. It consists of active circuits with nonlinear membrane conductances (marked as arrows) which define the ionic currents at the nodes of Ranvier, and passive circuits with constant resistance resulting from N layers of Schwann cell membranes. Every passive element symbolizes one internodal segment. The voltages V_e and V_i are average values of the segments. Passive segment length: Δx, active segment length: l. d is the diameter of the axon, $I_{ion,n}$ is the ionic current passing the membrane in the n$^{\text{th}}$ segment. Adapted from [34]

Stimulation', John Clark and Robert Plonsey[2] examined the potential distribution on both sides of the membrane and found, that only changes in the order of some mV occur on the extracellular side when an action potential is passing. However, about 97 to 99% of the voltage is carried by the inside of an isolated fibre. As long as no extracellular stimulation is applied, one can neglect the extracellular potential for simplified cases. [34]

The axon model corresponding to figure 8.1 is adequate for unmyelinated as well as myelinated axons as long as, the myelin sheath is assumed to be a perfect insulator of the internodal axolemma. In this case, the behaviour of the model is only dependent on the membrane dynamics in the node of Ranvier. The assumption that myelin is a perfect insulator is not consistent with experimental work, Donald McNeal described it as the "most serious error in the model". The effect of current leaking through the myelin sheath on the results according to this model is difficult to assess without resorting to a much complex simulation which would include sets of partial differential equations to describe the change in potential along the internodal regions as well as at the nodes. [30],[39]

In order to regard these findings, there is another model which assumes that the myelin sheath is an imperfect insulator in which some current can flow through the myelin. The electric network according to this model is presented in figure 8.2. The corresponding equation to (8.5) for the n^{th} nodal section is

$$\frac{\mathrm{d}V_n}{\mathrm{d}t} = \frac{1}{c_m}\cdot\left(-i_{ion,n} + \frac{1}{2l\rho_i}\cdot\left(\frac{d}{\Delta x_{n-1}}\cdot V_{n-1} - \left(\frac{d}{\Delta x_{n-1}} + \frac{d}{\Delta x_{n+1}}\right)\cdot V_n + \frac{d}{\Delta x_{n+1}}\cdot V_{n+1}\right)\right) \tag{8.6}$$

and for the n^{th} internodal section

$$\frac{\mathrm{d}V_n}{\mathrm{d}t} = \frac{N}{c_m}\cdot\left(-\frac{V_n}{N\cdot r} + \frac{d}{2\rho_i\Delta x_n^2}\cdot\Big(V_{n-1} - 2V_n + V_{n+1}\Big)\right) \tag{8.7}$$

r denotes the membrane resistivity, N is the number of membranes wrapped around the myelinated part of the axon.[34]

8.1 The Cable Equation

For analytical considerations of unmyelinated axons, it is often instructive to take the limit $\Delta x \to 0$; without an injected stimulating current equation (8.4) reads as

$$\frac{\partial(V_i - V_e)}{\partial t} = \frac{1}{c_m}\cdot\left(-i_{ion} + \frac{d}{4\rho_i}\cdot\frac{\partial^2 V_i}{\partial x^2}\right) \tag{8.8}$$

[2]Clark J. and Plonsey R. The extracellular potential field of the single active nerve fiber in a volume conductor. Biophysical Journal 8:842-864. 1968; Plonsey R. The active fiber in a volume conductor. IEEE-Trans. Biomed. Eng. BME-21, 371-381. 1974

V_i, V_e and i_{ion} are functions of t and x. By introducing the reduced membrane voltage $V = V_i - V_e - V_{rest}$ and by setting $V_e = 0$, $g_a = {}^{d}/_{4\rho_i}$, and $i_{ion} = g_m \cdot V$, equation (8.8) may be written in the simplified form

$$g_a \frac{\partial^2 V}{\partial x^2} = g_m V + c_m \frac{\partial V}{\partial t} \tag{8.9}$$

which, for constant g_m is called the "cable equation". Since g_m is approximately constant only near resting state, the cable equation can be used for subthreshold analysis. If the axon is stimulated by a constant subthreshold current, injected at $x = 0$, the membrane conductance g_m may be assumed to be constant. With this constant current we can observe the steady state solution $\left(\frac{\partial V}{\partial t} = 0\right)$ for all points along the axon. Equation (8.9) becomes

$$g_a \frac{\partial^2 V}{\partial x^2} = g_m V \tag{8.10}$$

which has the solution

$$V(x) = V(0) \cdot e^{-\frac{|x|}{\lambda}} \tag{8.11}$$

λ, which is defined as $\lambda^2 = \frac{g_a}{g_m}$, is called the "space constant". It gives the distance where V falls to $\frac{V}{e}$, i.e. V loses 63% of its value. [34]

Equation (8.9) can also be used as approximation for the space clamp reaction after a subthreshold stimulus. Here we get exponential decay again. Setting $\frac{\partial^2 V}{\partial x^2} = 0$ and assuming constant g_m, equation (8.9) reads as

$$0 = g_m V + c_m \frac{\partial V}{\partial t} \tag{8.12}$$

which has the following solution:

$$V(t) = V(0) \cdot e^{-\frac{t}{\tau}} \tag{8.13}$$

τ is called the "time constant" and gives the time when subthreshold excitation loses 63% of its value. Thus λ and τ characterize the subthreshold decay in time and space domain. [34]

Chapter 9

Results

9.1 Comparing HH with FH, CRRSS, SE, and SRB

First of all, it is important to note that the HH model is not appropriate for warm-blooded animals because of its heat block. When combined networks and standard HH-parameters are used to simulate an excitation process along the fibre, it turns out that action potentials will not propagate for temperatures higher than 31 ℃. [34]

A check with the model of a nerve cell used for this thesis resulted in a shrinkage of an action potential at 34 ℃; an action potential in an axon of 33 ℃ propagates in a normal manner. The amplitude of the peak which is propagating in an axon of a temperature of 33 ℃ after a minimal stimulus signal of 0.75 nA increases from 32 mV in the stimulating compartment to 47 mV in the 1.2 mm distant compartment and is still slightly increasing. This decrease of the amplitude at high temperatures—the amplitude of a squid axon at standard temperature (6.3 ℃) is about 100 mV—confirms Hodgkin and Katz's experiments on the largest axon of the stellar nerve of 'Loligo forbesi' from 1949[23], where the authors investigated temperature effects on the squid axon. They found out that the amplitude of the spike is not altered greatly except at temperatures above 30 ℃, where it falls rapidly. They observed an action potential of 62.6 mV at 30 ℃ and of 46.5 mV at 35 ℃ and found out that the temperature at which heat block occurred showed considerable variation.

Figure 9.1 shows action potential propagation at a nerve cell at 33 ℃ and 34 ℃. One can see that the spike on the right is shrinking although the stimulating current should be high enough (1.26 nA) in order to enable propagation. As quoted in [34], a heat block with a similar value of 33 ℃ was discovered through another method by Huxley[1].

As a consequence of the heat block, sodium, potassium and leakage conductances from the original model of Hodgkin and Huxley (HH model) are multiplied by a factor of 12 in

[1] Huxley A.F. Ion movements during nerve activity. Ann. N.Y. Acad. Sci. 81: 221-246, 1959

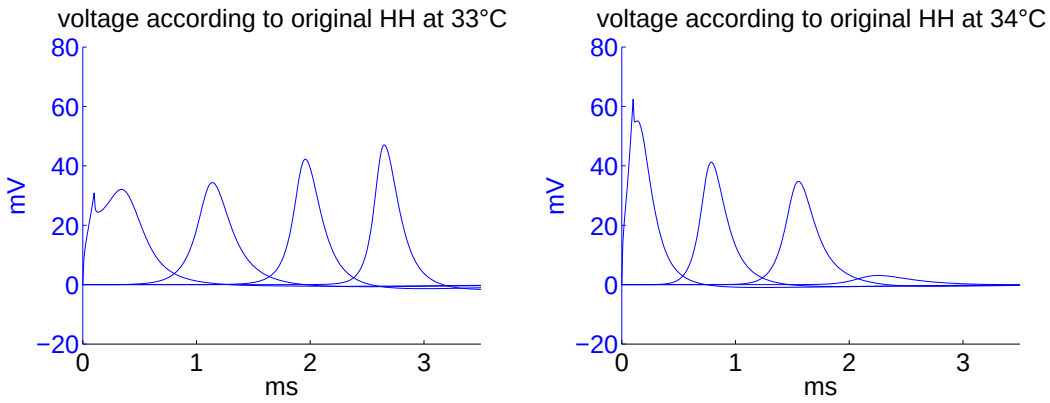

Figure 9.1: Heat block: Spike propagation at 33 ℃ (left) and 34 ℃ (right). At 34 ℃ the action potential can only be conducted within a certain distance. The x-axis represents the time in ms, the four graphs the reduced membrane voltage $V = V_i - V_e - V_{rest}$ (in mV) of the stimulated compartment, the 0.4 mm, 0.8 mm, and 1.2 mm distant compartment according to the original HH model.

order to get spike propagation and similar sodium conductance to the CRRSS model; the new conductances for the HH equations are: $g_{\mathrm{Na}} = 1440$, $g_{\mathrm{K}} = 432$, $g_{\mathrm{L}} = 3.6\,\mathrm{mS/cm^2}$. The other models can cope with a temperature of 37 ℃, their parameters do not need to be adapted.

The investigation was carried out by using ACSL (Advanced Continuous Simulation Language), a programming language which is designed for modeling and evaluating the performance of continuous systems described by time-dependent, nonlinear differential equations. Typical applications of ACSL include aerospace simulation, chemical process dynamics, toxicology models, robotics, and many others. ACSL has several built-in integration algorithms; for this investigation the Runge-Kutta algorithm of fourth order with fixed step size was used. Translator and runtime table size were expanded and double precision was applied. The communication interval—the interval at which the variables have their values recorded—was set to a tenth of the standard value, hence so was the integration step size. The parameter 'nsteps', which defines the integration step size in terms of the communication interval, was not changed. All numerical parameters are summarized in table 9.1. [24]

In section 9.1.1 local models—where current flow along the axon is prevented—of Hodgkin & Huxley (HH), Chiu, Ritchie, Rogart, Stagg, and Sweeney (CRRSS), Frankenhaeuser & Huxley (FH), Schwarz & Eikhof (SE), Schwarz, Reid, and Bostock (SRB), and FitzHugh, are analyzed. Section 9.1.2 explains the differences between the models when propagation along the axon is regarded. For the investigation, intracellular stimulation is applied, the stimulating current lasts for 0.1 ms and has a strength which is sufficient for each model to be excited, i.e. to generate an action potential.

9.1.1 Local Models (Space clamp experiments)

HH and CRRSS

Considering an axon under space clamp conditions, one can see some differences between the (adapted) HH and the CRRSS model. First, it takes more effort (a higher current) to stimulate and produce an action potential at a nerve cell whose ionic currents are modeled with the CRRSS equations. At 37 °C, it needs about 21 times as much stimulating current to generate an action potential, the 0.1 ms long pulse has to increase the voltage of the cell membrane by 19.81 mV. The membrane voltage of the CRRSS nerve fibre at the end of the stimulating current is 262% of the membrane voltage of the HH fibre, which must only be heightened by 7.55 mV. The shape of the generated spikes show differences too. Apart from the fact that the voltage of the CRRSS model must be higher at the end of stimulation, figure 9.2, which compares the action potential of six different models, shows that the falling phases of the spikes look different. The slope of the HH spike is more negative than the slope of the CRRSS spike, and in contrast to the CRRSS model, the undershoot only exists at the HH model. The action potential of the HH model needs another half millisecond to reach its resting level; the spike of the CRRSS model does not hyperpolarize, it reaches its resting level immediately after the falling phase.

The results of this simulation at three different temperatures are listed in table 9.2. As models for the cell membrane use current densities ($\mu A/cm^2$) rather than currents, the unit of excitation is $\mu A/cm^2$ as well. For comparison with propagating models, the stimulating current densities are multiplied by a factor that corresponds to a nerve cell segment which is modeled as a cylindric section with a diameter of 1 µm and a length of 10 µm. i_{stim} is the minimum stimulating current density that is necessary for generating an action potential. I_{inj} is the injected threshold current for a cell with a surface area of $10\pi\,\mu m^2$, which will be the lateral surface area of one segment of the nerve fibre at the propagating model. $V(0.1)$ is the reduced membrane voltage at the end of the stimulating current, i.e. after 0.1 ms. The number in brackets tells the percentage according to the (modified) HH model, i.e. the stimulating current density of the CRRSS model at 37 °C is 2111% of the stimulating current density of the HH model.

As regards the ionic currents, during an action potential Na^+ ions flow into and K^+ ions out of the cell. For this reason, Na^+ currents have a minus sign. We can also observe that more ions are passing the membrane in the CRRSS model. Analogue to the situation of the stimulating current density, ionic current densities i_{ion} are multiplied by a factor in order to become currents I_{ion}, which can be compared with the propagation models. As the CRRSS model does not have a K^+ current, the focus is on the Na^+ currents. The maximum

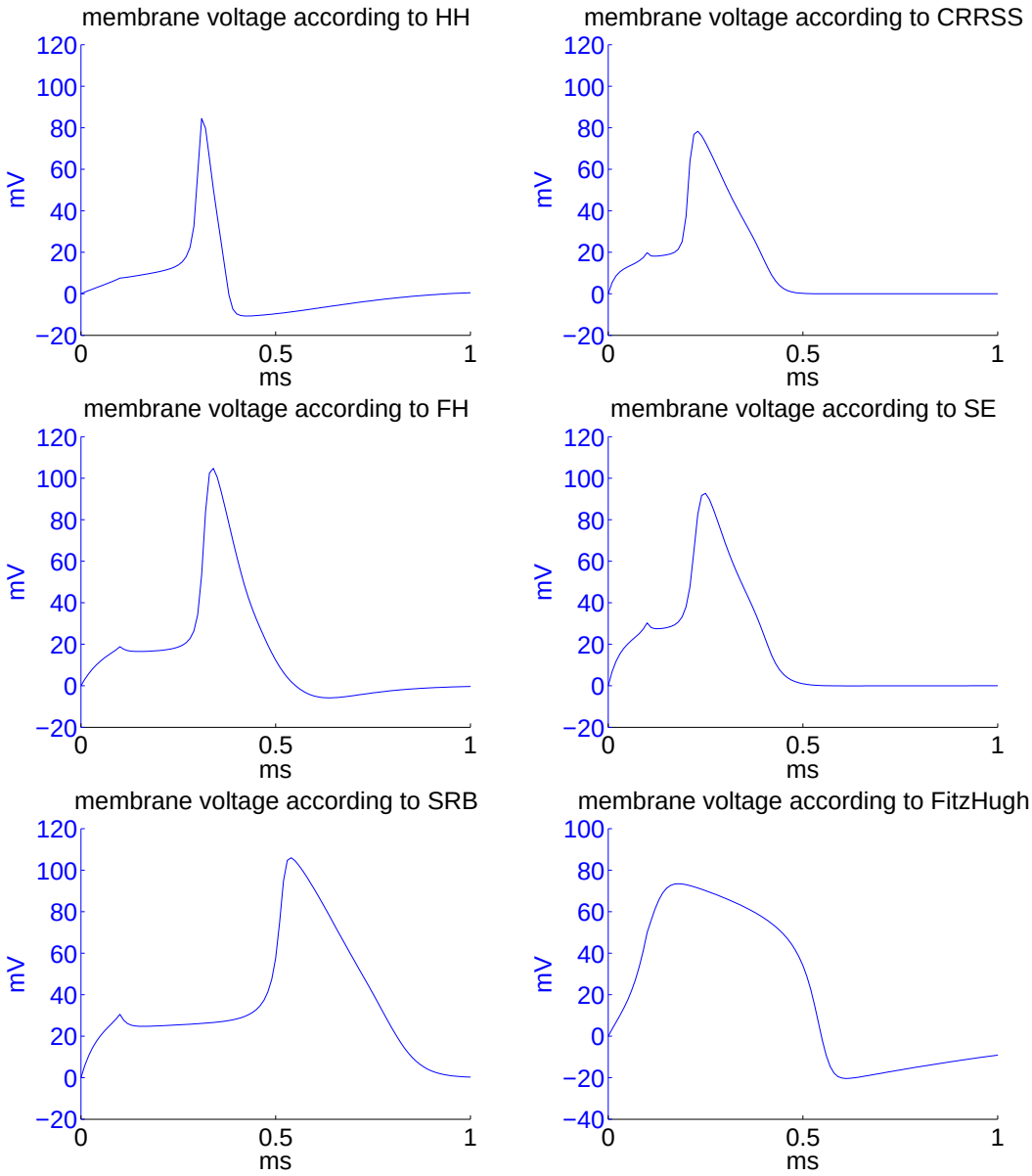

Figure 9.2: Time course of an action potential according to the local models of HH, CRRSS, FH, SE, SRB, and FitzHugh at 37 °C when stimulated with threshold current. The stimulating current densities are: 81 $\mu A/cm^2$ (HH), 1710 $\mu A/cm^2$ (CRRSS), 676 $\mu A/cm^2$ (FH), 2186 $\mu A/cm^2$ (SE), 1822 $\mu A/cm^2$ (SRB), and 1.1 (FitzHugh)

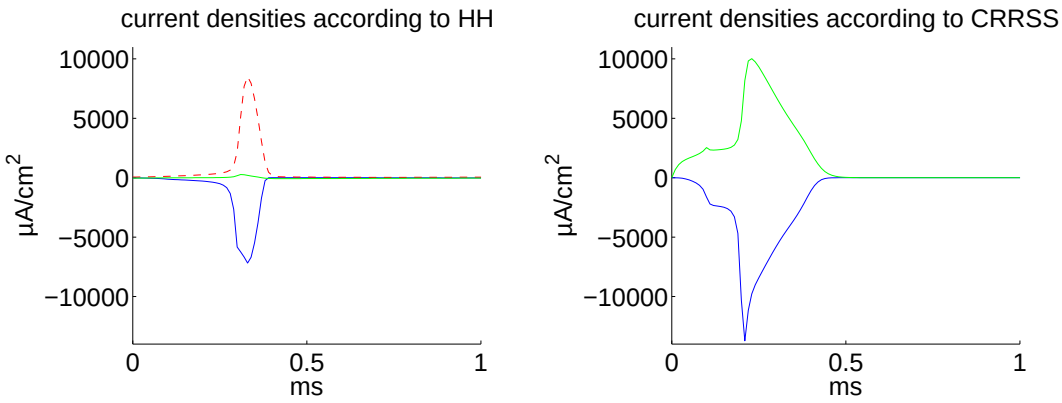

Figure 9.3: Time course of the ionic current densities across the membrane during an action potential according to the HH model (left) and the CRRSS model (right). The blue line indicates the Na^+ current density, the red dashed line the K^+ current density, the green line the leakage current density. As Na^+ ions flow into the cell, their current density has a minus sign.

magnitude of the sodium current density of the CRRSS model is about double the size of the HH model; 13733 $\mu A/cm^2$ is the maximum current density according to the CRRSS model, 7181 $\mu A/cm^2$ according to the HH model. The total number of Na^+ ions, which are passing the cell membrane during an action potential, is about three times the size of that in the HH model. 3.15 million sodium ions flow across the cell membrane in the CRRSS model, 1.06 million in the HH model. As one can see when comparing the currents, the leakage current of the HH model can be neglected. However, the leakage current of the CRRSS modeled cell is of the order of its Na^+ currents (see table 9.3 and figure 9.3).

FH and SE

Frankenhaeuser and Huxley separated a 'non-specific current' I_P from the complex delayed current, which is to a large extent carried by Na^+ ions. Their model was formulated for 20 °C, but Frankenhaeuser and Moore determined temperature coefficients for α_m, β_m, α_h, β_h, α_n, β_n, P_{Na}, and P_K to be 1.8, 1.7, 2.8, 2.9, 3.2, 2.8, 1.3, and 1.2, respectively. [14],[15],[16]

There are some similarities between the FH and the HH models with regard to action potentials at minimal stimulus. As regards the shape and the amount of current used for stimulation as well as the Na^+ current that flows from the outside to the inside of the cell during an action potential, the FH model is more similar to the HH model than to the CRRSS model. The stimulating current density of the FH model is eight times the current density of the HH model, a CRRSS model has a 21 as high stimulating current density. The

threshold, which the voltage of the FH membrane has to reach in order to generate a spike, is about 18.8 mV, which is near the threshold of the CRRSS model (19.81 mV), but through its hyperpolarization phase it differs from the latter. The magnitude of the spike is higher than in the HH or CRRSS model and is, apart from that of the SRB model, which is discussed later, the only one that exceeds 100 mV. When comparing the FH with the HH model, one can observe that on the one hand the maximum Na^+ current density of the FH model is 26% higher, but on the other hand the total amount of ions passing the FH membrane is more than double the size, which implies that the current flow takes longer across a FH modeled cell membrane than across a HH modeled cell membrane. This difference can be seen even more clearly when regarding the potassium currents. The maximum ionic current of the FH model is smaller than that of the HH model (69%), but the total amount of K^+ ions is 137% the size of its equivalent in the HH model. The non-specific current I_P is neglectable, the leakage current I_L about twelve times as high as in the HH model and the number of 'leakage' ions ten times as high. The sum of all currents of the FH model is more than twice that of the HH model.

The SE model, on the other hand, is similar to the CRRSS model. There is hardly any phase of hyperpolarization and the slope of the falling phase of the action potential is nearly the same as that of the CRRSS model. The minimal stimulating current to produce an action potential is even larger than the one of the CRRSS model. The SE model needs a stimulating current which is 27 times the strength of the HH stimulating current; a CRRSS nerve cell 'only' needs 21 times as much current as the HH model. The higher stimulus increases the membrane potential of the nerve cell even more, the voltage is raised by 30.27 mV, which is four times the membrane voltage of the HH model. Analogue to the FH model and the CRRSS model, it takes more time for the currents to pass the membrane. The maximum magnitude of the sodium current is 155% and the total number of sodium ions that pass the membrane during an action potential is 255% of the total numbers in the HH model. An analysis of the other currents shows that the potassium current of the SE model is so small that it can be neglected (the total amount of ions makes only 11% of that in the HH model); the leakage current on the other side is getting more important. The total number of 'leak' ions is 30 times the number of the HH model and is now of the order of its Na^+ current. This is quite the reverse situation one finds in the HH model, where the potassium current is of the order of its sodium current and the leakage current is negligible.

SRB and FitzHugh

Schwarz, Reid and Bostock distinguished between a fast potassium current $I_{K,fast}$ and a slow potassium current $I_{K,slow}$ in order to create a model for human nodes of Ranvier. [42]

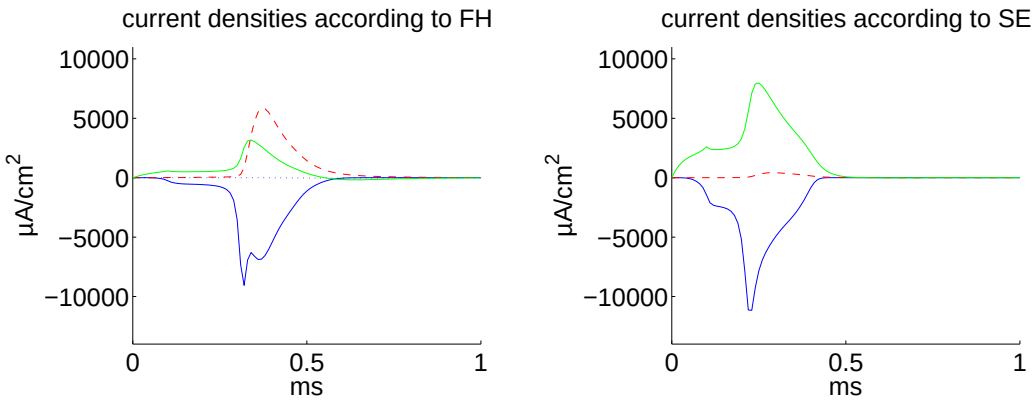

Figure 9.4: Time course of the ionic current densities across the membrane during an action potential according to the FH model (left) and the SE model (right). The blue line indicates the Na^+ current density, the red dashed line the K^+ current density, the green line the leakage current density, the blue dotted line the nonspecific current density i_P.

The first interesting difference one notes when looking at the membrane voltage when it is excited with threshold stimulus (see figure 9.2) is the long delay after which the steep slope of the action potential begins. About 0.5 ms go by until the voltage finally rises to a maximum value of 106 mV. The minimal stimulating current makes 2249% of the stimulating current of the HH model and raises the membrane voltage up to 30.54 mV. This is four times as high as the voltage of the HH model at the end of the stimulating signal.

The currents that flow across the membrane during an action potential are higher too. The maximum sodium current is 1.5 times as high as in the HH model but the total amount of ions passing the membrane is four times the value of that in the HH model. The leakage currents differ even more. In the SRB model, the maximum value of the leakage current is 24 times the value of that in the HH model and the factor of the total number of 'leakage ions' is even 41. One reason might be the delay after which the spike finally starts in the SRB model. A higher stimulating current would shorten this delay, as it would in any other model.

The FitzHugh model differs considerably from any previously discussed membrane model. This model does not include five (FH, SRB), four (HH, SE) or three (CRRSS) differential equations, but only two. The two variables of state represent excitability and refractoriness (see section 7.6). As the model does not include explicit equations for ionic currents, a comparison with other models cannot be made. Although the model does not include an equation for the membrane voltage either, it can be approximated (equation (7.64)). The reduced membrane voltage at the end of the minimal stimulus according to this equation is 18.81 mV, which is about two-and-a-half times of its value in the HH model. As the model has lost its physical interpretation, the parameter s, which may be interpreted as the stimulus

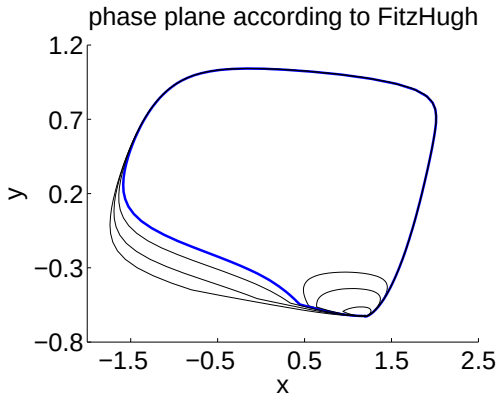

Figure 9.5: Phase plane of the FitzHugh model with $\beta = 7$ and standard parameters. The seven trajectories are the solutions to different stimulation strengths $s = 0.5$ (smallest "circle"), $0.9, 1.0, 1.1, 1.2, 1.5,$ and 2.0. The x-axis represents the state variable x, the y-axis the state variable y.

current density[34], does actually not have a physical unit. The minimal s that is necessary for producing an action potential has a strength of 1.1.

As mentioned above, the advantage of the FitzHugh model is that solutions according to different stimulating currents or starting values can be shown in a phase plane. The trajectories of figure 9.5 are the solutions according to the FitzHugh model when stimulated with values of 0.5 (smallest "circle"), 0.9, 1.0, 1.1 (thick blue line), 1.2, 1.5, and 2.0.

Summary

As it takes more time for the currents of the CRRSS, FH, SE, and SRB models to pass the membrane than for those of the adapted HH model, it is obvious that the action potential of the HH type itself is faster than all the others, i.e. that it takes less time for the spike to rise and fall. This can be seen in figure 9.2. It does not imply that an action potential of the HH type propagates faster than action potentials of the other types, for it takes approximately as much time as in the other models for excitation at minimal stimulus. But as we will see later, the propagation velocity of an HH action potential along the fibre is faster than those of the others.

9.1.2 Propagation Models

The basis for the investigation is an unmyelinated nerve fibre—or to be exact, the axon of an unmyelinated nerve fibre—which has a diameter of $1\,\mu m$[28] and an intracellular electrical resistivity ρ_i of $0.1\,k\Omega cm$[34]. Depending on the model, the specific capacitance of the cell

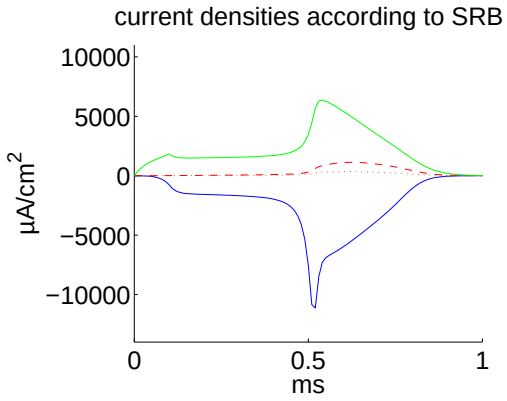

Figure 9.6: Time course of the ionic current densities across the membrane during an action potential according to the SRB model. The blue line indicates the Na^+ current density, the red dashed line the fast K^+ current density, the red dotted line the slow K^+ current density, the green line the leakage current density.

membrane is either 1 (HH), 2 (FH), 2.5 (CRRSS), or 2.8 (SE, SRB) $\mu F/cm^2$. The fibre is modeled as a long cylinder with a circular cross-section area. It is divided into 101 cylindric segments (or sections) with a length of 10 µm each and is stimulated in the 51^{st} compartment, which represents the middle of the axon. Within one section, the voltage and currents are individually approximated by a mean value, i.e. there is, for example, one (time dependent) voltage value for all ten micrometers that are united into a segment. Each segment of the fibre represents a space clamp experiment, which can be simulated as a local model. The simulation was carried out using equations for current densities rather than currents. These were calculated by appropriate formulas.

HH and CRRSS

Analogue to the space clamp analysis, it takes a higher current to stimulate the CRRSS model than the HH model. Under space clamp conditions, the stimulating current of the CRRSS model was 21 times that of the HH's current; within the propagation models the stimulating current of the CRRSS model is only five times that of the HH model. As currents can leak away to both sides of the compartment in which the stimulating electrode is inserted, it is clear that a higher stimulus current is needed to produce an action potential. In the case of the HH model, it takes more than thirteen times as much stimulating current for the cell when propagation is allowed than during a space clamp experiment. A CRRSS modeled cell only needs a current that is about three-and-a-half times higher.

In compartment models, the action potential propagation along the axon—when stimu-

lated with threshold current—produces a spike in the stimulating compartment which is lower than those of the of the following compartments. As can be seen in figure 9.7, the magnitude of the spike of the HH model increases from approximately 70 mV in the 51^{st} (stimulating) compartment to approximately 95 mV in the 70^{th} (distant) compartment. A spike according to the CRRSS model increases from 74 mV in the stimulating compartment (SC) to 91 mV in the distant compartment (DC), as do the ionic currents. The magnitude of the sodium current of the HH model increases from 1.83 nA to 2.71 nA, which corresponds to a factor of 1.48; the currents of the CRRSS model behave in a similar way. Its Na^+ current magnitude increases from 5.70 nA to 6.66 nA, which corresponds to an increasing factor of 1.17. The magnitude of the sodium current in the SC of the CRRSS model is three times the height of its equivalent in the HH model; the magnitude in the DC of the CRRSS model is two-and-a-half times the height of that of the HH model. If we stimulated with a higher current, the magnitude of the sodium currents in the stimulated would be higher and the difference to that in the distant compartment would get smaller. The shape of the spike has not significantly changed by contrast with the local models, as is also the case in the models of FH, SE and SRB. The alteration of the total number of sodium ions between the SC and the DC is 1.17 in the HH model and 0.92 in the CRRSS model. The drop in the total amount of sodium ions in the CRRSS model may be due to the shorter action potential in the 70^{th} compartment (see figure 9.7).

The propagation velocity along the fibre of the HH model is 1.67 m/s and of the CRRSS model 0.71 m/s, which corresponds to 43%. As the action potential has different properties in the stimulated region than in some distant compartment (it has a different shape and its peak has a smaller magnitude), the conduction speed of the spike is measured at some distance from the stimulated region—to be exact, between the 65^{th} and the 75^{th} compartment. One can see the faster propagation velocity of the HH model in Figure 9.7 as well as in Figure 9.9. Figure 9.7 shows the time course of the voltage in the stimulating compartment, which is represented by the first blue line, and in the 70^{th} compartment. Two closer spikes indicate a higher velocity; the greater the distance between two peaks, the slower the conduction speed of an action potential is. Figure 9.9 shows propagation along the fibre. The x-axis represents the whole axon, the graphs follow the membrane voltages along the axon at a specific time, $t = 0, 0.04, 0.08, \ldots, 1$ ms. At each time step, the graph is shifted to indicate the propagating effect. The spike of the HH model reaches the end of the fibre earlier than the one of the CRRSS model, which emerges clearly from the two graphs. One can also observe a later generation of an action potential at minimal stimulus in the stimulating compartment of the HH model (cp. also figure 9.7).

The total number of ions that are passing the CRRSS modeled membrane during an action

potential is higher than that of the HH modeled membrane. 4.36 million sodium ions pass the membrane at the 51^{st} compartment, 4 million ions pass it at the 70^{th} compartment. As only 1.09 million sodium ions cross the stimulating and 1.27 million the 70^{th} segment of the HH modeled cell, there are about four times more Na^+ ions involved in the excitation process of the CRRSS model than in the HH model. In the 70^{th} section, the sodium ions in the CRRSS model make 314% of those in the HH model.

FH and SE

The injected threshold current of the FH model has increased from 0.21 nA in the local model to 1.26 nA, which corresponds to an increase factor of six. This injected current is only three-and-a-half times the height of the injected current of the HH model, whereas the current of the local model was more than eight times the height of the HH model. The threshold voltage has also increased, from 18.8 mV to about 27 mV, which corresponds to a factor of 1.4. The increase of the maximum membrane voltage from 97 mV in the stimulated compartment to 105 mV in the distant is rather small.

Contrary to the HH model, the sodium current during an action potential in a FH modeled cell does not increase with increasing distance from the stimulated segment. In the stimulating compartment, the maximum magnitude of the Na^+ current is 4.01 nA whereas it is 3.71 nA in the distant compartment which corresponds to 92.5%. The total amount of sodium ions that cross the membrane also decreased from 3.31 million to 2.40 million ions. In comparison with the HH modeled cell, the number of sodium ions corresponds to a factor of three in the stimulating compartment and 1.8 in the 70^{th} compartment. With a conduction speed of 0.71 m/s, a spike of the FH model propagates as fast as one of the CRRSS model.

A SE modeled cell needs an about eight times stronger stimulus than a HH modeled cell which is quite different to the ratio of the two local models where SE needs a 27 times as high stimulus as HH. The membrane voltage at the end of the threshold current is about three times the voltage of the HH model.

The number of Na^+ ions passing the membrane in the SE model during an action potential decreases from 6 million in the stimulated segment to only 3 million ions in the distant section, although the maximum magnitude slightly increases from 4.28 nA to 4.93 nA. A similar property can be seen in the case of the leakage current. The total number of 'leak' ions is 4.28 million in the 51^{st} compartment and 2.84 million in the 70^{th}, whereas the maximum of the current increases from 1.88 nA to 2.17 nA. Only 210000 potassium ions pass the membrane in the stimulated segment, 110000 is the total number in the 70^{th} compartment and can therefor be neglected. The total number of sodium ions make 554% (51^{st} section) and 232% (70^{th} section) of a HH modeled axon, the total amount of potassium ions only 17% and 8%,

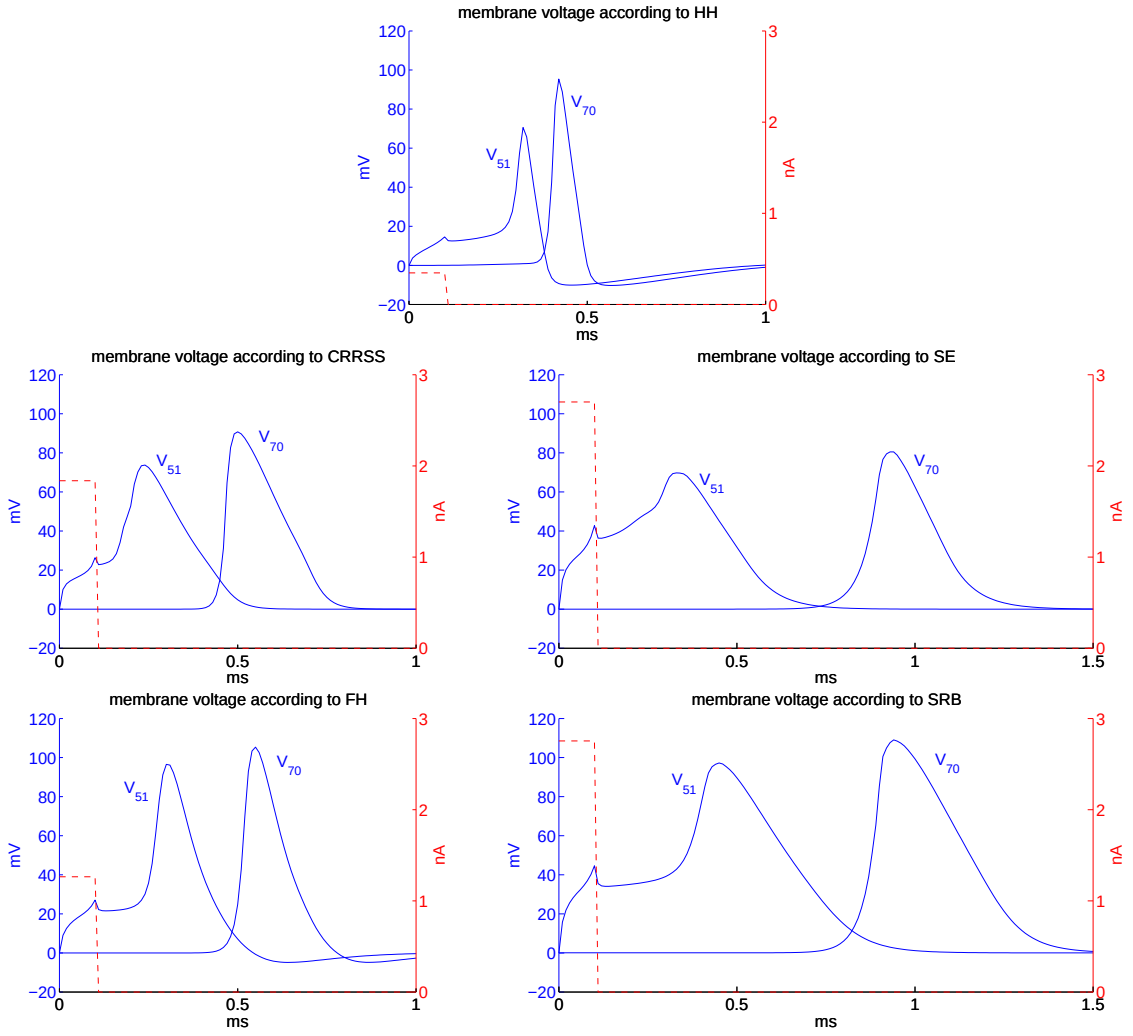

Figure 9.7: Time course of the injected threshold current (red dashed line) and resulting action potentials (blue lines) of the stimulated (51^{st}) and distant (70^{th}) compartment according to different membrane models, at 37 °C. The first blue line indicates the voltage in the stimulus compartment, the second blue line the voltage of the 70^{th} compartment. The injected currents are: 0.35 nA (HH), 1.84 nA (CRRSS), 1.26 nA (FH), 2.70 nA (SE), and 2.71 nA (SRB)

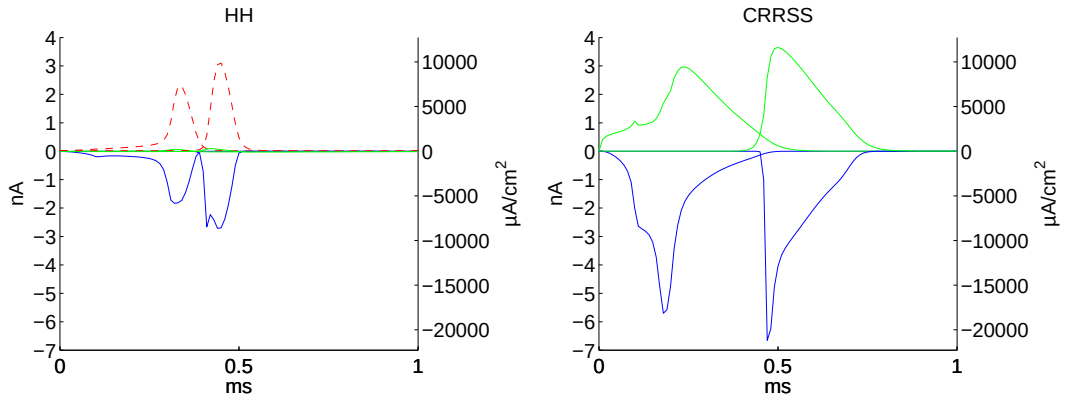

Figure 9.8: Time course of the ionic currents according to the HH model and the CRRSS model in the stimulated compartment (first set of lines) and in the distant compartment (second set of lines). The blue line represents the Na^+ current, the red dashed line the K^+ current, the green line the leakage current. The additional axis on the right of each graph is the scale of the appropriate current densities.

respecively. The maximum of the K^+ current in the stimulated region is 0.15 nA which is 6% of the appropriate value of the HH model. In the distant compartment, the maximum is only 0.10 nA any more which corresponds to 3% of the HH model. The amplitude of the leakage current as well as the total amount of not specified ions of the SE modeled nerve cell are higher and more than those of HH and FH. As seen in tables 9.9 to 9.11, there are 0.19 million (HH), 0.76 million (FH) and 2.84 million (SE) nonspecific ions passing the membrane at the 70^{th} segment, the maximum of the current is 0.10 (HH), 1 (FH) and 2.17 (SE) nA. The propagation velocity of a spike along the fibre is 0.30 m/s which is much slower compared to the HH model and is almost the slowest among all the examined models.

SRB

The SRB model needs a higher stimulating current than all the other models to generate an action potential. Its injected threshold current is 2.75 nA which is about eight times the height of the HH cell. The other models have smaller threshold currents: 1.84 nA (CRRSS), 1.26 nA (FH), 2.70 nA (SE). As one can observe, it is the model with the highest "transfer rate" of ions in the stimulated compartment too, especially when looking at the sodium currents. The number of Na^+ ions that pass the membrane is 7.68 million in the 51^{th} compartment and 4.26 million ions in the 70^{th} compartment. Only the CRRSS model with 4.36 million ions in the stimulated region and 4.00 million ions in the distant segment comes close to the SRB model. It is the model with most ionic movement, which can also be observed when comparing the

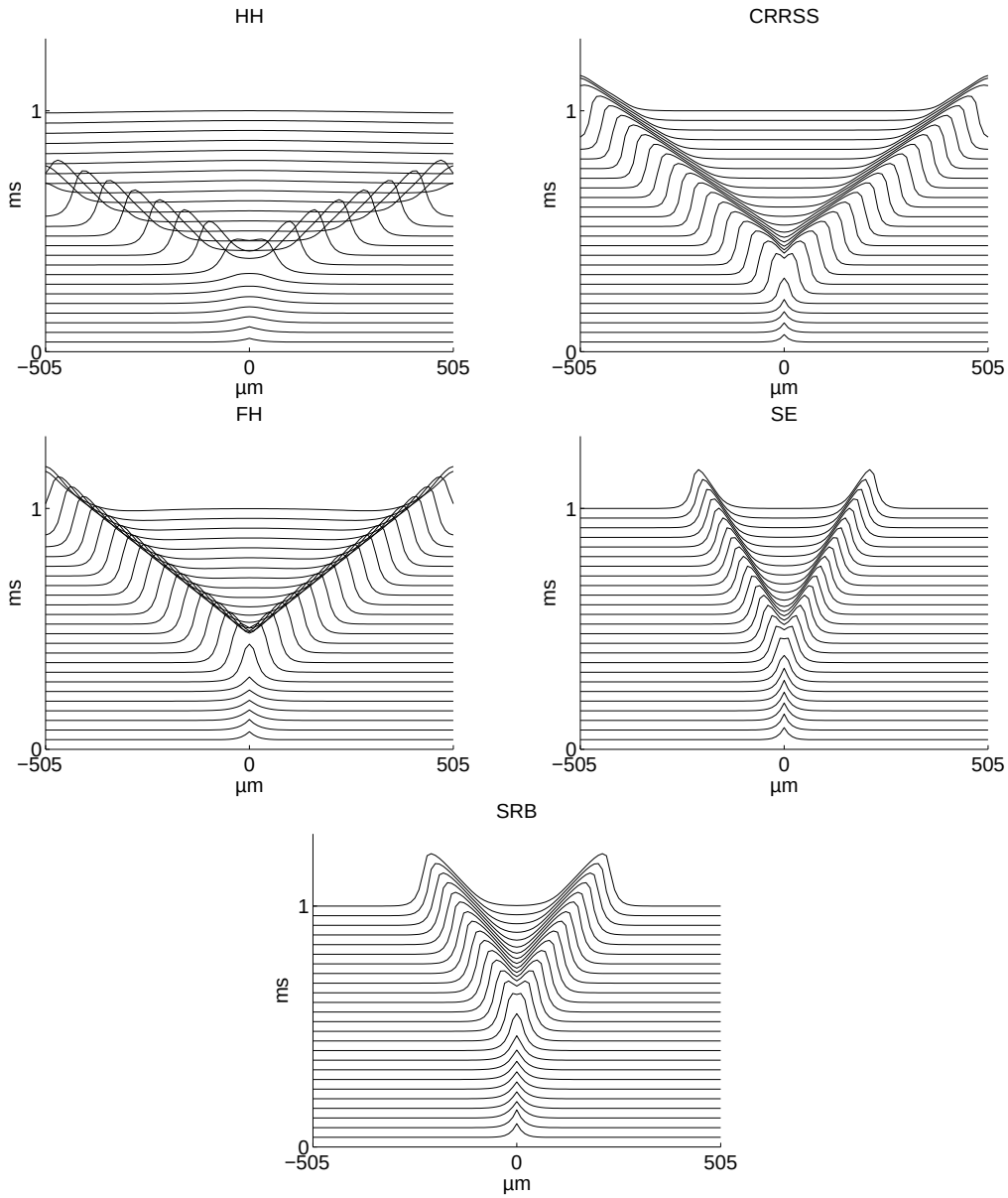

Figure 9.9: Action potential propagation along the axon after stimulation by threshold current in the middle at 37 ℃ according to the HH, CRRSS, FH, SE, and SRB models. Each line represents the membrane voltage along the whole axon at a determined time, $t = 0, 0.04, 0.08, \ldots, 1\,\text{ms}$.

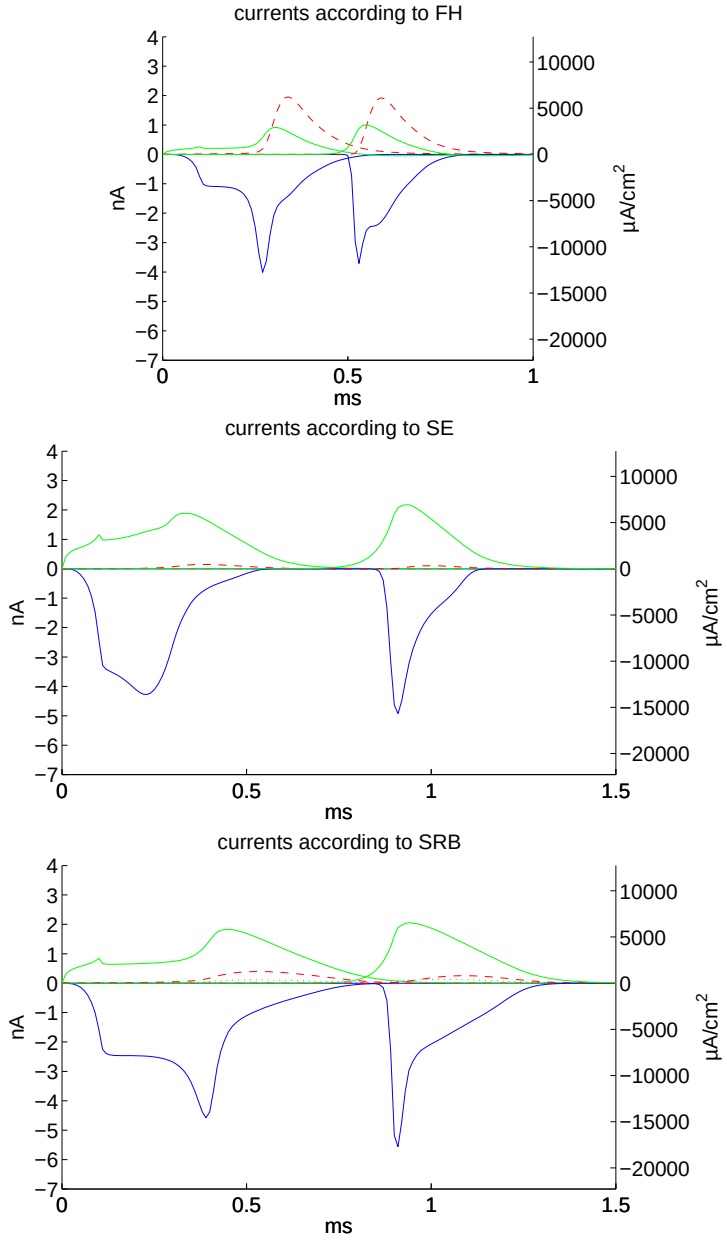

Figure 9.10: Time course of the ionic currents according to the FH model, the SE model, and the SRB model in the stimulated compartment (first set of lines) and in the distant compartment (second set of lines). The blue line represents the Na^+ current, the red dashed line the K^+ current (the slow potassium current of the SRB model is represented by the red dotted line), the green line the leakage current. The additional axis on the right of each graph is the scale of the appropriate current densities.

sum of all currents. In the distant compartment, about 8.5 million ions cross the membrane of the SRB model. Once again, the CRRSS model with 8 million crossing ions is the only model close to the SRB model in this matter.

The membrane voltage of 44.61 mV at the end of the stimulus is three times the voltage of the HH model and quite similar to the membrane voltage of the SE model (42.79 mV). The propagation velocity of an action potential along the fibre is slower than at any other model, with 0.37 $^{m}/_{s}$ it is only 22 % of the conduction speed of the HH model.

Summary

A comparison of sodium ions that cross the membrane in the distant section shows that the SRB model needs more ions for conducting an action potential along the fibre than any other examined model. With 4.26 million ions the SRB model is the model with most sodium ions passing the membrane, followed by the CRRSS model (4.00 million), the SE model (2.95 million), the FH model (2.40 million) and the HH model (1.27 million). The situation in the stimulated compartment is similar. The only difference is that in the SE modeled cell there are more Na^+ ions passing the membrane during an action potential than in a CRRSS modeled cell. 7.68 million ions are involved in the excitation process of the SRB model, 6.05 million ions in the SE modeled cell, 4.36 million ions in the CRRSS modeled cell, 3.31 million ions in the FH modeled cell and 1.09 million ions in the HH modeled cell.

An overall view of any ions moving into and out of the cell shows similar results. 8.52 million ions are involved in the propagation effect of the action potential in the 70^{th} section of the SRB cell, 8.01 million ions cross the CRRSS modeled cell, 5.90 million the SE modeled cell, 4.86 million the FH modeled cell and 2.87 million ions the HH modeled cell. Analogue to the situation of the sodium ions, the roles of CRRSS and SE swap when regarding the 51^{th} segment. The total amount of ions in the stimulated compartment is 13.56 million (SRB), 10.55 million (SE), 8.72 million (CRRSS), 6.15 million (FH) and 2.51 million (HH).

One section is modeled as a right circular cylinder with a lateral area of 31.4 μm^2, as the length of a section is 10 µm and the diameter is 1 µm. To generalize the investigations made above, one can calculate the total number of ions per centimetre of fibre length or per square centimetre of the lateral membrane area. Tables 9.9 to 9.12 list the total number of ions that cross the 1 µm thick membrane within a length of 1 cm as well as the total number of ions that cross a patch of 1 cm^2 of cell membrane. Calculations of the number of ions that pass one square centimetre of membrane area show that in the HH model $3479 \cdot 10^9$ sodium ions pass it in the stimulated region, $4054 \cdot 10^9$ ions pass it in the distant compartment. In the HH model, $3979 \cdot 10^9$ potassium ions pass one square centimetre of membrane in the stimulated compartment, $4465 \cdot 10^9$ ions in the distant compartment. These values seem to be very large,

but one has to take account of the large membrane area of $1\,\mathrm{cm}^2$: a $1\,\mu\mathrm{m}$ thick axon ought to be about 32 m long in order to have a membrane area of $1\,\mathrm{cm}^2$.

A unique issue of the HH model is that the number of ions crossing the membrane increases from the stimulated compartment to the distant compartment. The total number of sodium ions as well as the number of potassium and nonspecific leakage ions increase by a factor of 1.17 (sodium ions), 1.12 (potassium ions) and 1.13 (leakage ions). Except for the nonspecific P ions of the FH model, the total number of any ion type of any examined membrane model decreases from the 51^{st} to the 70^{th} compartment by factors between 0.96 (slow potassium ions of the SRB model) and 0.49 (sodium ions of the SE model). The increase of the maximum magnitude of all ionic currents from the 51^{st} to the 70^{th} compartment, which can be observed at the HH model, can also be seen at the model of CRRSS. Apart from the K^+ current of the SE model and the fast K^+ current of the SRB model, which, by the way, are really small, these two models show a similar property. Only the amplitudes of the sodium and potassium currents according to the model of FH decrease.

9.2 Factor for Conductance

As mentioned in section 9.1, the parameters of the original HH model are changed to get action potential propagation along an axon at 37 °C. Maximum sodium, potassium and leakage conductances are multiplied by a factor of 12. The aim of this section is the investigation of lower factors and to find the minimal factor for these conductances that is necessary for action potential propagation at 37 °C. As we have already been working on the model with a conductance factor of 12, this will be the reference model.

9.2.1 Minimal factor

The minimal factor by which the maximum ionic conductances of the HH model have to be multiplied is 1.5; multiplying them by a lower factor would forward a spike only within a certain distance. Figure 9.11 compares the action potentials of four HH models with different 'conductance factors' f. One can see that in the model with $f = 1.5$ only the propagation of a spike is ensured, the shape of the action potential has significantly changed. The maximum of the membrane voltage difference between the inside and the outside of the nerve cell in the 70^{th} compartment is only 35.36 mV any more and the action potential has a longer rising phase as well as a longer falling phase. As the resting potential of the HH model is $-70\,\mathrm{mV}$, there is actually no phase of 'depolarization'.

The conduction speed of an action potential decreases to $0.56\,\mathrm{m/s}$ which is only a third compared to the HH model with a conductance factor of 12. The 0.1 ms long injected stimulat-

ing current I_{inj} must be 0.69 nA high to heighten the membrane potential by about 30 mV in order to generate an action potential. Both, the injected threshold current and the threshold membrane potential, are about double the size of that in the reference model. The maximum magnitude of the sodium and potassium currents in the 70^{th} compartment according to the minimal factor model make 9 and 4% of the factor-12-HH respectivly, their amplitudes are 0.25 nA and 0.13 nA. Unlike the situation of the factor-12-HH, where more sodium and potassium ions are involved in the propagation of an action potential in the distant compartment than in the stimulated compartment, the total number of sodium and potassium ions in the distant section of the HH model with conductance factor 1.5 is lower than in the stimulating section. 0.22 million Na^+ ions cross the membrane in the 51^{st} section, 0.19 million in the 70^{th} section. K^+ ions behave in a similar way: 0.28 million ions flow through the ion channels in the stimulating compartment, 0.2 million in the distant compartment. To generalize the investigations made above, one can calulate the total number of of ions per centimetre of fibre length or per square centimetre of the membrane lateral area. Table 9.13 summarizes these calculations.

The minimum conductance factor model also differs from the factor-12-model with respect to the maximum of the potassium currents in the stimulated and in the distant compartment. The maximum in the stimulating compartment is 0.16 nA, which is higher than in the distant compartment (0.13 nA), whereas the maximum potassium current according to the factor-12-model increases from 2.30 nA (51^{st} compartment) to 3.10 nA (70^{th} compartment). The behaviour of the maximum magnitude of the sodium currents on the other hand does conform to the of the factor-12-model. There is a higher amplitude (0.25 nA) in the distant compartment than in the stimulated compartment (0.22 nA) which is 9 and 12% of the values of the HH model with a conductance factor of 12, respectively. Due to the fact that leakage currents can be neglected (see section 9.1.1) they are not investigated.

9.2.2 Factor analysis

In this section, four adapted HH models are analyzed. Original maximal ionic conductances g_{ion} are multiplied by different factors f, $f = 12, 8, 4, \text{and } 1.5$. The conductances for the already used factor-12-HH-model, which is our reference model, are $g_{\text{Na}} = 1440$, $g_{\text{K}} = 432$, $g_{\text{L}} = 3.6$, the conductances for the new models are $g_{\text{Na}} = 960$, $g_{\text{K}} = 288$, $g_{\text{L}} = 2.4$ for the HH model with $f = 8$, $g_{\text{Na}} = 480$, $g_{\text{K}} = 144$, $g_{\text{L}} = 1.2$ for the HH model with $f = 4$, and $g_{\text{Na}} = 180$, $g_{\text{K}} = 54$, $g_{\text{L}} = 0.45$ for the HH model with the minimal conductance factor ($f = 1.5$).

Figure 9.11 compares the action potentials of the four adapted HH models. One can see that with increasing f the maximum of the membrane voltage increases. As already

mentioned in the previous section, the factor-1.5-model is not suitable for real nerve cells, as the membrane voltage cannot depolarize the cell (the resting potential of the HH model is about $-70\,\mathrm{mV}$). The conduction speed also increases with increasing f, which is indicated by the smaller distance between two spikes. Calculation between the 65^{th} and 75^{th} compartment shows that propagation velocity along the axon of the minimal factor model is $0.56\,{}^{\mathrm{m}}/_{\mathrm{s}}$ which is 33% of the conduction speed of the factor-12-model, which conducts an action potential with $1.67\,{}^{\mathrm{m}}/_{\mathrm{s}}$. A spike according to the HH model with a conductance factor of 4 propagates with a speed that is 67% of the reference model's speed, the spike according to the factor-8-model with a velocity which is 86% of that of the reference model.

When focusing on the threshold current for the injected stimulating electrode, one can observe an increase with the decrease of the conductance factor. In the factor-12-model, the injected threshold current is 0.35 nA; multiplying the maximum ionic conductances by lower factors will increase the threshold current. The factor-8-model needs a 0.38 nA high current for excitation, the factor-4-model 0.46 nA, and the factor-1.5-model 0.69 nA. These values are 110%, 133%, and 200% of that of the reference model, respectively. Just as the minimal stimulating current increases with decreasing f, so does the threshold membrane voltage in the stimulated compartment. The injected current must increase the membrane voltage of the reference model by 14.57 mV, of the factor-8-model by 16.12 mV, of the factor-4-model by 19.71 mV, and of the factor-1.5-model by 30.59 mV in order to produce an action potential. These voltage values make 111%, 135%, and 210% of the voltage of the reference model and are quite similar to the alteration of the threshold injected stimulating currents.

Table 9.13 summarizes the measured data of the four investigated adapted HH models. The assumption that the total number of ions that are involved just in the propagation of an action potential, which can be measured in the distant compartment, decreases with decreasing conductance factor f makes sense, as a modification of g_{ion} can be interpreted as a change of the number of ion channels. Actually, changing f from 12 to 8, that is adapting f to 66% of that in the reference model, involves a decrease in the total number of sodium and potassium ions to 70% and 69% of the equivalents in the reference model, respectively. Changing f to 4, which is a modification to 33% of the reference model, results in a reduction of the total number to 38% of those in the factor-12-model; changing the factor to 1.5, which is 13% of 12, results in a reduction to 15% (Na^+ ions) and 14% (K^+ ions) of those in the reference model.

The maximum magnitudes of the sodium and potassium currents in the distant compartments are influenced by the change of f in a slightly similar way, even if the modification in percentage of f does not implicate an almost same modification in percentage of the maximum magnitude of the ionic currents. Changing f to 67% of the f of the reference model

results in an adaption in the maximum absolute value of the sodium current of 70% and in a maximum potassium current of 66% of the equivalents of the factor-12-model. Applying a conductance factor f of 4 to the HH model, which is a change to 33% of that in the reference model, induces a change of the maximum magnitude of the sodium current to 42% and of the potassium current to 29% of those in the factor-12-model. Setting $f = 1.5$ in the HH model, which is 13% of the f of our reference model, results in a decrease of amplitude of the sodium current to 9% and of potassium current to 4% of the equivalents in the factor-12-model.

The maximum absolute value of the currents in the stimulated compartment vary more largely. One attribute that all models have is that a reduction of f to x% of the f in the reference model implicates a reduction of the amplitudes of the currents to a value smaller than x% of those in the reference model. Additionally, the reduction of the amplitude of the K^+ currents is greater than of the Na^+ currents, i.e. for example, changing f to 33% of the reference model's f results in a change of the maximum amplitude of the potassium current to 8%, and of the sodium current to 9% of the equivalents in the reference model, respectively. It may be important to note that in the factor-4-model as well as in the factor-1.5-model the sodium's maximum absolute value in the stimulating compartment is reached right at the end of stimulation and not at the moment of the membrane voltage's peak. This distorts the observations from above to some extent. All measured data are collected in table 9.13.

9.3 Faster propagation

Faster propagation can be achieved by modeling the cell with segments that represent the part of an axon that is wrapped by a "Schwann cell"—the so-called myelin sheath—and with segments that represent the "Node of Ranvier" between them. Schwann cells surround the axon and prevent currents to cross the membrane or at least reduce them in order to enable higher propagation speed of an action potential. Ionic currents therefore can only occur at the small nodes.

9.3.1 Myelin as perfect insulator

Modeling myelin as a perfect insulator of the internodal axolemma totally prohibits ions from crossing the membrane at the myelinated regions. Ionic currents can only occur at the Nodes of Ranvier, the model is only dependent on the membrane dynamics there. [39]

Three different models were compared with the HH model of the unmyelinated nerve fibre. The length L of each myelinated part of the myelinated cell is 100 µm which corresponds to the ratio of internodal space to fibre diameter[30], the small nodes in between have lengths of $l = 10\,\mu m$ (first model), $l = 5\,\mu m$ (second model), and $l = 1\,\mu m$ (third model).

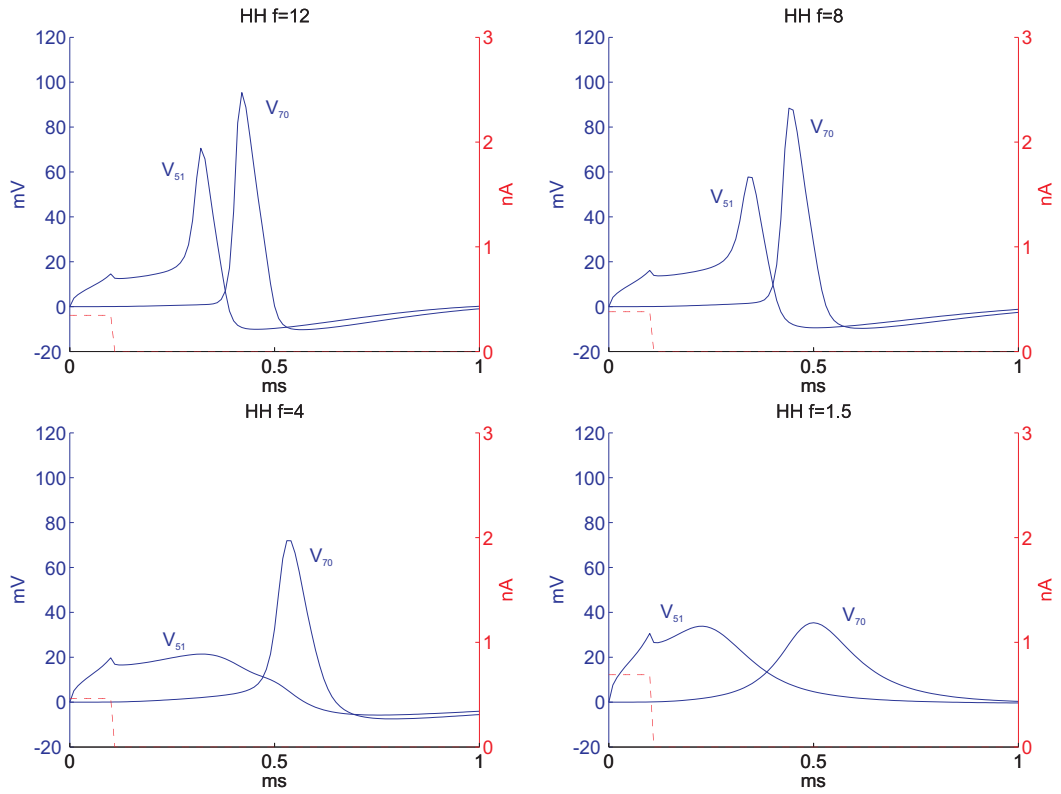

Figure 9.11: Time course of the reduced membrane voltage $V = V_i - V_e - V_{rest}$ in the stimulated (51^{st}) and in the distant (70^{th}) compartment after stimulation by threshold current at 37 °C according to HH models with adapted ionic conductances. Original sodium, potassium, and leakage conductances are multiplied by a factor f of 12, 8, 4, and 1.5. The first continuous blue line is the voltage of the stimulating compartment, the second continuous blue line is the voltage of the 70^{th} compartment. The red dashed line is the threshold current.

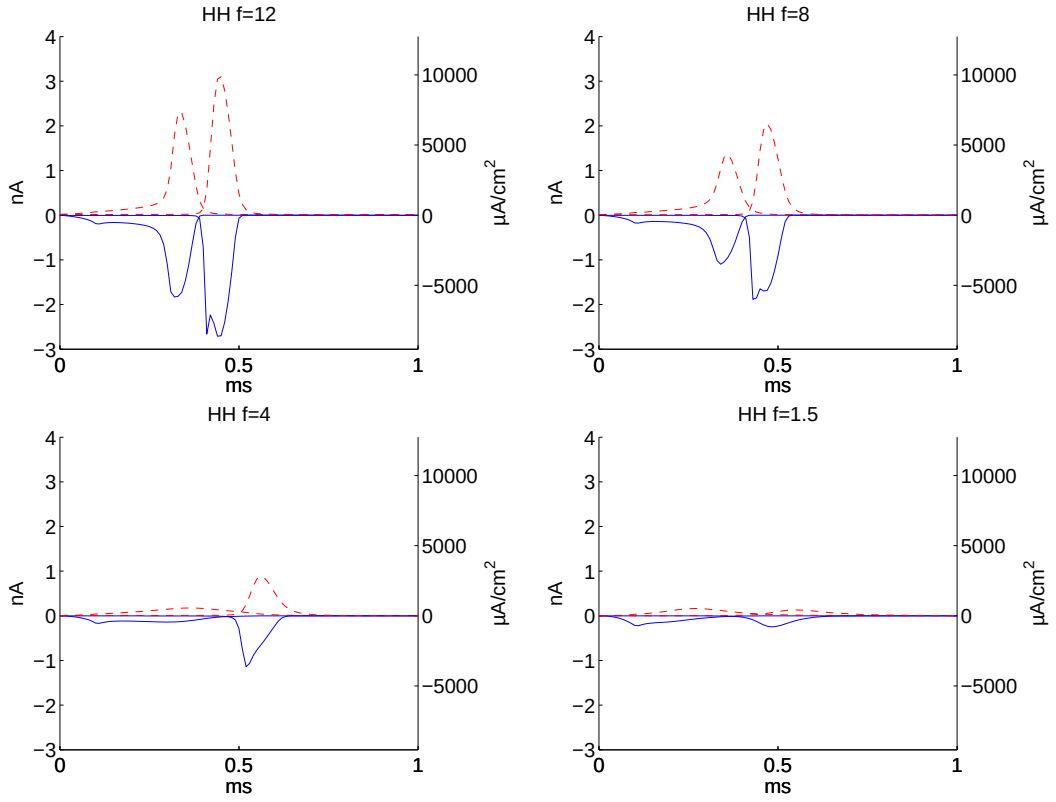

Figure 9.12: Time course of the ionic currents in the 51$^{\text{st}}$ (first set of lines) and in the 70$^{\text{th}}$ (second set of lines) compartment after stimulation by threshold currents at 37 ℃ according to HH models with adapted ionic conductances. Original sodium, potassium, and leakage conductances are multiplied by a factor f of 12, 8, 4, and 1.5. The blue continuous line is the sodium current, the red dashed line is the potassium current. The additional axis on the right of each graph is the scale of the appropriate current densities.

The currents in the first model ($l = 10\,\mu m$) in the distant compartment are similar to those in the HH model without myelinated regions. This is not surprising, as the segments of the unmyelinated nerve fibre are of the same size of the nodes of this myelinated model. Table 9.14 summarizes the measurements of the investigated models. The maximum magnitude of the currents are 100 and 101% of those in the unmyelinated HH model. The total number of ions that cross the membrane in the 70^{th} compartment, are 93% (sodium) and 98% (potassium) of those in the unmyelinated axon. The maximum sodium and potassium currents of the stimulating compartment are a little bit higher (121 and 115%, respectively), the total numbers of ions crossing the cell membrane are about the same size as those in the unmyelinated model (106 and 98%). The propagation velocity of an action potential along the axon as well as the stimulating threshold current differs even more. It takes only 27% of the stimulating threshold current of the unmyelinated HH model to generate an action potential, which on the other hand propagates faster. Its conduction speed is nearly three times the speed of a spike in the unmyelinated model. The threshold membrane voltage of the myelinated nerve fibre is 90% of the potential of the stimulated compartment at the end of the stimulus in the nonmyelinated fibre.

As regards the ionic currents in the model with a nodal gap width of $5\,\mu m$, the maximum magnitude as well as the total number of ions that cross the membrane is about half the size of the magnitude in the unmyelinated reference model. The amplitude of the sodium and potassium currents make 53 and 54% in the stimulated, 51 and 50% in the distant compartment of their equivalents in the unmyelinated model, respecively. As the geometry of the nerve cell has changed, one has to be careful with the interpretation of these findings. Ionic currents always depend on the geometry of the fibre; changing the surface of one section implicates a change in the ionic current (when assuming an unchanging current density). However, it is evident that comparing current densities and not currents, would overcome this problem. As the lateral surface area of one nodal section in the model with $l = 5\,\mu m$ is just the half of that in the model with $l = 10\,\mu m$ or of one section in the reference model, multiplying these currents by a factor of 2 gives comparable results. As regards the total number of ions crossing the membrane, the same problem would occur. By calculating the total number of ions per centimetre, this problem is avoided too. The total number of sodium ions per centimetre is very close to that of the unmyelinated HH model, in the stimulated region it is 99% and in the distant region 98% of that in the referece model, respectively. The amount of potassium ions per centimetre is 93% of that of the reference model, in the stimulated as well as in the distant compartment, respectively. The injected threshold current is 21% of that of the unmyelinated model. Once again, one has to take the geometric aspect into account. Calculating the stimulating current density results in 43% of that in

the reference model, which is higher than that in the myelinated nerve fibre with 10 µm long nodes. The conduction speed of the spike has increased to 6.56 m/s, which is about four times the speed of a spike in the unmyelinated nerve fibre.

The third model of a myelinated axon has a nodal gap width l of 1 µm. The conduction speed of an action potential is about 17 m/s, which is more than hundred times the speed of a spike in the model without myelin sheath. The maximum magnitudes of the ionic currents as well as the total amount of ions that are involved in the excitation process are about 10% of those in the reference model. This is not unexpected either, as the geometry of the nodes of Ranvier is different to that of former models. As regards the current densities, the maximum magnitude of the sodium current density in the stimulated compartment is 105% of that in the reference model, the maximum of the potassium current density 107% of that in the reference model. The current densities in the distant segment are both—sodium and potassium—100% of those in the unmyelinated model. The threshold stimulating current density in the myelinated model with $l = 1$ µm is 100% of that in the reference model, too. Geometric adjustment of the total number of ions that are responsible for propagating action potential along the fibre and comparison with the model for an unmyelinated axon shows that the amount of sodium ions per centimetre in the stimulated compartment as well as in the distant compartment are 98% of those in the reference model. The number of potassium ions in the stimulated and in the distant section make 93% of those in the reference model. The threshold voltage in the model for myelinated axons with a nodal gap with of 1 µm is slightly higher than those of the other models for myelinated nerve fibre and is equal to that of the reference model.

In order to be independent of geometry, figure 9.13 compares the threshold current densities in the unmyelinated reference model with those in the myelinated models. It is important to note that the graphs represent the membrane potentials of the 51^{st} and the 70^{th} compartment. The distance between these sections differs from model to model, so the conception that two closer action potentials implicate a faster propagation of the spike is wrong in this case. Figure 9.14 compares the sodium and potassium currents in the model for unmyelinated nerve fibre with those in the three models for myelinated nerve fibres. The first ordinate axis is the axis of the ionic current density, which has a physical unit of $\mu A/cm^2$; the second ordinate axis, which is located on the right of each graph, is the axis of appropriate currents. One can see that the current densities and the action potentials are of similar shape.

The propagation of a spike after a minimal stimulating current can be seen in figure 9.15. Basis for these four plots are the 101 compartments of the myelinated axon with 10 µm long internodes. Thus, the x-axis represents a 11.11 mm long axon. As the other models are dealing with shorter nodes, their number of compartments were adapted to fit in the frame

of the 11.11 mm long axon. The first (top left) graph represents the membrane voltage of the axon in the unmyelinated reference model. It is the same graph as in figure 9.9, the only difference is the scaling of the x-axis. The other graphs show the propagation of an action potential in the myelinated models with node lengths of 10 µm (top right), 5 µm (bottom left) and 1 µm (bottom right). It can be easily seen that the unmyelinated nerve fibre is the slowest, within 1 ms the spike is only conducted within 1.08 mm to both sides of the stimulated compartment. The conduction speed of an action potential in the models for myelinated nerve fibres is higher: A spike in the model with 10 µm long nodes is conducted within a distance of 3.74 mm within the first millisecond, a spike in the model with a nodal gap width of 5 µm within 5.04 mm. An action potential in the model with 1 µm long nodes even reaches the end of the investigated area after about 0.61 ms.

Some models of myelinated nerve fibres use a different inneraxonal resistance R^*, by replacing Δx in equation (8.3) by the internodal length L.[10],[30] The results according to these models are summarized in table 9.15. Comparing them with the results in table 9.14, one can see that there are only small differences.

The conduction speed of an action potential in the 'new' myelinated axon model with a node length of ten micrometers and in that with a node length of five micrometers is a little bit higher than that in the corresponding previously discussed myelinated models (5.24 and 7.00 m/s instead of 4.78 and 6.56 m/s, respectively). The threshold injected stimulating current as well as the total number of ions crossing the membrane are slightly higher in the 'new' model, too. The maximum magnitude of sodium and potassium currents are almost the same.

9.3.2 Myelin as passive element

The assumption that myelin is a perfect insulator is not consistent with experimental work (see e.g. chapter 8), so another model is created to regard this finding. In this section, the myelin sheath is modeled as an imperfect insulator, which means that some current can flow across the membrane and through the myelin layers of the internodes. Figure 8.2 shows the electrical network which is the model for the myelinated nerve fibre. The myelin sheath is simulated as an electric circuit consisting of a capacitor and a resistor, which are both dependent on the numbers of myelin layers that are wrapped round the axon. For this investigation, 35 myelin double layers are used with a thickness of 17 nm each. The diameter of a myelinated section is 1.595 µm, and due to the ratio of internodal space to fibre diameter of 100[30] the length of each myelinated region is 159.5 µm. The nodes of Ranvier have a length of 10 µm and a diameter of 1 µm each and are modeled with HH dynamics. The odd compartments represent nodes of Ranvier, the even compartments represent the internodes.

As the dimensions of this model are different to those of the models with perfect insulation,

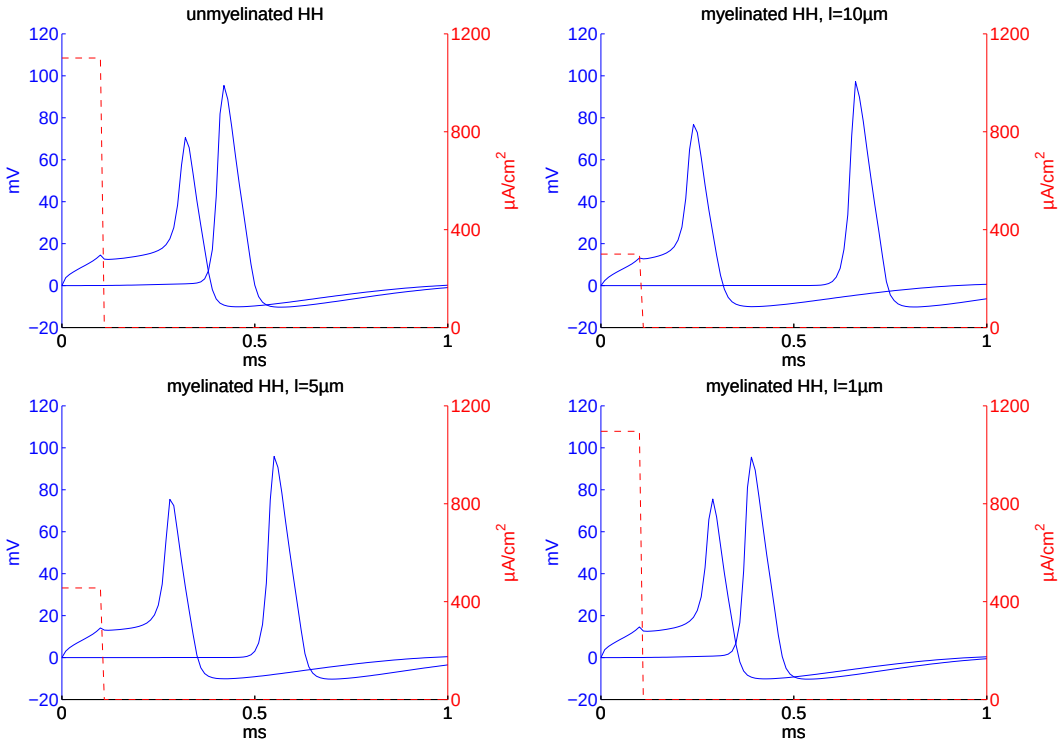

Figure 9.13: Time course of membrane potential in the stimulating and the distant compartment (blue solid lines) after stimulation by threshold current density (red dashed line) at 37 °C according to four different types of nerve cells with HH dynamics. An unmyelinated axon (top left) is compared with myelinated axons whose myelin sheath is a perfect insulator of the internodal axolemma. Myelinated regions (internodes) have a length L of 100 µm, the nodes in between have lengths l of 10 µm (top right), 5 µm (bottom left), and 1 µm (bottom right). The threshold current densities are 1101 $\mu A/cm^2$ in the unmyelinated HH model, 300 $\mu A/cm^2$ in the myelinated HH model with a nodal gap width l of 10 µm, 456 $\mu A/cm^2$ in that model with $l = 5$ µm, and 1096 $\mu A/cm^2$ in that model with $l = 1$ µm.

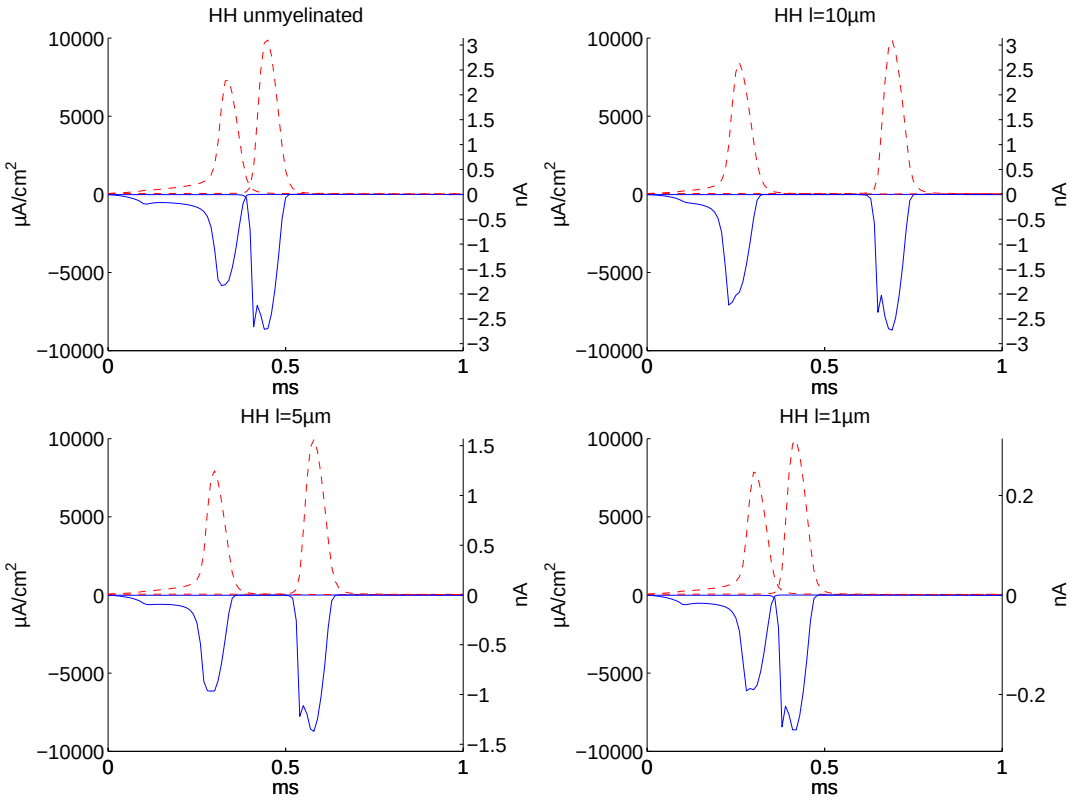

Figure 9.14: Time course of the ionic current densities in the stimulated (first set of lines) and in the distant (second set of lines) compartment after stimulation by threshold current at 37 °C according to four different types of nerve cells with HH dynamics. An unmyelinated axon (top left) is compared with myelinated axons whose myelin sheath is a perfect insulator of the internodal axolemma. Myelinated regions (internodes) have a length L of 100 µm, the nodes in between have lengths l of 10 µm (top right), 5 µm (bottom left), and 1 µm (bottom right). The additional axis on the right of each graph is the scale of the appropriate currents.

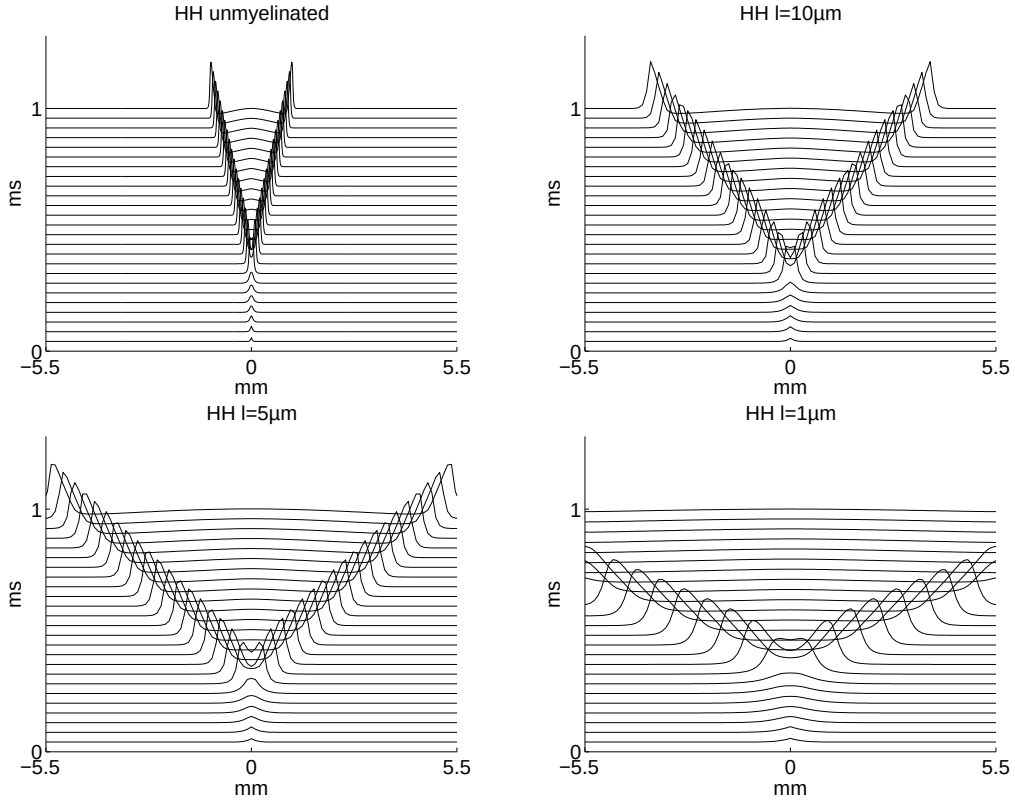

Figure 9.15: Action potential propagation along the axon after stimulation by threshold current in the middle at 37 °C according to four different types of nerve cell with HH dynamics. Each line represents the voltage along the 11110 µm long axon at a determined time, $t = 0, 0.04, 0.08, \ldots, 1$ ms. An unmyelinated axon (top left) is compared with myelinated axons whose myelin sheath is a perfect insulator of the internodal axolemma. Myelinated regions (internodes) have a length L of 100 µm, the nodes in between have lengths l of 10 µm (top right), 5 µm (bottom left), and 1 µm (bottom right).

where the myelinated parts are 100 µm long, one has to be cautious with a direct comparison. On the basis of the model with imperfect insulation of the internodes, the propagation velocity of a spike can be heightened up to nearly 10 $^{m}/_{s}$ which is more than five times the propagation speed of an action potential in the model for the unmyelinated nerve fibre. The threshold injected stimulating current has decreased to a value of 0.14 nA which is 39% of that in the unmyelinated model. The potential difference of the membrane has to be heightened by about the same size as that in the reference model to produce an action potenial. The treshold membrane voltage is 14.31 mV which is 98% of that in the unmyelinated model. The maximum magnitudes of the sodium and potassium currents of the stimulating compartment make 111% of those in the reference model. In the distant compartment the maximum amplitudes of the currents are 102 and 100% of those in the HH model without myelinated regions, respectively. As ionic currents can only occur at the nodes, the ionic currents of the 70^{th} compartment in the reference model are compared with the ionic currents of the 71^{st} compartment in the model for myelinated axons. The total number of sodium and potassium ions crossing the membrane during an action potential is about the same size of those in the unmyelinated model. The number of sodium ions passing the membrane in the stimlating compartment are 105% of those in the reference model, this percentage decreses within a distance; the number of sodium ions in the distant compartment is 101% of that in the unmyelinated HH model. The total number of potassium ions in the stimulated compartment are 103%, in the distant compartment 100% of those in the reference model.

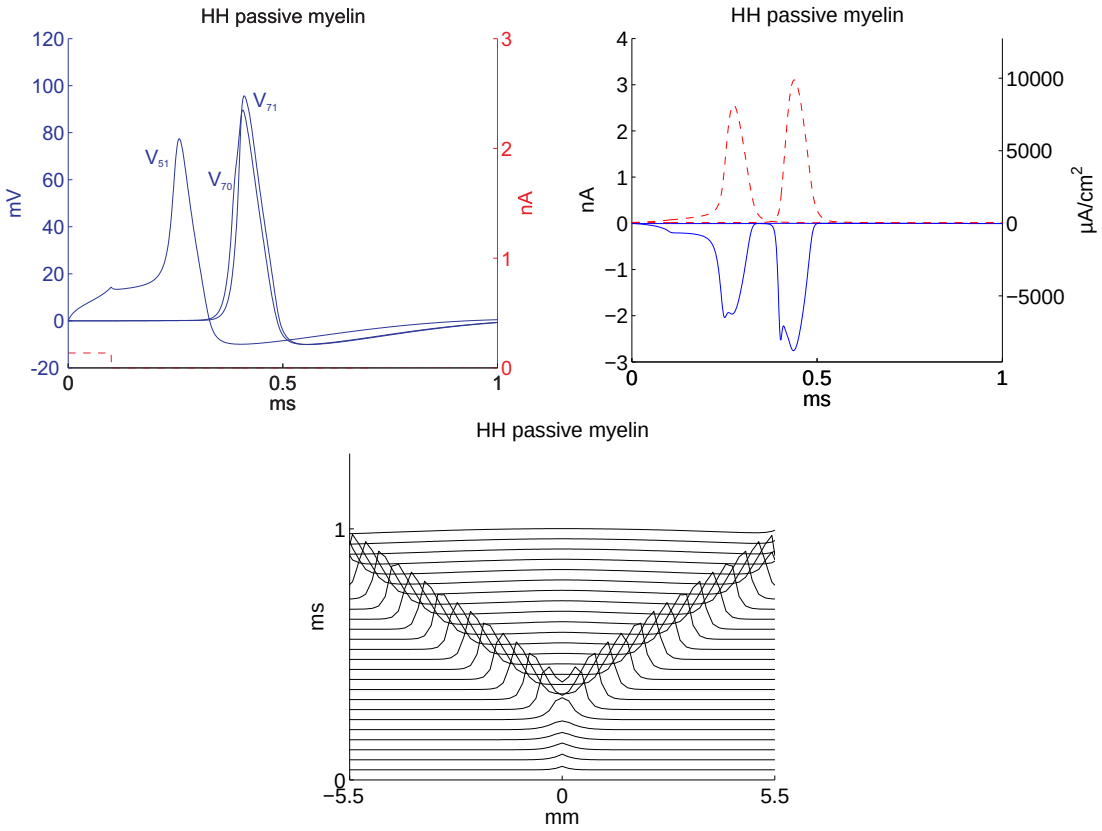

Figure 9.16: Exploring the model of a myelinated axon whose myelin sheath is an imperfect insulator of the internodal axolemma, i.e. some current can flow through the myelin. Top left: Time course of the threshold injected current (red dashed line) and resulting action potential (blue lines) of the stimulated node (V_{51}), distant internode (V_{70}), and distant node (V_{71}) at 37 °C. Top right: Time course of the ionic currents in the stimulated (first set of lines) and in the distant (second set of lines) node after stimulation by threshold current at 37 °C. Bottom: Action potential propagation along the axon after stimulation by threshold current in the middle at 37 °C. Each line represents the voltage along the axon at a determined time, $t = 0, 0.04, 0.08, \ldots, 1\,\text{ms}$.

Table 9.1: Numerical parameters that were used for simulation.

communication interval	0.01
integration algorithm	Runge-Kutta 4
precision	double
nsteps	10
integration step size	$\frac{0.01}{10} = 0.001$
translator table size	10000000
runtime table size	2000000

Table 9.2: Threshold stimulating current density i_{stim} and injected current I_{inj}, and membrane voltage after 0.1 ms according to the HH and CRRSS model at 6.3, 20, and 37 ℃. $[i_{stim}] = \mu\text{A}/\text{cm}^2$, $[I_{inj}] = \text{nA}$, $[V] = \text{mV}$.

	HH			CRRSS		
	i_{stim}	I_{inj}	$V(0.1)$	i_{stim}	I_{inj}	$V(0.1)$
6.3 ℃	129	0.04	9.16	3885 (3012%)	1.22	35.50 (388%)
20 ℃	73	0.02	5.68	2517 (3448%)	0.79	25.02 (441%)
37 ℃	81	0.03	7.55	1710 (2111%)	0.54	19.81 (262%)

Table 9.3: Maximum magnitude of current densities and currents, and total number of ions crossing the membrane during an action potential according to the HH and CRRSS model at 37 ℃. $[i_{ion}] = \mu\text{A}/\text{cm}^2$, $[I_{ion}] = \text{nA}$, [ions] = million.

	HH			CRRSS	
	Na^+	K^+	leak	Na^+	leak
$\max(\lvert i_{ion} \rvert)$	7181	8503	266	13733 (191%)	10024
$\max(\lvert I_{ion} \rvert)$	2.26	2.67	0.08	4.31 (191%)	3.15
# ions	1.06	1.13	0.10	3.15 (296%)	3.49

Table 9.4: Threshold stimulating current density i_{stim} and injected current I_{inj}, and membrane voltage after 0.1 ms according to the FH and SE model. $[i_{stim}] = \mu A/cm^2, [I_{inj}] = nA, [V] = mV$.

	FH	SE
i_{stim}	676 (835%)	2186 (2699%)
I_{inj}	0.21	0.69
$V(0.1)$	18.80 (249%)	30.27 (401%)

Table 9.5: Maximum magnitude of current densities and currents, and total number of ions crossing the membrane during an action potential according to the FH model. $[i_{ion}] = \mu A/cm^2$, $[I_{ion}] = nA$, [ions] = million

	Na^+	K^+	P	leak
$\max(\lvert i_{ion}\rvert)$	9057 (126%)	5827 (69%)	23	3173
$\max(\lvert I_{ion}\rvert)$	2.85	1.83	0.01	1.00
# ions	2.30 (216%)	1.54 (137%)	0.02	1.07

Table 9.6: Maximum magnitude of current densities and currents, and total number of ions crossing the membrane during an action potential according to the SE model. $[i_{ion}] = \mu A/cm^2$, $[I_{ion}] = nA$, [ions] = million

	Na^+	K^+	leak
$\max(\lvert i_{ion}\rvert)$	11157 (155%)	421 (5%)	7973 (2997%)
$\max(\lvert I_{ion}\rvert)$	3.51	0.13	2.50
# ions	2.71 (255%)	0.12 (11%)	3.02 (2962%)

Table 9.7: Threshold stimulating current density i_{stim} and injected current I_{inj}, and membrane voltage after 0.1 ms according to the SRB and FitzHugh model. $[i_{stim}] = {}^{\mu A}/_{cm^2}$, $[I_{inj}] =$ nA, $[V] =$ mV.

	SRB	FitzHugh
i_{stim}	1822 (2249%)	—
I_{inj}	0.57	—
$V(0.1)$	30.54 (405%)	18.81 (249%)

Table 9.8: Maximum magnitude of current densities and currents, and total number of ions crossing the membrane during an action potential according to the SRB model. $[i_{ion}] = {}^{\mu A}/_{cm^2}$, $[I_{ion}] =$ nA, [ions] = million

	Na^+	K^+_{fast}	K^+_{slow}	leak
$\max(\lvert i_{ion} \rvert)$	11138 (155%)	1125	346	6359 (2393%)
$\max(\lvert I_{ion} \rvert)$	3.50	0.35	0.11	2.00
ions	4.63 (435%)	0.62	0.21	4.17 (4111%)

Table 9.9: Maximum magnitude of ionic currents as well as total number of ions passing the membrane in the stimulated compartment (SC) and in the distant compartment (DC) per cm of fibre length and per cm^2 of membrane area. Simulation at 37 °C. Propagation velocity v along the fibre is measured between the 65^{th} and 75^{th} compartments. $V(0.1)$ is the potential of the membrane at the end of stimulation. The value in brackets tells the percentage in comparison to the HH model. $[I_{ion}] = [I_{inj}] =$ nA, [# ions/cm] = million, [# ions/cm^2] = 10^9, $[v] = {}^{\text{m}}/_{\text{s}}$, $[V] =$ mV

	HH			CRRSS	
	Na^+	K^+	leak	Na^+	leak
max($\lvert I_{ion}\rvert$) SC	1.83	2.30	0.07	5.70 (311%)	2.97 (4373%)
max($\lvert I_{ion}\rvert$) DC	2.71	3.10	0.10	6.66 (245%)	3.65 (3807%)
# ions/cm SC	1093	1250	172	4361 (399%)	4361 (2541%)
# ions/cm DC	1274	1403	193	4004 (314%)	4004 (2071%)
# ions/cm^2 SC	3479	3979	546	13883 (399%)	13883 (2541%)
# ions/cm^2 DC	4054	4465	615	12743 (314%)	12744 (2071%)
I_{inj}	0.35			1.84 (531%)	
v	1.67			0.71 (43%)	
$V(0.1)$	14.57			26.33 (181%)	

Table 9.10: Maximum magnitude of ionic currents as well as total number of ions passing the membrane in the stimulated compartment (SC) and in the distant compartment (DC) per cm of fibre length and per cm^2 of membrane area. Simulation at 37 °C. Propagation velocity v along the fibre is measured between the 65^{th} and 75^{th} compartment. $V(0.1)$ is the potential of the membrane at the end of stimulation. The value in brackets tells the percentage in comparison to the HH model. $[I_{ion}] = [I_{inj}] =$ nA, [# ions/cm] = million, [# ions/cm^2] = 10^9, $[v] =$ m/s, $[V] =$ mV

	FH			
	Na^+	K^+	P	leak
max($\lvert I_{ion} \rvert$) SC	4.01 (219%)	1.95 (85%)	0.01	0.92 (1354%)
max($\lvert I_{ion} \rvert$) DC	3.71 (137%)	1.93 (62%)	0.01	1.00 (1045%)
# ions/cm SC	3308 (303%)	1802 (144%)	30	1013 (590%)
# ions/cm DC	2396 (188%)	1671 (119%)	35	760 (393%)
# ions/cm^2 SC	10529 (303%)	5736 (144%)	95	3224 (590%)
# ions/cm^2 DC	7627 (188%)	5319 (119%)	112	2418 (393%)
I_{inj}	1.26 (365%)			
v	0.71 (43%)			
$V(0.1)$	27.04 (186%)			

Table 9.11: Maximum magnitude of ionic currents as well as total number of ions passing the membrane in the stimulated compartment (SC) and in the distant compartment (DC) per cm of fibre length and per cm^2 of membrane area. Simulation at 37 °C. Propagation velocity v along the fibre is measured between the 65^{th} and 75^{th} compartment. $V(0.1)$ is the potential of the membrane at the end of stimulation. The value in brackets tells the percentage in comparison to the HH model. $[I_{ion}] = [I_{inj}] =$ nA, [# ions/cm] = million, [# ions/cm^2] = 10^9, $[v] =$ m/s, $[V] =$ mV

	SE		
	Na^+	K^+	leak
max($\|I_{ion}\|$) SC	4.28 (233%)	0.15 (6%)	1.88 (2777%)
max($\|I_{ion}\|$) DC	4.93 (182%)	0.10 (3%)	2.17 (2268%)
# ions/cm SC	6054 (554%)	213 (17%)	4279 (2493%)
# ions/cm DC	2950 (232%)	114 (8%)	2836 (1468%)
# ions/cm^2 SC	19270 (554%)	678 (17%)	13621 (2493%)
# ions/cm^2 DC	9390 (232%)	362 (8%)	9029 (1468%)
I_{inj}	2.70 (781%)		
v	0.30 (18%)		
$V(0.1)$	42.79 (294%)		

Table 9.12: Maximum magnitude of ionic currents as well as total number of ions passing the membrane in the stimulated compartment (SC) and in the distant compartment (DC) per cm of fibre length and per cm^2 of membrane area. Simulation at 37 °C. Propagation velocity v along the fibre is measured between the 65^{th} and 75^{th} compartment. $V(0.1)$ is the potential of the membrane at the end of stimulation. The value in brackets tells the percentage in comparison to the HH model. $[I_{ion}] = [I_{inj}] =$ nA, [# ions/cm] = million, [# ions/cm^2] = 10^9, $[v] = {}^{\text{m}}/_{\text{s}}$, $[V] =$ mV

	SRB			
	Na^+	K_f^+	K_s^+	leak
max($\lvert I_{ion}\rvert$) SC	4.58 (250%)	0.40	0.11	1.83
max($\lvert I_{ion}\rvert$) DC	5.56 (303%)	0.25	0.13	2.06
# ions/cm SC	7683 (703%)	836	257	4785 (2788%)
# ions/cm DC	4259 (334%)	428	246	3584 (1855%)
# ions/cm^2 SC	24455 (703%)	2661	819	15231 (2788%)
# ions/cm^2 DC	13555 (334%)	1362	784	11409 (1855%)
I_{inj}	2.75 (796%)			
v	0.37 (22%)			
$V(0.1)$	44.61 (306%)			

Table 9.13: Maximum magnitude of ionic currents as well as total number of ions passing the membrane in the stimulated compartment (SC) and in the distant compartment (DC) per cm of fibre length and per cm^2 of membrane area. Simulation at 37 °C. Propagation velocity v along the fibre is measured between the 65^{th} and 75^{th} compartment. $V(0.1)$ is the potential of the membrane at the end of stimulation. The value in brackets tells the percentage in comparison to the HH model with a conductance factor f (a factor, by which the ionic conductances of the original HH model are multiplied) of 12. $[I_{ion}] = [I_{inj}] =$ nA, $[\#\ ^{\text{ions}}/_{\text{cm}}] =$ million, $[\#\ ^{\text{ions}}/_{\text{cm}^2}] = 10^9$, $[v] = {}^{\text{m}}/_{\text{s}}$, $[V] =$ mV

	HH ($f = 12$)	HH $f = 8$ (67%)	HH $f = 4$ (33%)	HH $f = 1.5$ (13%)
max($\lvert I_{\text{Na}} \rvert$) SC	1.83	1.10 (60%)	0.17 (9%)	0.22 (12%)
max($\lvert I_{\text{K}} \rvert$) SC	2.30	1.36 (59%)	0.18 (8%)	0.16 (7%)
max($\lvert I_{\text{Na}} \rvert$) DC	2.71	1.89 (70%)	1.14 (42%)	0.25 (9%)
max($\lvert I_{\text{K}} \rvert$) DC	3.10	2.05 (66%)	0.89 (29%)	0.13 (4%)
# Na^+ $^{\text{ions}}/_{\text{cm}}$ SC	1093	758 (69%)	295 (27%)	220 (20%)
# K^+ $^{\text{ions}}/_{\text{cm}}$ SC	1250	872 (70%)	375 (30%)	275 (22%)
# Na^+ $^{\text{ions}}/_{\text{cm}}$ DC	1274	886 (70%)	484 (38%)	188 (15%)
# K^+ $^{\text{ions}}/_{\text{cm}}$ DC	1403	973 (69%)	529 (38%)	200 (14%)
# Na^+ $^{\text{ions}}/_{\text{cm}^2}$ SC	3479	2412 (69%)	939 (27%)	700 (20%)
# K^+ $^{\text{ions}}/_{\text{cm}^2}$ SC	3979	2775 (70%)	1194 (30%)	875 (22%)
# Na^+ $^{\text{ions}}/_{\text{cm}^2}$ DC	4054	2820 (70%)	1540 (38%)	599 (15%)
# K^+ $^{\text{ions}}/_{\text{cm}^2}$ DC	4465	3097 (69%)	1684 (38%)	636 (14%)
I_{inj}	0.35	0.38 (110%)	0.46 (133%)	0.69 (200%)
v	1.67	1.43 (86%)	1.11 (67%)	0.56 (33%)
$V(0.1)$	14.57	16.12 (111%)	19.71 (135%)	30.59 (210%)

Table 9.14: Maximum magnitude of ionic currents as well as total number of ions passing the membrane in the stimulated compartment (SC) and in the distant compartment (DC) per cm of fibre length and per cm^2 of membrane area. Simulation at 37 °C. Propagation velocity v along the fibre is measured between the 65^{th} and 75^{th} compartments. $V(0.1)$ is the potential of the membrane at the end of stimulation. The value in brackets tells the percentage in comparison to the unmyelinated HH model. Myelin sheath is a perfect insulator, the length l of the internode is 100 µm, the length l of the node varies from model to model. Total number of ions is measured after 2 ms. $[I_{ion}] = [I_{inj}] = \text{nA}$, $[\#\ ^{\text{ions}}/_{\text{cm}}] = \text{million}$, $[\#\ ^{\text{ions}}/_{\text{cm}^2}] = 10^9$, $[v] = {}^{\text{m}}/_{\text{s}}$, $[V] = \text{mV}$

	HH (unmyelin.)	HH $l = 10\,\mu\text{m}$	HH $l = 5\,\mu\text{m}$	HH $l = 1\,\mu\text{m}$
$\max(\lvert I_{\text{Na}}\rvert)$ SC	1.83	2.22 (121%)	0.97 (53%)	0.19 (11%)
$\max(\lvert I_{\text{K}}\rvert)$ SC	2.30	2.65 (115%)	1.25 (54%)	0.25 (11%)
$\max(\lvert I_{\text{Na}}\rvert)$ DC	2.71	2.73 (101%)	1.37 (51%)	0.27 (10%)
$\max(\lvert I_{\text{K}}\rvert)$ DC	3.10	3.10 (100%)	1.56 (50%)	0.31 (10%)
$\#\ \text{Na}^+\ {}^{\text{ions}}/_{\text{cm}}$ SC	1093	1155 (106%)	1081 (99%)	1076 (98%)
$\#\ \text{K}^+\ {}^{\text{ions}}/_{\text{cm}}$ SC	1250	1222 (98%)	1158 (93%)	1166 (93%)
$\#\ \text{Na}^+\ {}^{\text{ions}}/_{\text{cm}}$ DC	1274	1246 (98%)	1249 (98%)	1245 (98%)
$\#\ \text{K}^+\ {}^{\text{ions}}/_{\text{cm}}$ DC	1403	1307 (93%)	1309 (93%)	1301 (93%)
$\#\ \text{Na}^+\ {}^{\text{ions}}/_{\text{cm}^2}$ SC	3479	3678 (106%)	3440 (99%)	3426 (98%)
$\#\ \text{K}^+\ {}^{\text{ions}}/_{\text{cm}^2}$ SC	3979	3889 (98%)	3685 (93%)	3713 (93%)
$\#\ \text{Na}^+\ {}^{\text{ions}}/_{\text{cm}^2}$ DC	4054	3965 (98%)	3976 (98%)	3963 (98%)
$\#\ \text{K}^+\ {}^{\text{ions}}/_{\text{cm}^2}$ DC	4465	4160 (93%)	4165 (93%)	4142 (93%)
I_{inj}	0.35	0.09 (27%)	0.07 (21%)	0.03 (10%)
v	1.67	4.78 (287%)	6.56 (394%)	16.83 (1010%)
$V(0.1)$	14.57	13.12 (90%)	14.11 (97%)	14.58 (100%)

Table 9.15: Maximum magnitude of ionic currents as well as total number of ions passing the membrane in the stimulated compartment (SC) and in the distant compartment (DC) per cm of fibre length and per cm^2 of membrane area. Simulation at 37 °C. Propagation velocity v along the fibre is measured between the 65^{th} and 75^{th} compartments. $V(0.1)$ is the potential of the membrane at the end of stimulation. The value in brackets tells the percentage in comparison to the unmyelinated HH model. Myelin sheath is a perfect insulator, the length L of the internode is 100 µm, the length l of the node varies from model to model. Total number of ions is measured after 2 ms. Adapted R^* for the inneraxonal resistance was used. $[I_{ion}] = [I_{inj}] =$ nA, [# ions/cm] = million, [# ions/cm^2] = 10^9, $[v] =$ m/s, $[V] =$ mV

	HH (unmyelin.)	HH $l = 10$ µm	HH $l = 5$ µm	HH $l = 1$ µm
max($\lvert I_{Na}\rvert$) SC	1.83	1.96 (107%)	1.00 (54%)	0.18 (10%)
max($\lvert I_{K}\rvert$) SC	2.30	2.46 (107%)	1.29 (56%)	0.23 (10%)
max($\lvert I_{Na}\rvert$) DC	2.71	2.75 (102%)	1.37 (51%)	0.27 (10%)
max($\lvert I_{K}\rvert$) DC	3.10	3.10 (100%)	1.54 (50%)	0.31 (10%)
# Na^+ ions/cm SC	1093	1141 (104%)	1124 (103%)	1093 (100%)
# K^+ ions/cm SC	1250	1276 (102%)	1278 (102%)	1250 (100%)
# Na^+ ions/cm DC	1274	1272 (100%)	1278 (100%)	1274 (100%)
# K^+ ions/cm DC	1403	1401 (100%)	1406 (100%)	1403 (100%)
# Na^+ ions/cm^2 SC	3479	3630 (104%)	3578 (103%)	3479 (100%)
# K^+ ions/cm^2 SC	3979	4062 (102%)	4067 (102%)	3979 (100%)
# Na^+ ions/cm^2 DC	4054	4050 (100%)	4068 (100%)	4054 (100%)
# K^+ ions/cm^2 DC	4465	4458 (100%)	4476 (100%)	4465 (100%)
I_{inj}	0.35	0.10 (29%)	0.07 (21%)	0.03 (10%)
v	1.67	5.24 (314%)	7.00 (420%)	16.83 (1010%)
$V(0.1)$	14.57	13.22 (91%)	14.18 (97%)	14.57 (100%)

Table 9.16: Maximum magnitude of ionic currents as well as total number of ions passing the membrane in the stimulated compartment (SC) and in the distant compartment (DC) per cm of fibre length and per cm^2 of membrane area. In the model in which the myelin sheaths are an imperfect isolator the distant compartment is the 71^{st} compartment. Simulation at 37 °C. Propagation velocity v along the fibre is measured between the 65^{th} and 75^{th} compartments. $V(0.1)$ is the potential of the membrane at the end of stimulation, i.e. the threshold membrane potential. The value in brackets tells the percentage in comparison to the unmyelinated HH model. Myelin sheath is an imperfect insulator, the length Δx of the internode is 159.5 µm, the length l of the node is 10 µm. Diameter of a node is 1 µm, diameter of an internode is 1.595 µm. Total number of ions is measured after 2 ms. $[I_{ion}] = [I_{inj}] = \text{nA}$, $[v] = {}^{\text{m}}/_{\text{s}}$, $[V] = \text{mV}$, $[\#\ {}^{\text{ions}}/_{\text{cm}}] = \text{million}$, $[\#\ {}^{\text{ions}}/_{\text{cm}^2}] = 10^9$

	HH	HH with passive myelin
$\max(\lvert I_{\text{Na}}\rvert)$ SC	1.83	2.04 (111%)
$\max(\lvert I_{\text{K}}\rvert)$ SC	2.30	2.56 (111%)
$\max(\lvert I_{\text{Na}}\rvert)$ DC	2.71	2.76 (102%)
$\max(\lvert I_{\text{K}}\rvert)$ DC	3.10	3.10 (100%)
$\#\ \text{Na}^+\ {}^{\text{ions}}/_{\text{cm}}$ SC	1093	1145 (105%)
$\#\ \text{K}^+\ {}^{\text{ions}}/_{\text{cm}}$ SC	1250	1288 (103%)
$\#\ \text{Na}^+\ {}^{\text{ions}}/_{\text{cm}}$ DC	1274	1281 (101%)
$\#\ \text{K}^+\ {}^{\text{ions}}/_{\text{cm}}$ DC	1403	1404 (100%)
$\#\ \text{Na}^+\ {}^{\text{ions}}/_{\text{cm}^2}$ SC	3479	3643 (105%)
$\#\ \text{K}^+\ {}^{\text{ions}}/_{\text{cm}^2}$ SC	3979	4098 (103%)
$\#\ \text{Na}^+\ {}^{\text{ions}}/_{\text{cm}^2}$ DC	4054	4078 (101%)
$\#\ \text{K}^+\ {}^{\text{ions}}/_{\text{cm}^2}$ DC	4465	4470 (100%)
I_{inj}	0.35	0.14 (39%)
v	1.67	9.74 (584%)
$V(0.1)$	14.57	14.31 (98%)

Chapter 10

Discussion

In this thesis, the action potential and the propagation effect of a spike according to an adapted HH model are investigated. The multiplying factor of 12 for the maximum ionic conductances of the HH model enables the generation and transmission of an action potential along the membrane of a nerve cell at a temperature of 37 °C. It changes the maximum sodium, potassium and leakage conductance of the HH model so that g_{Na} almost equals the maximum sodium conductance of the CRRSS model, which is a model for mammalian myelinated nerve fibres. Conduction velocity, stimulating threshold current and other properties of the HH model are compared with those of models found in literature.

Local models, where current flow along the axon is prevented, as well as different propagation models are examined and compared with each other. Adapted HH models with different factors for the ionic conductances are analyzed, and models for myelinated nerve fibres with different insulating properties are investigated.

The conduction velocity of an action potential along a 1 µm thick unmyelinated axon with an internal resistivity of 0.1 kΩcm and HH dynamics is 1.67 m/s, which is higher than the velocity of an action potential according to the other investigated membrane models. As regards the HH model of a myelinated nerve fibre whose myelin sheaths are modeled as perfect insulators of the internodal axolemma, the conduction speed of a spike is 16 m/s. As shown in chapter 4, one can calculate the velocity for thicker unmyelinated axons by applying the rule that an axon with a diameter of k µm increases the speed by a factor of $\sqrt{k}$, i.e. an axon with a diameter of 3 µm can conduct an action potential by $v = \sqrt{3} \cdot 1.67$ m/s. Changing the diameter of a myelinated nerve fibre by a factor of k leads to an adaption in propagation velocity along the fibre by a factor of k; a four times thicker axon conducts an action potential by $v = 4 \cdot 16$ m/s.

The injected stimulating threshold current in the HH model is smaller than those in the other models. In the CRRSS model, for example, the stimulating current has to be more than

five times that in the HH model to generate an action potential. The threshold membrane voltage in the HH model is smaller than in the other models, too. The membrane voltage in the CRRSS model must be heightened by 181% of the membrane voltage in the HH model in order to produce an action potential. Apart from the conduction speed of a spike and threshold stimulating current and threshold membrane voltage, the CRRSS model differs from the HH model in many ways. The maximum amplitudes of the sodium currents in the propagation model with CRRSS dynamics are two-and-a-half times (in the distant compartment) and three times (in the stimulating compartment) the height of the corresponding maximum amplitudes in the HH model. The total number of sodium ions involved in the excitation of a CRRSS nerve cell is three times (in the distant compartment) and four times (in the stimulating compartment) of those in the HH model. The total number of any ions in the CRRSS model that cross the membrane in the stimulated compartment is 3.5 times that in the HH model. In the distant compartment, 2.8 times as many ions are involved in the conduction of an action potential in the CRRSS model as in the HH model.

It is important to note that the action potentials according to the adapted HH model are very short. Figures 9.13 and 9.16 show the time courses of spikes according to unmyelinated and myelinated HH propagation models. Figure 9.7, which compares propagation models according to unmyelinated nerve fibres of different membrane models, shows that an action potential according to the HH model is unusually short. This can also be seen in figure 9.2, which compares the local models of the investigated membrane models. In particular, the shape of the spike according to the adapted HH model is different to that of the CRRSS and the SRB model, which are created for modeling the membrane of a mammalian myelinated nerve fibre and a human myelinated nerve fibre, respectively. This indicates that the adapted HH model is not adequate for modeling the membrane of warm blooded animals. In general, action potentials last for one millisecond which is much longer than the action potentials according to the adapted HH model. However, the model may be appropriate for the membrane of a squid with a temperature of 37°C.

One reason for these differences might be that the value of Q_{10} within the temperature coefficient k in the HH model is not equal to three for all temperatures, but changes with temperature. Another reason could be that the HH model does not take account of different sodium channel types. In the central nervous system, action potentials are described by high threshold sodium channels $Na_v1.2$ and low threshold sodium channels $Na_v1.6$.[38]

Bibliography

[1] http://www.usm.maine.edu/psy/broida/101/neuron.JPG.

[2] H. Bostock, M. Baker, and G. Reid. Changes in excitability of human motor axons underlying post-ischaemic fasciculations: evidence for two stable states. *The Journal of Physiology*, 441:537–557, 1991.

[3] C.M. Bowe, J.D. Kocsis, and S.G. Waxman. Differences between mammalian ventral and dorsal roots in response to blockade of potassium channels during maturation. *Proceedings of the Royal Society of London. Series B, Biological Sciences*, 224:355–366, 1985.

[4] T. Brismar. Potential clamp analysis of membrane currents in rat myelinated nerve fibres. *The Journal of Physiology*, 298:171–184, 1980.

[5] S.Y. Chiu, J.M. Ritchie, R.B. Rogart, and D. Stagg. A quantitative description of membrane currents in rabbit myelinated nerve. *The Journal of Physiology*, 292:149–166, 1979.

[6] F.A. Dodge and B. Frankenhaeuser. Sodium currents in the myelinated nerve fibre of Xenopus leavis investigated with the voltage clamp technique. *The Journal of Physiology*, 148:188–200, 1959.

[7] R. FitzHugh. Mathematical models of threshold phenomena in the nerve membrane. *Bulletin of mathematical biophysics*, 17:257–278, 1955.

[8] R. FitzHugh. Thresholds and Plateaus in the Hodgkin-Huxley Nerve Equations. *The Journal of General Physiology*, 43:867–896, 1960.

[9] R. FitzHugh. Impulses and physiological states in theoretical models of nerve membrane. *Biophysical Journal*, 1:445–466, 1961.

[10] R. FitzHugh. Computation of impulse initiation and saltatory conduction in a myelinated nerve fiber. *Biophysical Journal*, 2:11–21, 1962.

[11] R. FitzHugh and H.P. Schwan. *Biological engineering*, chapter 1. New York, McGraw-Hill, 1969.

[12] B. Frankenhaeuser. Quantitative description of sodium currents in myelinated nerve fibres of Xenopus leavis. *The Journal of Physiology*, 151:491–501, 1960.

[13] B. Frankenhaeuser. Potassium permeability in myelinated nerve fibres of Xenopus leavis. *The Journal of Physiology*, 160:54–61, 1962.

[14] B. Frankenhaeuser. A quantitative description of potassium currents in myelinated nerve fibres of Xenopus leavis. *The Journal of Physiology*, 169:424–430, 1963.

[15] B. Frankenhaeuser and A.F. Huxley. The action potential in the myelinated nerve fibre of Xenopus leavis as computed on the basis of voltage clamp data. *The Journal of Physiology*, 171:302–315, 1964.

[16] B. Frankenhaeuser and L.E. Moore. The effect of temperature on the sodium and potassium permeability changes in myelinated nerve fibres of Xenopus leavis. *The Journal of Physiology*, 169:431–437, 1963.

[17] B. Hille. *Ionic Channels of Excitable Membranes*. Sinauer Associates Inc., second edition, 1992.

[18] A.L. Hodgkin and A.F. Huxley. The components of membrane conductance in the giant axon of Loligo. *The Journal of Physiology*, 116:473–496, 1952.

[19] A.L. Hodgkin and A.F. Huxley. Currents carried by sodium and potassium ions through the membrane of the giant axon of Loligo. *The Journal of Physiology*, 116:449–472, 1952.

[20] A.L. Hodgkin and A.F. Huxley. The dual effect of membrane potential on sodium conductance in the giant axon of Loligo. *The Journal of Physiology*, 116:497–506, 1952.

[21] A.L. Hodgkin and A.F. Huxley. A quantitative description of membrane current and its application to conduction and excitation in nerve. *The Journal of Physiology*, 117:500–544, 1952.

[22] A.L. Hodgkin, A.F. Huxley, and B. Katz. Measurement of current-voltage relations in the membrane of the giant axon of Loligo. *The Journal of Physiology*, 116:424–448, 1952.

[23] A.L. Hodgkin and B. Katz. The effect of temperature on the electrical activity of the giant axon of the squid. *The Journal of Physiology*, 109:240–249, 1949.

[24] AEgis Technologies Group Inc. *Advanced Continuous Simulation Language (ACSL) Reference Manual*. AEgis Software, Huntsville, 1999.

[25] D. Junge. *Nerve and Muscle Excitation*, chapter 1, 2 and 6. Sinauer Associates Inc., third edition, 1992.

[26] E.R. Kandel, J.H. Schwartz, and T.M. Jessel. *Principles of Neural Science*. McGraw-Hill, New York, fourth edition, 2000.

[27] B. Katz. *Nerve, muscle and synapse*. McGraw-Hill, New York, 1966.

[28] K. Kunsch and S. Kunsch. *Der Mensch in Zahlen*. Spektrum Akademischer Verlag, third edition, 2007.

[29] G.G. Matthews. *Neurobiology: molecules, cells, and systems*. Blackwell Science, Inc., 2001.

[30] D.R. McNeal. Analysis of a Model for Excitation of Myelinated Nerve. *IEEE Transactions on biomedical engineering*, BME-23 (4):329–337, 1976.

[31] H. Pfützner. *Angewandte Biophysik*. Springer-Verlag, 2003.

[32] F. Rattay. Ways to Approximate Current-Distance Relations for Electrically Stimulated Fibers. *Journal of Theoretical Biology*, 125 (3):339–349, 1987.

[33] F. Rattay. Analysis of models for extracellular fiber stimulation. *IEEE Transactions on biomedical engineering*, 36 (7):676–682, 1989.

[34] F. Rattay. *Electrical Nerve Stimulation - Theory, Experiments and Application*. Springer-Verlag, 1990.

[35] F. Rattay. The basic mechanism for the electrical stimulation of the nervous system. *Neuroscience*, 89 (2):335–346, 1999.

[36] F. Rattay and M. Aberham. Modeling axon membranes for functional electrical stimulation. *IEEE Transactions on biomedical engineering*, 40 (12):1201–1209, 1993.

[37] F. Rattay, R.J. Greenberg, and S. Resatz. Neuron modeling. In *Handbook of Neuroprosthetic Methods*, chapter 3. CRC Press LLC, 2003.

[38] F. Rattay and C. Wenger. Which elements of the mammalian central nervous system are excited by low current stimulation with microelectrodes? *Neuroscience*, 170:339–407, 2010.

[39] A.G. Richardson, C.C. McIntyre, and W.M. Grill. Modelling the effects of electric fields on nerve fibres: influence of the myelin sheath. *Medical & Biological Engineering & Computing*, 38 (4):438–446, 2000.

[40] J. Röper and J.R. Schwarz. Heterogeneous distribution of fast and slow potassium channels in myelinated rat nerve fibres. *The Journal of Physiology*, 416:93–110, 1989.

[41] J.R. Schwarz and G. Eikhof. Na currents and action potentials in rat myelinated nerve fibres at 20 and 30 ℃. *Pflügers Archiv — European Journal of Physiology*, 409:569–577, 1987.

[42] J.R. Schwarz, G. Reid, and H. Bostock. Action potentials and membrane currents in the human node of ranvier. *European Journal of Physiology*, 430:283–292, 1995.

[43] J.D. Sweeney, J.T. Mortimer, and D. Durand. Modeling of mammalian myelinated nerve for functional neuromuscular stimulation. *IEEE 9^{th} Annual Conference of Engineering in Medicine and Biology Society*, pages 1577–1578, 1987.